2012-07-29

Propagation and Scattering of Optical Light Beams in Free Space, in Atmosphere, and in Biological Media

Serkan Sahin
University of Miami, sahserkan@hotmail.com

UNIVERSITY OF MIAMI

PROPAGATION AND SCATTERING OF OPTICAL LIGHT BEAMS IN FREE SPACE, IN ATMOSPHERE AND IN BIOLOGICAL MEDIA

By

Serkan Sahin

A DISSERTATION

Submitted to the Faculty
of the University of Miami
in partial fulfillment of the requirements for
the degree of Doctor of Philosophy

Coral Gables, Florida

August 2012

UNIVERSITY OF MIAMI

A dissertation submitted in partial fulfillment of
the requirements for the degree of
Doctor of Philosophy

PROPAGATION AND SCATTERING OF OPTICAL LIGHT BEAMS IN FREE SPACE, IN ATMOSPHERE, AND IN BIOLOGICAL MEDIA

Serkan Sahin

Approved:

_____ Olga Korotkova, Ph.D. Associate Professor of Physics	_____ M. Brian Blake, Ph.D. Dean of the Graduate School
_____ Howard Gordon, Ph.D. Professor of Physics	_____ Kenneth Voss, Ph.D. Professor of Physics

_____
Greg Gbur, Ph.D.
Associate Professor of Physics
University of North Carolina at Charlotte

SAHIN, SERKAN. (Ph.D., Physics)

Propagation and Scattering of Optical Light Beams in Free Space, in Atmosphere, and in Biological Media (August 2012)

Abstract of a dissertation at the University of Miami.

Dissertation supervised by Professor Olga Korotkova.
No. of pages in text. (116)

With their first production implemented around 1960's, lasers have afterwards proven to be excellent light sources in building the technology. Subsequently, it has been shown that the extraordinary properties of lasers are related to their coherence properties. Recent developments in optics make it possible to synthesize partially coherent light beams from fully coherent ones. In the last several decades it was seen that using partially coherent light sources may be advantageous, in the areas such as laser surface processing, fiber and free-space optical communications, and medical diagnostics.

In this thesis, I study extensively the generation, the propagation in different media, and the scattering of partially coherent light beams with respect to their spectral polarization and coherence states. For instance, I analyze the evolution of recently introduced degree of cross-polarization of light fields in free space; then develop a novel partially coherent light source which acquires and keeps a flat intensity profile around the axis at any distance in the far field; and investigate the interaction of electromagnetic random light with the human eye lens.

A part of the thesis treats the effect of atmospheric turbulence on random light beams. Due to random variations in the refractive index, atmospheric turbulence modulates all

physical and statistical properties of propagating beams. I have explored the possibility of employing the polarimetric domain of the beam for scintillation reduction, which positively affects the performance of free-space communication systems. I also discuss novel techniques for the sensing of rough targets in the turbulent atmosphere by polarization and coherence properties of light.

The other contribution to the thesis is the investigation of light scattering from deterministic or random collections of particles, within the validity of first Born approximation. In the case of a random collection, I introduce and model the new quantity (named pair-structure function) describing correlations among particles, the knowledge of which is necessary for the rigorous predictions of scattered radiation's statistics. Also, by introducing the multi-Gaussian family of functions for scattering potentials, we demonstrate a realistic model for semi-hard edges of particles and bubble-like particles.

To my parents

Acknowledgments

I would like to thank a number of people for their support during my Ph.D. years. First of all I would like to express my gratitude to my advisor, Professor Olga Korotkova. It was a great pleasure to work under her supervision. From her patience and time grew my understanding. I am very grateful to Professor Greg Gbur for sharing excellent studies with me besides his comments on my thesis. I would like to thank all the members of the University of Miami Physics Department for their friendship and warmth. Especially, I would like to thank Professor Kenneth Voss for his comments and for his help during my Ph.D., Professor Howard Gordon for his comments and for being a member of my committee. I owe my deepest gratitude to Professor Carolyna Van Vliet and Professor Thomas Curtright for their support and motivation, and I have enjoyed and learned a lot in their teachings. Finally I would like to thank my family and friends, they never left me alone and always supported and motivated me in desperate times.

Table of Contents

List of Figures

Chapter 1

Introduction

1.1 Brief history of classical statistical optics

A single quantitative measure of the coherence properties of a light field, called the degree of coherence, was introduced by Zernike [1]. It provides the basis for the development of modern coherence theory. The definition of the degree of coherence was later extended [2], but the essence of the Zernike's approach was retained, which is: the degree of coherence of an optical field is proportional to the visibility of fringes in double-slit interference experiment. Before the development of lasers in the 1960s, optical coherence was practically unknown and an underestimated subject. However, the situation changed once it was realized that the remarkable physical properties of laser light depended on its coherence properties. The experiments by Hanbury Brown and Twiss [3] stimulated further interest in optical coherence theory, showing that correlations between fluctuations of mutually coherent beams of thermal light could be measured by photoelectric correlation and two-photon coincidence counting experiments.

In 1970's and 80's scalar coherence theory was developed. Among its most interesting findings are the relations between the source coherence state and the field spectral and diffraction properties [4].

In the last several decades, considerable progress has been made in generalizing the coherence theory of scalar wave fields to the domain of electromagnetic theory, which helped reveal the relation between coherence and polarization properties of light fields [5]. As early as in 1994, James [6] showed that the degree of polarization of

partially coherent light beams can change even in free space. Afterwards, the number of studies on the effect of different media on coherence and polarization properties of light beams increased considerably due to their practical importance. In particular, the effect of atmospheric and oceanic turbulence as well as of biological media on random, electromagnetic wave propagation are now under intense research.

1.2 Random optical fields

The discussion in this section is based on the principles of classical coherence theory of Refs. [2] and [5]. Let us first consider a complex random process $z(t) = x(t)+iy(t)$, with t denoting the time. This form is called the complex representation of the real analytic signal $x(t)$. If the real signal $x(t)$ has a narrow bandwidth $\Delta\omega$ which is small relative to its mean frequency $\bar{\omega}$ then it is called a *quasi-monochromatic* signal. One often represents it in the form $x(t) = a(t)\cos[\psi(t) - \bar{\omega}t]$ under the condition $\Delta\omega/\bar{\omega} \ll 1$, where $a(t)$, $\psi(t)$, and ω are the amplitude, the phase factor, and the angular frequency, respectively. The function $z(t)$ may then be identified with a *complex envelope of the narrow-band signal* $x(t)$. The statistical properties of the complex process $z(t)$ are characterized by the sequence of probability densities

$$p_1(z,t), p_2(z_1,z_2,t_1,t_2), p_3(z_1,z_2,z_3,t_1,t_2,t_3), ... \tag{1.1}$$

Here $p_1(z,t)d^2z$ ($d^2z = dxdy$) represents the probability that $z(t)$ will take on a value within the element $(x, x+dx; y, y+dy)$ at time t. These probability density functions are employed for finding the ensemble average of the process

$$\langle z(t)\rangle_e = \int z p_1(z,t) d^2z, \tag{1.2}$$

where the integration extends over all possible values of z. The joint probability p_2

allows us to define the ensemble average of the product $z^*(t_1)z(t_2)$, which is called the autocorrelation function $\Gamma(t_1, t_2)$

$$\Gamma(t_1, t_2) = \langle z^*(t_1)z(t_2)\rangle_e = \int z_1^* z_2 p_2(z_1, z_2, t_1, t_2) d^2 z_1 d^2 z_2, \tag{1.3}$$

where the asterisks denotes the complex conjugate. If the statistical behavior of a random process does not change with time then such a process is called *statistically stationary*. The mathematical meaning of this statement is that the probability densities $p_1, p_2, p_3...$ are time-shift invariant, i.e., $\langle z^*(t_1)z(t_2)\rangle_e = \langle z^*(t_1 + T)z(t_2 + T)\rangle_e$, for any value of T. Processes in which the statistics are time-shift invariant only up to the second order are called *wide-sense stationary*. The mean $\langle z(t)\rangle_e$ is then independent of t and the autocorrelation is a function only of the time difference $\tau = t_2 - t_1$, that is

$$\Gamma(\tau) = \langle z^*(t)z(t + \tau)\rangle_e. \tag{1.4}$$

If a process is *ergodic* an ensemble average can always be replaced by a time average [2]. From now on we will assume that all the ensembles considered are both wide-sense stationary and ergodic. Therefore, the subscript e on the angular brackets will be omitted.

An important property of a stationary random process is its spectral density $S(\omega)$. The spectral density provides a measure of the strength of the fluctuations in every specific Fourier component of $z(t)$. The Wiener-Khintchine theorem ([7], Ch. 16.4) states that the autocorrelation function $\Gamma(\tau)$ forms a Fourier-transform pair with the spectral density $S(\omega)$, i.e.,

$$S(\omega) = \frac{1}{2\pi} \int_{-\infty}^{\infty} \Gamma(\tau) e^{i\omega\tau} d\tau. \tag{1.5}$$

$$\Gamma(\tau) = \int_{-\infty}^{\infty} S(\omega) e^{-i\omega\tau} d\tau. \tag{1.6}$$

This theorem is readily generalized from a single random process $z(t)$ to a pair of random processes $z_1(t)$ and $z_2(t)$ which are jointly stationary, at least in the wide sense, i.e. the cross-correlation between the two processes, $\Gamma_{12}(\tau) = \langle z_1^*(t) z_2(t+\tau) \rangle$, depends only on the time difference $\tau = t_2 - t_1$. This extension is called the generalized Wiener-Khintchine theorem, and according to it the cross-spectral density $W_{12}(\omega)$ for the pair of processes and its Fourier transform are related as

$$W_{12}(\omega) = \frac{1}{2\pi} \int_{-\infty}^{\infty} \Gamma_{12}(\tau) e^{i\omega\tau} d\tau. \tag{1.7}$$

$$\Gamma_{12}(\tau) = \int_{-\infty}^{\infty} W_{12}(\omega) e^{-i\omega\tau} d\tau. \tag{1.8}$$

We can now turn our attention to the fundamentals of scalar coherence theory for any spatially varying fields. Let $V(\mathbf{r}, t)$ be a member of an ensemble $\{V(\mathbf{r}, t)\}$ representing a component of the fluctuating electric field, where $\mathbf{r}$ is the position vector of a point in space. The cross-correlation function of the spatially varying field is known as the *mutual coherence function*:

$$\Gamma(\mathbf{r}_1, \mathbf{r}_2; \tau) = \langle V^*(\mathbf{r}_1; t) V(\mathbf{r}_2; t+\tau) \rangle. \tag{1.9}$$

The normalized version of the mutual coherence function is known as the complex degree of coherence

$$\gamma(\mathbf{r}_1, \mathbf{r}_2; \tau) = \frac{\Gamma(\mathbf{r}_1, \mathbf{r}_2; \tau)}{\sqrt{I(\mathbf{r}_1)} \sqrt{I(\mathbf{r}_2)}}, \tag{1.10}$$

where

$$I(\mathbf{r}) = \Gamma(\mathbf{r}, \mathbf{r}; 0), \tag{1.11}$$

is the averaged intensity at position r. The magnitude of the degree of coherence can be shown to be limited as $0 \leq |\gamma(\mathbf{r}_1, \mathbf{r}_2; \tau)| \leq 1$.

It is implied by the generalized Wiener-Khintchine theorem, Eq. (1.7), that the cross-spectral density function of the time-harmonic field $V(\mathbf{r}; t) = U(\mathbf{r}; \omega)e^{-i\omega t}$, with $U(\mathbf{r}; \omega)$ being its space-dependent part, is just the Fourier transform of the mutual coherence function, i.e.

$$W(\mathbf{r}_1, \mathbf{r}_2; \omega) = \frac{1}{2\pi} \int_{-\infty}^{\infty} \Gamma(\mathbf{r}_1, \mathbf{r}_2; \tau) e^{i\omega\tau} d\tau. \tag{1.12}$$

It is also proven ([5], Ch.4) that the cross-spectral density of a statistically stationary fluctuating field can be expressed as a cross-correlation function of an ensemble $U(\mathbf{r}; \omega)$ of space-frequency realizations

$$W(\mathbf{r}_1, \mathbf{r}_2; \omega) = \langle U^*(\mathbf{r}_1; \omega) U(\mathbf{r}_2; \omega) \rangle, \tag{1.13}$$

where the angular brackets now represent the average taken over an ensemble of space-frequency realizations. The normalization of the cross-spectral density function

$$\mu(\mathbf{r}_1, \mathbf{r}_2; \omega) = \frac{W(\mathbf{r}_1, \mathbf{r}_2; \omega)}{\sqrt{S(\mathbf{r}_1; \omega)}\sqrt{S(\mathbf{r}_2; \omega)}}, \tag{1.14}$$

is called the spectral degree of coherence and has a certain similarity with $\gamma(\mathbf{r}_1, \mathbf{r}_2; \tau)$. Here

$$S(\mathbf{r}; \omega) = W(\mathbf{r}, \mathbf{r}; \omega) = \langle |U(\mathbf{r}; \omega)|^2 \rangle, \tag{1.15}$$

is the spectral density of the field, the average of the squared modulus of the Fourier frequency components of the fluctuating field $V(\mathbf{r}; t)$.

So far we have described coherence theory in the scalar domain. In order to

explore the polarization properties of light fields one needs to expand the scalar formulation into vectorial situation. The basic quantity of the electromagnetic theory of stochastic, statistically stationary beams is the so-called electric cross-spectral density matrix $[W_{ij}(\mathbf{r}_1, \mathbf{r}_2; \omega)]$ defined as

$$\overleftrightarrow{W}(\mathbf{r}_1, \mathbf{r}_2; \omega) = [W_{ij}(\mathbf{r}_1, \mathbf{r}_2; \omega)] = \begin{pmatrix} W_{xx}(\mathbf{r}_1, \mathbf{r}_2; \omega) & W_{xy}(\mathbf{r}_1, \mathbf{r}_2; \omega) \\ W_{yx}(\mathbf{r}_1, \mathbf{r}_2; \omega) & W_{yy}(\mathbf{r}_1, \mathbf{r}_2; \omega) \end{pmatrix}, \tag{1.16}$$

where $i = x, y,\ j = x, y$. The matrix with elements $W_{ij}(\mathbf{r}_1, \mathbf{r}_2; \omega)$ is a function of two spatial arguments capable of elucidating the coherence features, moreover the components of the matrix can determine the polarization features of the fluctuating electromagnetic beam. In terms of the electric field we can express the cross-spectral density matrix as

$$\overleftrightarrow{W}(\mathbf{r}_1, \mathbf{r}_2; \omega) = \begin{pmatrix} \langle E_x^*(\mathbf{r}_1; \omega) E_x(\mathbf{r}_2; \omega) \rangle & \langle E_x^*(\mathbf{r}_1; \omega) E_y(\mathbf{r}_2; \omega) \rangle \\ \langle E_y^*(\mathbf{r}_1; \omega) E_x(\mathbf{r}_2; \omega) \rangle & \langle E_y^*(\mathbf{r}_1; \omega) E_y(\mathbf{r}_2; \omega) \rangle \end{pmatrix}, \tag{1.17}$$

where $E_x(\mathbf{r}; \omega)$ and $E_y(\mathbf{r}; \omega)$ are the mutually orthogonal components of the (complex) electric field vector, and are members of suitably constructed statistical ensembles.

The difference between the scalar and the electromagnetic degrees of coherence is that the latter takes into account both components of the electric field being defined as the normalized trace of the cross-spectral density matrix [5]:

$$\eta(\mathbf{r}_1, \mathbf{r}_2; \omega) = \frac{TrW(\mathbf{r}_1, \mathbf{r}_2; \omega)}{\sqrt{S(\mathbf{r}_1; \omega)}\sqrt{S(\mathbf{r}_2; \omega)}}, \tag{1.18}$$

the spectral density becoming the trace of the cross-spectral density matrix at a single point, i.e.

$$S(\mathbf{r};\omega) = Tr\overleftrightarrow{W}(\mathbf{r},\mathbf{r};\omega) = W_{xx}(\mathbf{r},\mathbf{r};\omega) + W_{yy}(\mathbf{r},\mathbf{r};\omega). \tag{1.19}$$

While coherence theory considers correlations of the field at two points, polarization is concerned with the correlation of two field components at a single point. For instance, the main measure for such a correlation is called the *spectral degree of polarization*, defined as

$$P(\mathbf{r};\omega) = \sqrt{1 - \frac{4\det\overleftrightarrow{W}(\mathbf{r},\mathbf{r};\omega)}{[Tr\overleftrightarrow{W}(\mathbf{r},\mathbf{r};\omega)]^2}}, \tag{1.20}$$

where *det* and *Tr* stand for the determinant and trace. We note here that the complete description of polarization properties of the field can be made via the set of four Stokes parameters [5] which are related to the cross-spectral density matrix of the beam by the formulas

$$\begin{aligned} S_0(\mathbf{r}) &= W_{xx}(\mathbf{r},\mathbf{r}) + W_{yy}(\mathbf{r},\mathbf{r}) \\ S_1(\mathbf{r}) &= W_{xx}(\mathbf{r},\mathbf{r}) - W_{yy}(\mathbf{r},\mathbf{r}) \\ S_2(\mathbf{r}) &= W_{xy}(\mathbf{r},\mathbf{r}) + W_{yx}(\mathbf{r},\mathbf{r}) \\ S_3(\mathbf{r}) &= i[W_{yx}(\mathbf{r},\mathbf{r}) - W_{yy}(\mathbf{r},\mathbf{r})]. \end{aligned} \tag{1.21}$$

From the knowledge of the Stokes parameters it is possible to evaluate the parameters of the polarization ellipse which is associated with the completely polarized portion of the beam. Three parameters are required in order to uniquely specify the polarization ellipse, for instance, the orientation angle and its minor and major semi-axes [8]

$$\theta(\mathbf{r}) = \frac{1}{2}\tan^{-1}\left[\frac{S_2(\mathbf{r})}{S_1(\mathbf{r})}\right] \tag{1.22}$$

and

$$A_{\pm}(\mathbf{r}) = \left[\frac{S_0(\mathbf{r}) \pm \sqrt{S_1^2(\mathbf{r}) + S_2^2(\mathbf{r})}}{S_3(\mathbf{r})}\right]^{1/2} \tag{1.23}$$

where the choice of $\pm$ signs correspond to values of major and minor semi-axes, respectively.

One can also construct the generalized spectral Stokes parameters [9] via the elements of cross-spectral density matrix in the following order

$$\begin{aligned} S_0(\mathbf{r}_1, \mathbf{r}_2, \omega) &= W_{xx}(\mathbf{r}_1, \mathbf{r}_2, \omega) + W_{yy}(\mathbf{r}_1, \mathbf{r}_2, \omega) \\ S_1(\mathbf{r}_1, \mathbf{r}_2, \omega) &= W_{xx}(\mathbf{r}_1, \mathbf{r}_2, \omega) - W_{yy}(\mathbf{r}_1, \mathbf{r}_2, \omega) \\ S_2(\mathbf{r}_1, \mathbf{r}_2, \omega) &= W_{xy}(\mathbf{r}_1, \mathbf{r}_2, \omega) + W_{yx}(\mathbf{r}_1, \mathbf{r}_2, \omega) \\ S_3(\mathbf{r}_1, \mathbf{r}_2, \omega) &= i[W_{yx}(\mathbf{r}_1, \mathbf{r}_2, \omega) - W_{xy}(\mathbf{r}_1, \mathbf{r}_2, \omega)], \end{aligned} \tag{1.24}$$

which makes it possible to determine both the coherence and the polarization properties of an electromagnetic beam. It is evident that the generalized Stokes parameters reduce to ordinary Stokes parameters when the two points coincide: $\mathbf{r}_1 = \mathbf{r}_2 = \mathbf{r}$.

The most tractable and illustrative model for electromagnetic random sources and fields is the electromagnetic Gaussian Schell-model (EGSM) [10] (see Fig. 1.1 for illustration). It is used in the majority of analytic and numerical calculations relating to the stochastic electromagnetic beams. Generally, the components of the cross-spectral density matrix of the EGSM beam in the plane of the source have the form

$$W_{ij}(\boldsymbol{\rho}_1', \boldsymbol{\rho}_2'; \omega) = [S_i(\boldsymbol{\rho}_1'; \omega)]^{\frac{1}{2}} [S_j(\boldsymbol{\rho}_2'; \omega)]^{\frac{1}{2}} \mu_{ij}(\boldsymbol{\rho}_1', \boldsymbol{\rho}_2'; \omega), \tag{1.25}$$

where $\boldsymbol{\rho}'$ is the two dimensional vector in the source plane, $S_i(\boldsymbol{\rho}_1'; \omega)$ and $S_j(\boldsymbol{\rho}_2'; \omega)$ are the spectral density distributions and $\mu_{ij}(\boldsymbol{\rho}_1', \boldsymbol{\rho}_2'; \omega)$ are the spectral correlation

coefficients defined respectively by the Gaussian distributions

$$S_j(\boldsymbol{\rho}';\omega) = I_j \exp\Big[-\frac{\boldsymbol{\rho}'^2}{2\sigma^2}\Big], \tag{1.26}$$

$$\mu_{ij}(\boldsymbol{\rho}'_1,\boldsymbol{\rho}'_2;\omega) = B_{ij} \exp\Big[-\frac{|\boldsymbol{\rho}'_2-\boldsymbol{\rho}'_1|^2}{2\delta_{ij}^2}\Big]. \tag{1.27}$$

Here I_j are the squares of the amplitudes of the electric field components, σ^2 is the variance of the intensity distribution across the source, $B_{ij} = |B_{ij}|e^{i\varphi_{ij}}$ is the single point correlation coefficient, and δ_{ij}^2 are the variances of the correlations between the components of the electric field vector. All of the parameters entering this model may depend on frequency ω and have to satisfy relations derived in [11] and [12].

On substituting from Eqs. (1.26) and (1.27) into Eq. (1.25) we find the exact expression for the elements of the cross-spectral density matrix of electromagnetic Gaussian Schell-model sources:

$$W_{ij}(\boldsymbol{\rho}'_1,\boldsymbol{\rho}'_2;\omega) = (I_iI_j)^{1/2}B_{ij} \exp\Big[-\frac{\boldsymbol{\rho}'^2_1+\boldsymbol{\rho}'^2_2}{4\sigma^2}\Big] \exp\Big[-\frac{|\boldsymbol{\rho}'_2-\boldsymbol{\rho}'_1|^2}{2\delta_{ij}^2}\Big]. \tag{1.28}$$

Figure 1.1: A simulated typical transverse intensity cross-section of a Gaussian Schell-model beam

1.3 Huygens-Fresnel integral for light propagation in free space

In free space each member $V(\mathbf{r},t)$ of the ensemble of wavefields satisfies the wave equation ([5], Ch. 3.5). By using the Wiener-Khintchine theorem it was proven that the cross-spectral density satisfies two Helmholtz equations which shows that the correlation function behaves as a wave, as well [2]. As a result, these correlation functions in general change on propagation, even in free space. Further, free-space propagation of electromagnetic beams can be reduced to propagation of scalar light beams, since no coupling of the field components occur.

Suppose that the electric cross-spectral density matrix of a beam in the source plane has the form

$$\overleftrightarrow{W}^{(0)}(\boldsymbol{\rho}_1',\boldsymbol{\rho}_2';\omega)=\begin{pmatrix} W_{xx}^{(0)}(\boldsymbol{\rho}_1',\boldsymbol{\rho}_2';\omega) & W_{xy}^{(0)}(\boldsymbol{\rho}_1',\boldsymbol{\rho}_2';\omega) \\ W_{yx}^{(0)}(\boldsymbol{\rho}_1',\boldsymbol{\rho}_2';\omega) & W_{yy}^{(0)}(\boldsymbol{\rho}_1',\boldsymbol{\rho}_2';\omega) \end{pmatrix}, \tag{1.29}$$

where

$$W_{ij}^{(0)}(\boldsymbol{\rho}_1',\boldsymbol{\rho}_2';\omega)=\langle E_i^{(0)^*}(\boldsymbol{\rho}_1';\omega)E_j^{(0)}(\boldsymbol{\rho}_2';\omega)\rangle. \tag{1.30}$$

The propagation of each component of the electromagnetic field is governed by the formula

$$E_j(\mathbf{r};\omega)=\int E_j^{(0)}(\boldsymbol{\rho}';\omega)G(\boldsymbol{\rho}-\boldsymbol{\rho}',z;\omega)d^2\boldsymbol{\rho}', \tag{1.31}$$

where G denotes the Green's function for paraxial propagation from the source point $Q(\boldsymbol{\rho}')$ to the field point $P(\mathbf{r})$, $\mathbf{r}\equiv(\boldsymbol{\rho},z)$:

$$G(\boldsymbol{\rho}-\boldsymbol{\rho}',z;\omega)=\frac{-ik}{2\pi z}\exp[ik|\boldsymbol{\rho}-\boldsymbol{\rho}'|^2/2z], \tag{1.32}$$

with the wavenumber $k = \omega/c$, c being the speed of light in vacuum.

On substituting from Eq. (1.32) into Eq. (1.31) we first express the propagating field via the field in the source plane, then by substituting from Eq. (1.31) into Eq. (1.17) it can be found that the electric cross-spectral density matrix of the beam at a pair of points in a transverse plane $z > 0$ is given by the formula ([5],Ch. 9.4)

$$\overleftrightarrow{W}(\mathbf{r}_1, \mathbf{r}_2; \omega) = \int\int \overleftrightarrow{W}^{(0)}(\boldsymbol{\rho}_1', \boldsymbol{\rho}_2'; \omega) K_f(\boldsymbol{\rho}_1, \boldsymbol{\rho}_2, \boldsymbol{\rho}_1', \boldsymbol{\rho}_2', z; \omega) d^2\boldsymbol{\rho}_1' d^2\boldsymbol{\rho}_2', \tag{1.33}$$

where

$$K_f(\boldsymbol{\rho}_1, \boldsymbol{\rho}_2, \boldsymbol{\rho}_1', \boldsymbol{\rho}_2', z; \omega) = G^*(\boldsymbol{\rho}_1 - \boldsymbol{\rho}_1', z; \omega) G(\boldsymbol{\rho}_2 - \boldsymbol{\rho}_2', z; \omega). \tag{1.34}$$

Here, the subscript f stands for free space. Equation (1.33) is the general formula for propagation of beams in free space. By simply dropping the subscripts i and j one obtains the propagation of scalar fields. However, if there exists three components of the initial field then the propagation of such vector fields can not be treated component by component (see [13] and [14]).

1.4 Extended Huygens-Fresnel integral for light propagation in turbulent atmosphere

Generally, statistical properties of a partially coherent beam propagating in the turbulent atmosphere are affected by two mechanisms. One is associated with the correlation properties of the source, being called *correlation-induced*, and the second is due to the atmosphere itself, which we call the *turbulence-induced* changes. Since the combined effect of the correlation-induced and the turbulence-induced changes on the beam can be controlled to some extent by the choice of the source parameters, the theory we describe here may have applications in the problems involving sensing

of random media (the turbulent atmosphere, ocean and objects embedded in such media), in the development of more efficient schemes for imaging by laser radars and for free-space optical communication systems, and even in the turbulent models of biological media [15]-[16].

Suppose again that the light field is a beam-like, propagating from the plane $z = 0$ into the half-space $z > 0$ (close to z-axis), filled with the turbulent atmosphere. $\mathbf{r} = (\boldsymbol{\rho}, z)$ is the position vector at a point in the half-space $z > 0$, $\boldsymbol{\rho}$ denoting a two-dimensional transverse vector perpendicular to the direction of propagation of the beam. Let $E^{(0)}(\boldsymbol{\rho}', 0; \omega)$ represent the electric field vector at the point $(\boldsymbol{\rho}', 0)$ in the source plane $z = 0$. The field at any point in the half-space $z > 0$ at which the beam propagates can be expressed by the following well-known formula based on the so-called extended Huygens-Fresnel principle ([17], [18]):

$$\begin{aligned} E_j(\mathbf{r}; \omega) = &- \frac{ik}{2\pi z} \exp[ikz] \int E_j^{(0)}(\boldsymbol{\rho}'; \omega) \\ &\times \exp\Big[ik\frac{(\boldsymbol{\rho} - \boldsymbol{\rho}')^2}{2z}\Big] \exp[\psi(\boldsymbol{\rho}, \boldsymbol{\rho}', z; \omega)] d^2\rho', \end{aligned} \tag{1.35}$$

the integration extending over the source plane, ψ is a random complex phase factor which represents the effect of the turbulent atmosphere on a monochromatic spherical wave, and $j = x, y$.

If the beam is not monochromatic but is polychromatic and partially coherent then it is described by a correlation matrix (Eq. (1.16)) rather than by the field vector. The elements of the cross-spectral density matrix at two points $(\boldsymbol{\rho}_1, z)$ and $(\boldsymbol{\rho}_2, z)$ in a transverse plane $z = const > 0$ may be obtained on substituting from equation (1.35) into equation (1.17) and one then finds that

$$\begin{aligned} W_{ij}(\mathbf{r}_1, \mathbf{r}_2; \omega) = &\Big(\frac{k}{2\pi z}\Big)^2 \int\int W_{ij}^{(0)}(\boldsymbol{\rho}_1', \boldsymbol{\rho}_2'; \omega) \exp\Big[-ik\frac{(\boldsymbol{\rho}_1 - \boldsymbol{\rho}_1')^2 - (\boldsymbol{\rho}_2 - \boldsymbol{\rho}_2')^2}{2z}\Big] \\ &\times \langle \exp[\psi^*(\boldsymbol{\rho}_1, \boldsymbol{\rho}_1', z; \omega) + \psi(\boldsymbol{\rho}_2, \boldsymbol{\rho}_2', z; \omega)] \rangle d^2\rho_1' d^2\rho_2'. \end{aligned} \tag{1.36}$$

It is assumed here that the fluctuations in the light beam and of the turbulent atmosphere are mutually independent. Equation (1.36) can be written in a compact form as

$$W_{ij}(\mathbf{r}_1, \mathbf{r}_2; \omega) = \int\int W_{ij}^{(0)}(\boldsymbol{\rho}_1', \boldsymbol{\rho}_2'; \omega) K_t(\boldsymbol{\rho}_1, \boldsymbol{\rho}_2, \boldsymbol{\rho}_1', \boldsymbol{\rho}_2', z; \omega) d^2\rho_1' d^2\rho_2', \tag{1.37}$$

where

$$\begin{aligned} K_t(\boldsymbol{\rho}_1, \boldsymbol{\rho}_2, \boldsymbol{\rho}_1', \boldsymbol{\rho}_2', z; \omega) = &\Big(\frac{k}{2\pi z}\Big)^2 \exp\Big[-ik\frac{(\boldsymbol{\rho}_1 - \boldsymbol{\rho}_1')^2 - (\boldsymbol{\rho}_2 - \boldsymbol{\rho}_2')^2}{2z}\Big] \\ &\times \langle \exp[\psi^*(\boldsymbol{\rho}_1, \boldsymbol{\rho}_1', z; \omega) + \psi(\boldsymbol{\rho}_2, \boldsymbol{\rho}_2', z; \omega)]\rangle. \end{aligned} \tag{1.38}$$

Analytic formulas for the components of the matrix (1.37) can be derived only by approximating the phase structure function, given by the expression in the angular brackets in Equation (1.38). One possibility is the following form for the phase structure function [17]

$$\begin{aligned} &\langle \exp[\psi^*(\boldsymbol{\rho}_1, \boldsymbol{\rho}_1', z; \omega) + \psi(\boldsymbol{\rho}_2, \boldsymbol{\rho}_2', z; \omega)]\rangle = \\ &= \exp\left[-\frac{\pi^2 k^2 z}{3}(\mathbf{r}_1' - \mathbf{r}_2')^2 \int_0^\infty \kappa^3 \Phi_n(\kappa) d\kappa\right], \end{aligned} \tag{1.39}$$

where $\Phi_n(\kappa)$ is the one-dimensional power spectrum of atmospheric fluctuations.

1.5 Collins' diffraction integral for light propagation in optical systems

Within the last few years considerable attention has been paid to interaction of partially coherent and partially polarized beams with optical systems. This section formulates propagation of random beams through an aligned paraxial optical ABCD system.

The ABCD matrix analysis (also known as ray transfer matrix analysis) is a ray tracing technique used in the design of any optical systems, particularly lens systems. It involves the construction of a ray transfer matrix which describes the optical system; tracing of a light path through the system, and then evaluation of the beam characteristics by the Collins diffraction formula. More generally, the ABCD method is capable of analyzing any interaction between light and the system such as reflection, refraction, diffraction.

The connection between ray optics and diffraction theory was first established by Collins [19]. According to this theory, the propagation of the source field, $E_j^{(0)}(\boldsymbol{\rho}';\omega)$, is governed by the following integral

$$\begin{aligned} E(\mathbf{r};\omega) = \frac{-ik}{2\pi B(z)} \exp[ikL_0] \int\int E_j^{(0)}(\boldsymbol{\rho}';\omega) \\ \times \exp\Big[\frac{ik}{2B(z)}\Big\{A(z)(\boldsymbol{\rho}'^2) - 2(\boldsymbol{\rho}\cdot\boldsymbol{\rho}') + D(z)(\boldsymbol{\rho}^2)\Big\}\Big] d^2\rho', \end{aligned} \tag{1.40}$$

where L_0 is the axial optical distance between the two planes, and A(z), B(z), D(z) are the elements of the 2×2 ray transfer matrix of the system

$$\overleftrightarrow{T}_s(z) = \begin{pmatrix} A(z) & B(z) \\ C(z) & D(z) \end{pmatrix}. \tag{1.41}$$

For example, $A(z) = 1$, $B(z) = z$, $C(z) = 0$, $D(z) = 1$ in free space.

Propagation of the cross-spectral density matrix of random beams through a paraxial optical ABCD system, on the other hand, can be obtained by employing

Eq. (1.40) in Eq. (1.17) [19]-[20], and one obtains

$$\begin{aligned} W_{ij}(\mathbf{r}_1,\mathbf{r}_2;\omega) &= \left(\frac{k}{2\pi B(z)}\right)^2 \int\int W_{ij}(\boldsymbol{\rho}_1',\boldsymbol{\rho}_2';\omega) \\ &\times \exp\Big[\frac{ik}{2B(z)}\Big\{A(z)(\boldsymbol{\rho}_1'^2-\boldsymbol{\rho}_2'^2) - 2(\boldsymbol{\rho}_1\cdot\boldsymbol{\rho}_1' - \boldsymbol{\rho}_2\cdot\boldsymbol{\rho}_2') \\ &+ D(z)(\boldsymbol{\rho}_1^2-\boldsymbol{\rho}_2^2)\Big\}\Big] d^2\rho_1' d^2\rho_2', \end{aligned} \tag{1.42}$$

Equation (1.42) can also be written in a compact form as

$$W_{ij}(\mathbf{r}_1,\mathbf{r}_2;\omega) = \int\int W_{ij}(\boldsymbol{\rho}_1',\boldsymbol{\rho}_2';\omega) K_s(\boldsymbol{\rho}_1,\boldsymbol{\rho}_2,\boldsymbol{\rho}_1',\boldsymbol{\rho}_2',z;\omega) d^2\rho_1' d^2\rho_2', \tag{1.43}$$

where the propagation kernel $K_s(\boldsymbol{\rho}_1,\boldsymbol{\rho}_2,\boldsymbol{\rho}_1',\boldsymbol{\rho}_2',z;\omega)$ is given by the expression

$$\begin{aligned} K_s(\boldsymbol{\rho}_1,\boldsymbol{\rho}_2,\boldsymbol{\rho}_1',\boldsymbol{\rho}_2',z;\omega) &= \Big(\frac{k}{2\pi B(z)}\Big)^2 \\ \times \exp\Big[\frac{ik}{2B(z)}\Big\{A(z)(\boldsymbol{\rho}_1'^2-\boldsymbol{\rho}_2'^2) &- 2(\boldsymbol{\rho}_1\cdot\boldsymbol{\rho}_1' - \boldsymbol{\rho}_2\cdot\boldsymbol{\rho}_2') + D(z)(\boldsymbol{\rho}_1^2-\boldsymbol{\rho}_2^2)\Big\}\Big]. \end{aligned} \tag{1.44}$$

1.6 Weak potential scattering of light

Light scattering is a broad subject; in this section we will only discuss the fundamentals of one type: scattering of scalar light on a linear, isotropic, statistically stationary medium. We will formulate scattering of both deterministic and stochastic wavefields on media of both deterministic and stochastic nature. Let us first consider the scattering of an incident monochromatic wave

$$V^{(i)}(\mathbf{r},t) = U^{(i)}(\mathbf{r},\omega)e^{-i\omega t}, \tag{1.45}$$

and assume that the total field after the scattering process can be expressed in the same form

$$V^{(t)}(\mathbf{r},t) = U^{(t)}(\mathbf{r},\omega)e^{-i\omega t}. \tag{1.46}$$

The total field produced on scattering then satisfies the scalar wave equation ([21], Ch. 13)

$$\nabla^2 U^{(t)}(\mathbf{r},\omega) + k^2 n^2(\mathbf{r},\omega) U^{(t)}(\mathbf{r},\omega) = 0. \tag{1.47}$$

It is convenient to re-write this equation, extracting the scattering potential, in the form

$$\nabla^2 U^{(t)}(\mathbf{r},\omega) + k^2 U^{(t)}(\mathbf{r},\omega) = -4\pi F(\mathbf{r},\omega) U^{(t)}(\mathbf{r},\omega), \tag{1.48}$$

where the function

$$F(\mathbf{r},\omega) = \frac{1}{4\pi} k^2 [n^2(\mathbf{r},\omega) - 1], \tag{1.49}$$

is called the *scattering potential* of the medium. In this analysis, we have assumed that the physical properties of the medium are completely characterized by the refractive index $n(\mathbf{r},\omega)$.

Let us now express the total field $U^{(t)}(\mathbf{r},\omega)$ produced on scattering as the sum of the incident field $U^{(i)}(\mathbf{r},\omega)$ and the scattered filed $U^{(s)}(\mathbf{r},\omega)$:

$$U^{(t)}(\mathbf{r},\omega) = U^{(i)}(\mathbf{r},\omega) + U^{(s)}(\mathbf{r},\omega). \tag{1.50}$$

The second term on the right hand side of Eq. (1.50) can be regarded as the definition of the scattered field. The incident field is usually a plane wave which satisfies the Helmholtz equation throughout all space

$$(\nabla^2 + k^2) U^{(i)}(\mathbf{r},\omega) = 0. \tag{1.51}$$

It can be shown using Eqs. (1.48), (1.50), and (1.51) (see also Ch. 13.1.1 of [21])

that the total field obeys the following integral equation

$$U^{(t)}(\mathbf{r},\omega) = U^{(i)}(\mathbf{r},\omega) + \int_V F(\mathbf{r}',\omega)U^{(t)}(\mathbf{r}',\omega)G(\mathbf{r},\mathbf{r}',\omega)d^3r', \tag{1.52}$$

where $\mathbf{r}'$ is a point within the scatterer, and $G(\mathbf{r},\mathbf{r}',\omega)$ is the outgoing free-space Green function of the Helmholtz operator

$$G(\mathbf{r},\mathbf{r}',\omega) = \frac{e^{ik|\mathbf{r}-\mathbf{r}'|}}{|\mathbf{r}-\mathbf{r}'|}. \tag{1.53}$$

In order to solve Eq. (1.52) we will now reduce the problem to the weak scattering condition. Scattering is called weak if there is a slight variation in the refractive index of the scatterer from unity ($n \approx 1$). Weak scattering condition is also known as the "first-order Born approximation" and assumes that

$$|U^{(s)}(\mathbf{r}',\omega)| \ll |U^{(i)}(\mathbf{r}',\omega)|, \tag{1.54}$$

throughout the scatterer. Reference [22] provides more information on the validity regime of the first-order Born approximation. Within the validity of first-order Born approximation, the integral equation (1.52) then becomes

$$U^{(t)}(\mathbf{r},\omega) \approx U^{(i)}(\mathbf{r},\omega) + \int_V F(\mathbf{r}',\omega)U^{(i)}(\mathbf{r}',\omega)G(\mathbf{r},\mathbf{r}',\omega)d^3r'. \tag{1.55}$$

If we take into account Eq. (1.50), and express the second term in Eq. (1.55) as the scattered field, then we arrive at the formula

$$U^{(s)}(\mathbf{r},\omega) \approx \int_V F(\mathbf{r}',\omega)U^{(i)}(\mathbf{r}',\omega)G(\mathbf{r},\mathbf{r}',\omega)d^3r'. \tag{1.56}$$

We will now generalize the above theory to partially coherent waves and illustrate

it via polychromatic plane waves. Here, we assume, as always, that the fluctuations in light are statistically stationary, at least in the wide sense. The cross-spectral density of the incident light may be expressed as

$$W^{(i)}(\mathbf{r}_1, \mathbf{r}_2, \omega) = \langle U^{(i)^*}(\mathbf{r}_1, \omega) U^{(i)}(\mathbf{r}_2, \omega) \rangle, \tag{1.57}$$

where the angular brackets denote the average over a statistical ensemble of monochromatic realizations. The total field, $U^{(t)}(\mathbf{r}, t)$, may likewise be expressed via monochromatic realizations, and its cross-spectral density function may be represented as

$$W^{(t)}(\mathbf{r}_1, \mathbf{r}_2, \omega) = \langle U^{(t)^*}(\mathbf{r}_1, \omega) U^{(t)}(\mathbf{r}_2, \omega) \rangle. \tag{1.58}$$

Consider now the total field which was expressed as the incident field plus the scattered field. When we substitute from Eq. (1.50) into Eq. (1.58) we obtain the formula

$$W^{(t)}(\mathbf{r}_1, \mathbf{r}_2, \omega) = W^{(i)}(\mathbf{r}_1, \mathbf{r}_2, \omega) + W^{(is)}(\mathbf{r}_1, \mathbf{r}_2, \omega) + W^{(si)}(\mathbf{r}_1, \mathbf{r}_2, \omega) + W^{(s)}(\mathbf{r}_1, \mathbf{r}_2, \omega), \tag{1.59}$$

where the scattered cross-spectral density is

$$W^{(s)}(\mathbf{r}_1, \mathbf{r}_2, \omega) = \langle U^{(s)^*}(\mathbf{r}_1, \omega) U^{(s)}(\mathbf{r}_2, \omega) \rangle, \tag{1.60}$$

while the cross-spectral density of the cross-terms are

$$W^{(is)}(\mathbf{r}_1, \mathbf{r}_2, \omega) = \langle U^{(i)^*}(\mathbf{r}_1, \omega) U^{(s)}(\mathbf{r}_2, \omega) \rangle, \tag{1.61}$$

and

$$W^{(si)}(\mathbf{r}_1, \mathbf{r}_2, \omega) = W^{(is)^*}(\mathbf{r}_1, \mathbf{r}_2, \omega) = \langle U^{(s)^*}(\mathbf{r}_1, \omega) U^{(i)}(\mathbf{r}_2, \omega) \rangle. \tag{1.62}$$

Let us now simplify the analysis by only considering the scattered part. On substitution from Eq. (1.56) into Eq. (1.60) we find that the scattered cross-spectral density is given by the formula

$$W^{(s)}(\mathbf{r}_1,\mathbf{r}_2,\omega)=\int\limits_V\int\limits_V W^{(i)}(\mathbf{r}_1',\mathbf{r}_2',\omega)F^*(\mathbf{r}_1',\omega)F(\mathbf{r}_2',\omega) \times G^*(\mathbf{r}_1,\mathbf{r}_1',\omega)G(\mathbf{r}_2,\mathbf{r}_2',\omega)d^3r_1'd^3r_2', \tag{1.63}$$

being valid for scattering of arbitrary random fields from deterministic media. For scattering from random media we first define the *correlation function of the scattering potential* by the equation

$$C_F(\mathbf{r}_1',\mathbf{r}_2',\omega)=\langle F^*(\mathbf{r}_1',\omega)F(\mathbf{r}_2',\omega)\rangle, \tag{1.64}$$

where angular brackets denote the average taken over an ensemble of realizations of the scattering medium, and then we obtain the cross-spectral density of the scattered field on random media as

$$W^{(s)}(\mathbf{r}_1,\mathbf{r}_2,\omega)=\int\limits_V\int\limits_V W^{(i)}(\mathbf{r}_1',\mathbf{r}_2',\omega)C_F(\mathbf{r}_1',\mathbf{r}_2',\omega) \times G^*(\mathbf{r}_1,\mathbf{r}_1',\omega)G(\mathbf{r}_2,\mathbf{r}_2',\omega)d^3r_1'd^3r_2'. \tag{1.65}$$

Note that if the medium is deterministic then the correlation function reduces to a product, i.e.

$$C_F(\mathbf{r}_1',\mathbf{r}_2',\omega)=F^*(\mathbf{r}_1',\omega)F(\mathbf{r}_2',\omega). \tag{1.66}$$

The formulas that we have reviewed in this section can be used to elucidate a wide range of phenomena occurring on scattering of light of any state of coherence, on a deterministic or on a random media.

Chapter 2

Light Beams in Free Space and Systems

2.1 Motivation

As is well known controllable propagation and modulation of light beams have extensive uses in many practical areas of optics. For example, polarization and coherence properties of beams can be used in free space communication systems, for increasing their capacity, for improving the sensitivity in medical diagnostics applications and for material surface processing. Hence, in this chapter, we will examine several important topics relating to such needs.

In section 2.2, based on the unified theory of coherence and polarization and the extended Huygens-Fresnel integral, the free-space evolution of the recently introduced spectral degree of cross-polarization of a stochastic electromagnetic beam is studied. This is perhaps the only important characteristics of a random beam not previously investigated in the literature.

Planar, scalar, Schell-model and quasi-homogeneous optical light sources with correlations which are Fourier transforms of multi-Gaussian functions are introduced in section 2.3. This development leads to a very special class of beams having flat intensity profiles around optical axis for all propagation distances in the far zone of the source. The development of novel model beams, predictions on how their properties are modified on propagation and passage through systems are of profound current interest.

In section 2.4 we present the first account of interaction between stochastic light

beams and the crystalline human eye lens. The aim of this investigation is to reveal the dependence of light propagation within the eye on the statistics of its illumination.

2.2 Free-space propagation of the spectral degree of cross-polarization

In 2004, Ellis and Dogariu [23] proposed to generalize the concept of the degree of polarization to two spatial arguments and called the new quantity the mutual degree of cross-polarization (MDCP) which was meant to provide the measure of statistical similarity between the ordinary degrees of polarization at two given points. Later, Shirai and Wolf [24], on deriving the formula for intensity correlations of a stochastic electromagnetic beam whose fluctuations obey Gaussian statistics, obtained another quantity, which they called the spectral degree of cross-polarization (SDCP). It is also a function of two spatial arguments and reduces to the usual degree of polarization when the two points coincide. The SDCP has a form and meaning very similar to the MDCP but involves a different normalization factor and therefore has different bounds (while MDCP takes values from -1 to 1, the SDCP is generally unbounded). Since the SDCP is a derived quantity entering important expressions for classical fourth-order interference, while the MDCP is introduced heuristically, we will focus our attention on the former quantity.

In this section we perform qualitative and quantitative analysis of the evolution of the SDCP of a typical stochastic electromagnetic beam in free space. Numerous numerical examples illustrate the changes in this quantity for a number of chosen typical beams and propagation distances. In particular, we will separately consider the cases when the electric field components are uncorrelated and partially correlated in the source plane.

2.2.1 Theoretical background

As before, we assume that a beam is generated in the plane $z = 0$ and it propagates in free space into the positive half-space $z > 0$, close to the positive z-direction. The second-order statistical properties of such a beam at angular frequency ω may be characterized by the 2×2 cross-spectral density matrix, Eq. (1.29). On free-space (paraxial) propagation the relation between the cross-spectral density matrix in the source plane and that at points $(\boldsymbol{\rho}_1,\, z_1)$ and $(\boldsymbol{\rho}_2,\, z_2)$, $z_1, z_2 > 0$ is given by the law [2]

$$\begin{aligned} W_{ij}(\boldsymbol{\rho}_1, z_1; \boldsymbol{\rho}_2, z_2; \omega) &= \Big(\frac{k}{2\pi}\Big)^2 \frac{1}{z_1 z_2} \int\limits_{\boldsymbol{\rho}_1'} \int\limits_{\boldsymbol{\rho}_2'} W_{ij}^{(0)}(\boldsymbol{\rho}_1', \boldsymbol{\rho}_2'; \omega) \\ &\times \exp\Big[-ik\Big(\frac{(\boldsymbol{\rho}_1 - \boldsymbol{\rho}_1')^2}{2z_1} - \frac{(\boldsymbol{\rho}_2 - \boldsymbol{\rho}_2')^2}{2z_2}\Big)\Big] d^2\boldsymbol{\rho}_1' d^2\boldsymbol{\rho}_2'. \end{aligned} \tag{2.1}$$

This law is obtained by straightforward use of Eqs. (1.32)-(1.34).

We will now assume that the beam is generated by an electromagnetic Gaussian Schell-model source. On substituting from Eq. (1.28) into Eq. (2.1), after tedious integral calculation, we obtain, for the elements of the electromagnetic cross-spectral density matrix of the beam propagating in free space, the expressions

$$\begin{aligned} W_{ij}(\boldsymbol{\rho}_1, z_1; \boldsymbol{\rho}_2, z_2; \omega) &= \frac{B_{ij}\sqrt{I_i}\sqrt{I_j}}{\triangle_{ij}^2(z_1, z_2)} \\ &\times \exp\Big[-\frac{1}{8\sigma^2} + i\frac{z_2 - z_1}{8k\sigma^2}\Big(\frac{1}{4\sigma^2} + \frac{1}{\delta_{ij}^2}\Big)\frac{(\boldsymbol{\rho}_1 + \boldsymbol{\rho}_2)^2}{\triangle_{ij}^2(z_1, z_2)}\Big] \\ &\times \exp\Big[-\frac{(\boldsymbol{\rho}_1 - \boldsymbol{\rho}_2)^2}{2\triangle_{ij}^2(z_1, z_2)}\frac{1}{4\sigma^2} + \frac{1}{\delta_{ij}^2}\Big] \exp\Big[-i\frac{k(\boldsymbol{\rho}_1^2 - \boldsymbol{\rho}_2^2)}{2R_{ij}(z_1, z_2)}\Big], \end{aligned} \tag{2.2}$$

where

$$\triangle_{ij}^2(z_1, z_2) = 1 + \frac{z_1 z_2}{k^2\sigma^2}\Big(\frac{1}{4\sigma^2} + \frac{1}{\delta_{ij}^2}\Big) + i\frac{z_2 - z_1}{k}\Big(\frac{1}{2\sigma^2} + \frac{1}{\delta_{ij}^2}\Big), \tag{2.3}$$

$$R_{ij}(z_1, z_2) = \sqrt{z_1 z_2}\Big[1 + \frac{k^2\sigma^2}{z_1 z_2}(\frac{1}{4\sigma^2} + \frac{1}{\delta_{ij}^2})^{-1}\Big]. \tag{2.4}$$

In particular, when in Eq. (2.2) $z_1 = z_2 = z$ we obtain the transverse cross-spectral density matrix (see also [25] where a similar expression is derived for a scalar beam)

$$\begin{aligned} W_{ij}(\boldsymbol{\rho}_1, z; \boldsymbol{\rho}_2, z; \omega) &= \frac{B_{ij}\sqrt{I_i}\sqrt{I_j}}{\triangle_{ij}^2(z)} \exp\Big[-\frac{(\boldsymbol{\rho}_1 + \boldsymbol{\rho}_2)^2}{8\sigma^2\triangle_{ij}^2(z)}\Big] \\ &\times \exp\Big[-\frac{(\boldsymbol{\rho}_1 - \boldsymbol{\rho}_2)^2}{2\triangle_{ij}^2(z)}\frac{1}{4\sigma^2} + \frac{1}{\delta_{ij}^2}\Big] \exp\Big[-i\frac{k(\boldsymbol{\rho}_1^2 - \boldsymbol{\rho}_2^2)}{2R_{ij}(z)}\Big], \end{aligned} \tag{2.5}$$

where

$$\triangle_{ij}^2(z) = 1 + \frac{z^2}{k^2\sigma^2}\Big(\frac{1}{4\sigma^2} + \frac{1}{\delta_{ij}^2}\Big), \tag{2.6}$$

$$R_{ij}(z) = z\Big[1 + \frac{k^2\sigma^2}{z^2}\Big(\frac{1}{4\sigma^2} + \frac{1}{\delta_{ij}^2}\Big)^{-1}\Big]. \tag{2.7}$$

These expressions also agree with those given in [10].

In the other special case, when in Eq. (2.2) $\boldsymbol{\rho}_1 = \boldsymbol{\rho}_2 = \boldsymbol{\rho}$, we obtain the longitudinal cross-spectral density matrix

$$\begin{aligned} W_{ij}(\boldsymbol{\rho}, z_1; \boldsymbol{\rho}, z_2; \omega) &= \frac{B_{ij}\sqrt{I_i}\sqrt{I_j}}{\triangle_{ij}^2(z_1, z_2)} \\ &\times \exp\Big[-\frac{1}{2\sigma^2} + i\frac{z_2 - z_1}{2k\sigma^2}\Big(\frac{1}{4\sigma^2} + \frac{1}{\delta_{ij}^2}\Big)\frac{\boldsymbol{\rho}^2}{\triangle_{ij}^2(z_1, z_2)}\Big], \end{aligned} \tag{2.8}$$

where $\triangle_{ij}^2(z_1, z_2)$ was given in Eq. (2.3). Note that the phase factor R_{ij} does not enter the formula in this case.

The spectral degree of cross-polarization of a stochastic electromagnetic beam-like field at two spatial positions ($\boldsymbol{\rho}_1$, z_1) and ($\boldsymbol{\rho}_2$, z_2), at frequency ω, was introduced in

[24] by means of the formula

$$P(\boldsymbol{\rho}_1, z_1; \boldsymbol{\rho}_2, z_2; \omega) = \sqrt{1 - \frac{4 \det \overleftrightarrow{W}(\boldsymbol{\rho}_1, z_1; \boldsymbol{\rho}_2, z_2; \omega)}{[Tr \overleftrightarrow{W}(\boldsymbol{\rho}_1, z_1; \boldsymbol{\rho}_2, z_2; \omega)]^2}}. \tag{2.9}$$

Combination of formulae (2.1) and (2.9) can now be used for evaluation of the SDCP at any two positions within the beam.

2.2.2 Uncorrelated electric field components

We will first discuss the cross-polarization changes in the case when the two components of the electric field are uncorrelated and hence the cross-spectral density matrix has no off-diagonal components. We recall that in this case the ordinary degree of polarization usually exhibits drastic changes on propagation in free space as compared to those for beams with partially correlated field components.

In figure 2.1 we show the contours of the degree of cross-polarization $P(\boldsymbol{\rho}_1 = 0, z_1 = 1m; \boldsymbol{\rho}_2 = \boldsymbol{\rho}, z_2 = z)$ of the EGSM beam propagating in free space for several different values of source correlation coefficients δ_{yy}, while δ_{xx} is chosen to be 0.5 mm, with $I_x = 3I_y$. Such contour plots allow illustration of both transverse and longitudinal components of the SDCP at the same time. When the correlation coefficients δ_{yy} and δ_{xx} coincide (figure 2.1(b)) the beam is scalar-like and the contour becomes degenerate. When the correlation coefficients δ_{yy} and δ_{xx} approach the rms width of the beam σ, the changes in the SDCP become significant only with a slight change in δ_{xx} (compare figures 2.1(c) and (d)).

In order to illustrate how the initial parameters of the EGSM beam affect its degree of cross-polarization $P(\boldsymbol{\rho}_1 = 0, z_1 = 1m; \boldsymbol{\rho}_2 = \boldsymbol{\rho}, z_2 = z)$ on propagation in free space more explicitly, the SDCP curves at different planes $z = const.$ are given in figures 2.2 and 2.3. In particular, one can see from figure 2.2 how the changes in the

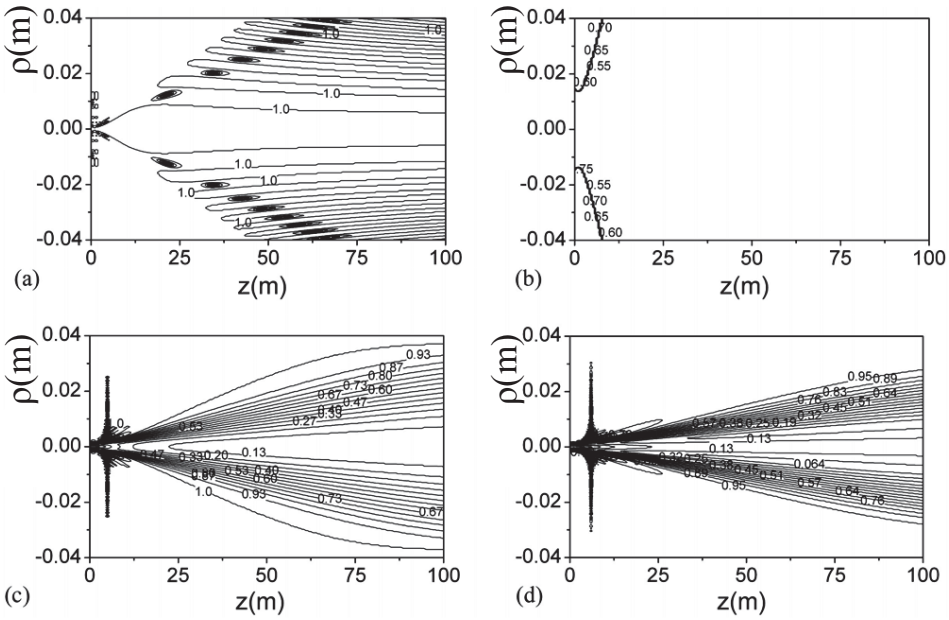

Figure 2.1: The contour of the degree of cross-polarization $p(\boldsymbol{\rho}_1 = 0, z_1 = 1m; \boldsymbol{\rho}_2 = \boldsymbol{\rho}, z_2 = z; \omega)$ of the EGSM beam propagating in free space. a) $\delta_{yy} = 0.1$ mm, b) $\delta_{yy} = 0.5$ mm, c) $\delta_{yy} = 0.8$ mm, d) $\delta_{yy} = 1$ mm. The values of the parameters of the beams are: $\lambda = 632.8$ mm, $\delta_{xx} = 0.5$ mm, $I_x = 3I_y$, $\sigma = 5$ mm.

SDCP depend on the initial ordinary degree of polarization, which in this case simply depends on the ratio of intensities of the two components of the beam:

$$P(\boldsymbol{\rho}) = \frac{I_x(\boldsymbol{\rho})/I_y(\boldsymbol{\rho}) - 1}{I_x(\boldsymbol{\rho})/I_y(\boldsymbol{\rho}) + 1}. \tag{2.10}$$

For the four ratios $I_x(\boldsymbol{\rho})/I_y(\boldsymbol{\rho})$ of our choice: 1, 5/3, 3 and 19 the degree of polarization takes values 0 (unpolarized beam), 1/4, 1/2 and 9/10 (almost polarized beam). We note that even though in the plane $z = 1$, where the transverse SDCP is smaller than 1 for all values of $\boldsymbol{\rho}$ (see figure 2.2(a)), in other planes it is no longer just confined to the interval between 0 and 1, and will be generally larger than 1 (see figures 2.2(b) and (c)). It is also seen from figure 2.2 that both the degree of polarization of the source and the propagation distance affect the degree of cross-polarization.

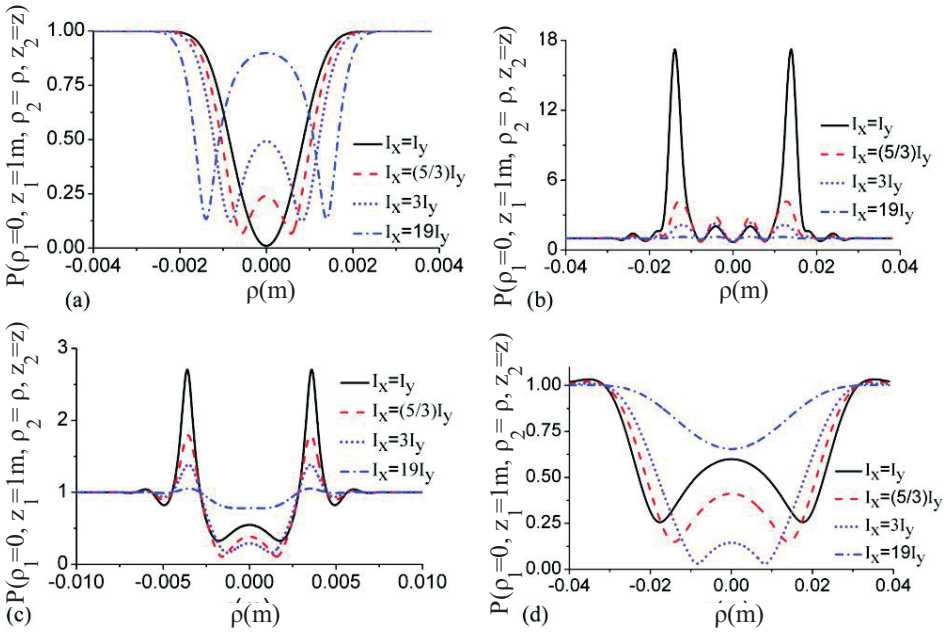

Figure 2.2: The degree of cross-polarization of the EGSM beam propagating in free space for different values of the initial degree of polarization: a) $z = 1$ m, b) $z = 6$ m, c) $z = 10$ m, d) $z = 100$ m. The other calculation parameters are: $\delta_{xx} = 0.5$ mm, $\delta_{yy} = 1$ mm, $\sigma = 5$ cm.

The influence of the source correlation coefficients and the propagation distance on the degree of cross-polarization is shown in figure 2.3. In particular, in the general case, when the correlation coefficients are the same (dashed curves) the SDCP remains constant for almost the whole range of $\boldsymbol{\rho}$ (in figure 2.3(b) variation in SDCP for large values of $\boldsymbol{\rho}$ is due to violation of non-paraxial regime). We also note that in cases when both correlation coefficients δ_{yy} and δ_{xx} are small compared to the rms width of the beam σ, it is clearly seen that the changes in the SDCP not only propagate with distance z from the source but also spread with radial distance $\boldsymbol{\rho}$ from the axis of the beam (compare the solid curves in all four figures of 2.3(a)(d)).

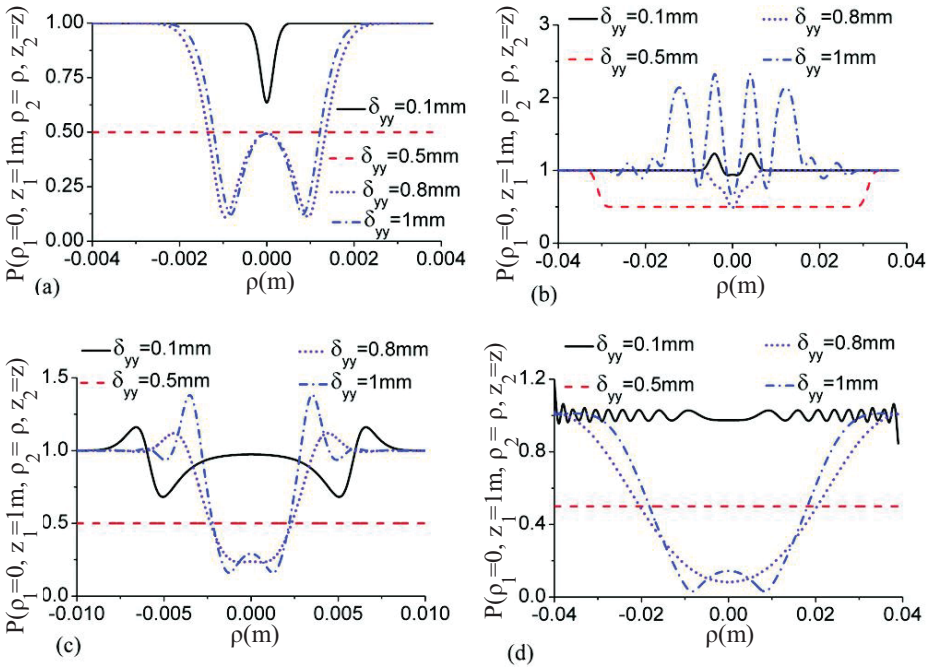

Figure 2.3: The degree of cross-polarization of the EGSM beam propagating in free space for different values of δ_{yy}: a) $z = 1$ m, b) $z = 6$ m, c) $z = 10$ m, d) $z = 100$ m. The other calculation parameters are: $\delta_{xx} = 0.5$ mm, $I_x = 3I_y$, $\sigma = 5$ cm.

2.2.3 Correlated electric field components

Figures 2.4-2.6 illustrate the behavior of the SDCP in the more general case than discussed in section 2.2.2, namely when the two transverse components of the electric field are partially correlated. In this situation the cross-spectral matrix has non-zero off-diagonal elements. Since the dependence of the SDCP on initial intensities and correlation coefficients was explored in detail in section 2.2.2, here we will primarily focus our attention on the dependence of the SDCP on the coefficient B_{xy}. In the EGSM beam, this coefficient alone provides the measure of correlation of the x and y components of the electric field in the source plane. Moreover, if in the source plane $I_x = I_y$, then B_{xy} solely determines the degree of polarization of the source:

$$P(\boldsymbol{\rho}) = B_{xy}. \tag{2.11}$$

In figures 2.4-2.6, four values of B_{xy} (or, equivalently, $P(\boldsymbol{\rho})$) were chosen: 0, 0.1, 0.2 and 0.3. Higher values of B_{xy} cannot be applied due to some intrinsic constraints on the choice of parameters of the EGSM sources [12]. Also we will only consider in this section the purely transverse or purely longitudinal SDCP, since the general SDCP was discussed in detail above, and usually polarization properties in transverse planes or at a fixed radial position but different distances from the source plane are of most interest.

Figure 2.4 shows the spatial distribution of the transverse SDCP for four aforementioned values of the coefficient B_{xy}. One can see that the change in B_{xy} results in the change in the SDCP especially in the central part of the beam. The same as for the ordinary degree of polarization, in this case of correlated field components, the changes in the SDCP are not as dramatic as for that of the beam with uncorrelated field components.

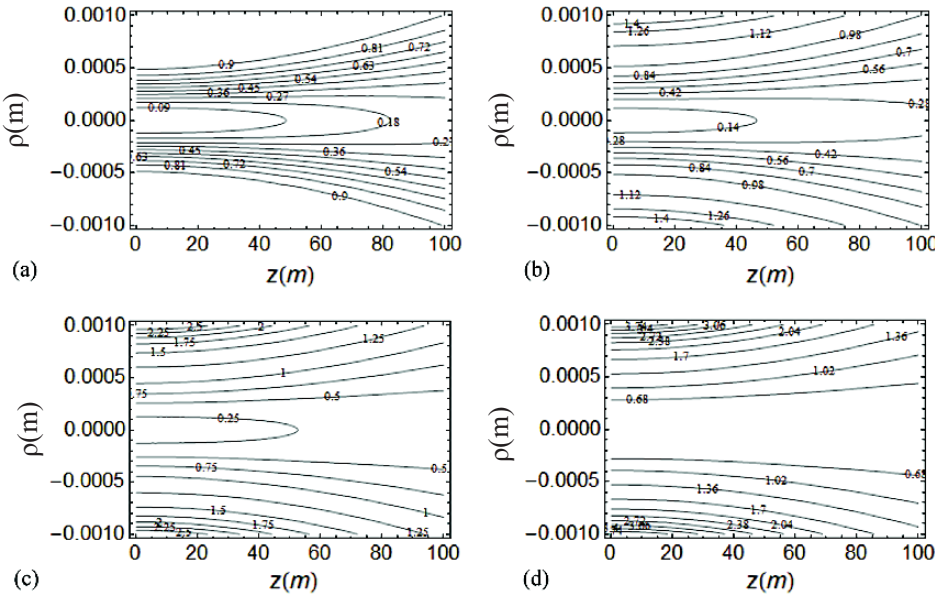

Figure 2.4: Contours of the transverse SDCP $p(\boldsymbol{\rho}_1 = 0, \boldsymbol{\rho}_2 = \boldsymbol{\rho}, z_1 = z_2 = z; \omega)$ of the EGSM beam propagating in free space. a) $B_{xy} = 0$, b) $B_{xy} = 0.1$, c) $B_{xy} = 0.2$, d) $B_{xy} = 0.3$. The values of the parameters of the beams are: $\delta_{xx} = 0.15$ mm, $\delta_{yy} = 0.225$ mm, $\delta_{xy} = \delta_{yx} = 0.25$ mm, $I_x = I_y$,$\sigma = 5$ cm.

Figure 2.5 illustrates the dependence of the transverse SDCP calculated for a pair of points in the fixed plane z on the radial distance $\mathbf{r}$. We see that with the increasing propagation distance the SDCP becomes more uniform across the transverse cross-section, saturating at certain non-zero values, depending on the coefficient B_{xy}. This result is in striking contrast with the behavior of the spectral degree of coherence which always tends to 1 at sufficiently large distances on free-space propagation.

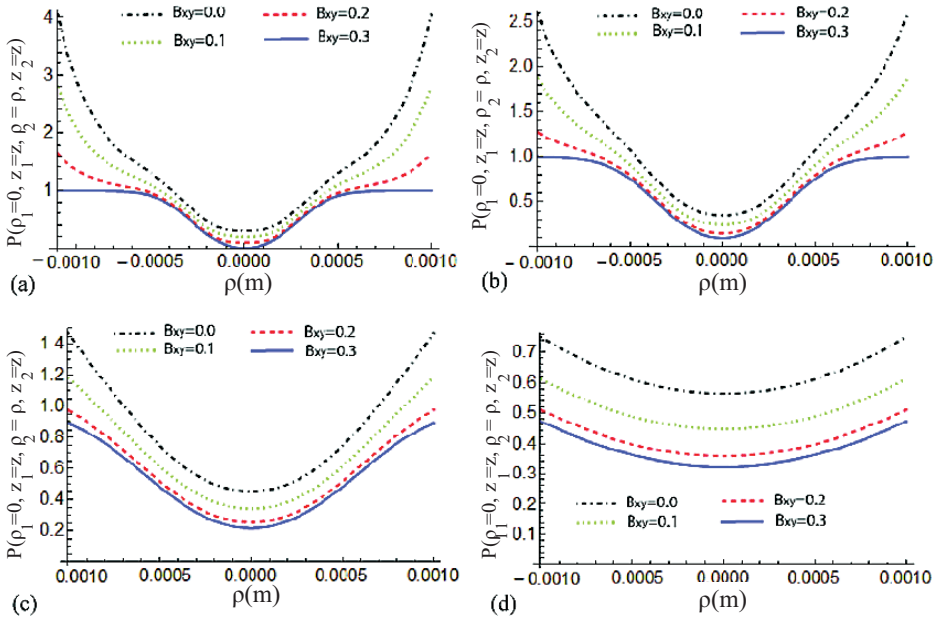

Figure 2.5: The transverse degree of cross-polarization of the EGSM beam propagating in free space for different values of B_{xy}: a) $z = 1$ m, b) $z = 50$ m, c) $z = 100$ m, d) $z = 200$ m. The other parameters are the same as in figure 2.4.

Figure 2.6 illustrates the dependence of the longitudinal SDCP at a pair of points on the axis of the beam at four values of distance z_1 from the source while distance z_2 varies, for several chosen values of coefficient B_{xy}. We note that the change is pronounced only for relatively small separation distances $|z_1 - z_2|$; for larger separations the SDCP saturates at certain fixed values, not necessarily 0. It is also seen that the longitudinal SDCP changes its shape with distance z_1. Parameter B_{xy}, on the other

hand, influences the magnitude rather than the shape of the SDCP.

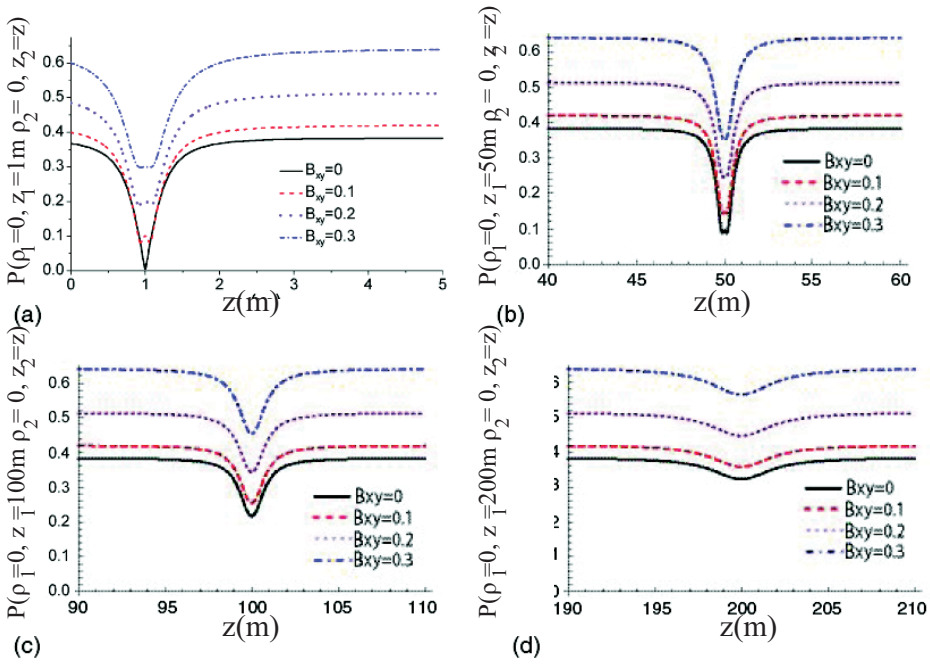

Figure 2.6: The longitudinal SDCP of the EGSM beam propagating in free space for different values of B_{xy}: a) $z = 1$ m, b) $z = 50$ m, c) $z = 100$ m, d) $z = 200$ m. The other parameters are the same as in figure 2.4.

2.3 Light sources generating far fields with tunable flat profiles

It is well-known in statistical optics that the structure of the correlation function of a field in the source plane is closely related to the intensity distribution of its far field ([2], p. 236). Moreover, for some model sources it is possible to obtain analytic relations between these two quantities. For instance, for quasi-homogeneous sources the so-called reciprocity relations are known to be of Fourier type ([2], p. 243). For model sources of the Schell type [26], on the other hand, it is possible to obtain formulas for the major statistical characteristics of the field propagating

to any distance from the source and to analyze how source correlations gradually affect the field ([2], p. 276). Surprisingly few analytical models for the planar source correlation functions have been developed so far: the Gaussian Schell-model (GSM) sources, the J_n-Bessel correlated sources [27], the I_n-Bessel-correlated sources [28], the non-uniform GSM sources [29] and the Lambertian sources ([2], p. 248) might constitute the full list of models. The difficulty in developing new models stems from the fact that a genuine correlation function must satisfy a number of restrictions ([2], Sec. 4.7.1). To alleviate this task a sufficient condition in a simple integral form for the genuine correlation function was derived in [30] and has already led to a model in [29]. We will use such a condition to introduce yet another, and very special, model source and beam.

2.3.1 The model for the source

In this section we introduce a model for the *correlation function* of a planar source which is based on the multi-Gaussian family of functions. Such functions have previously been employed for modeling beam amplitudes [31] and scattering potentials [32]. Generally, multi-Gaussian functions make it possible to control the width of the flat center of the profile and the slope of its edge by the choice of two parameters. But being employed for modeling the correlation, rather than for the field itself, the multi-Gaussian function can serve as a unique tool for generating far fields with flat intensity profiles.

Let us set the spectral degree of coherence $\mu(\boldsymbol{\rho}_1, \boldsymbol{\rho}_2; \omega)$, at a pair of points in the source plane with position vectors $\boldsymbol{\rho}_1$ and $\boldsymbol{\rho}_2$ and frequency ω in the following form

$$\mu(\boldsymbol{\rho}_1, \boldsymbol{\rho}_2; \omega) = \frac{1}{C_0} \sum_{m=1}^{M} \binom{M}{m} \frac{(-1)^{m-1}}{m} \exp\left[-\frac{|\boldsymbol{\rho}_2 - \boldsymbol{\rho}_1|^2}{2m\delta^2}\right], \tag{2.12}$$

where $C_0 = \sum_{m=1}^{M} \frac{(-1)^{m-1}}{m}\binom{M}{m}$ is the normalization factor, $\binom{M}{m}$ stand for binomial coefficients and δ is a correlation width. As is illustrated in Fig. 2.7, the profile function defined by Eq. (2.12) visually resembles a Bessel-correlated source or a Lambertian source (see [2], Figs. 5.9 and 5.10), however is given by a different functional form. As in the case of a Bessel function whose Taylor's expansion is a sum of sign-alternating terms, the modified multi-Gaussian function is also represented by a sum of positive and negative exponentials.

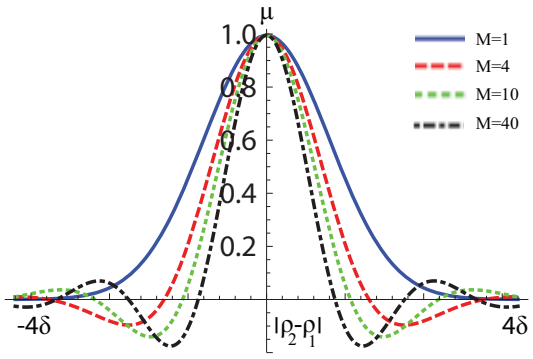

Figure 2.7: Illustration of the degree of coherence for several values of M.

As is evident from Refs. [2] and [30] not any degree of coherence defines a physically meaningful random source. For instance, for a Schell-model source, for which the cross-spectral density function has the form

$$W^{(0)}(\boldsymbol{\rho}_1, \boldsymbol{\rho}_2; \omega) = \sqrt{S(\boldsymbol{\rho}_1; \omega)}\sqrt{S(\boldsymbol{\rho}_2; \omega)}\mu(\boldsymbol{\rho}_2 - \boldsymbol{\rho}_1; \omega), \tag{2.13}$$

$S(\boldsymbol{\rho})$ being the spectral density at $\boldsymbol{\rho}$, the sufficient condition for the cross-spectral density to be genuine is that it must be expressed by the integral

$$W^{(0)}(\boldsymbol{\rho}_1, \boldsymbol{\rho}_2; \omega) = \int p(\boldsymbol{v}; \omega) H^*(\boldsymbol{\rho}_1, \boldsymbol{v}; \omega) H(\boldsymbol{\rho}_2, \boldsymbol{v}; \omega) d^2\boldsymbol{v}, \tag{2.14}$$

where $H(\boldsymbol{\rho}, \boldsymbol{v})$ is an arbitrary kernel and $p(\boldsymbol{v})$ is a nonnegative, Fourier-transformable function. Following [30] we assume that function $H(\boldsymbol{\rho}, \boldsymbol{v})$ has the form

$$H(\boldsymbol{\rho}, \boldsymbol{v}; \omega) = \tau(\boldsymbol{\rho}; \omega) \exp[-i\boldsymbol{v} \cdot \boldsymbol{\rho}], \tag{2.15}$$

and hence $W^{(0)}$ becomes

$$W^{(0)}(\boldsymbol{\rho}_1, \boldsymbol{\rho}_2; \omega) = \tau^*(\boldsymbol{\rho}_1; \omega)\tau(\boldsymbol{\rho}_2; \omega)\widetilde{p}(\boldsymbol{\rho}_1 - \boldsymbol{\rho}_2; \omega), \tag{2.16}$$

where $\tau(\boldsymbol{\rho}; \omega)$ is a (possibly complex) profile function, tilde denotes the Fourier transform.

The choice of $p(\boldsymbol{v})$ defines a family of sources with different correlation functions. On taking the Fourier transform of Eq. (2.12) we arrive at:

$$p(\boldsymbol{v}; \omega) = \frac{\delta^2}{C_0} \sum_{m=1}^{M} \frac{(-1)^{m-1}}{M} \binom{M}{m} \exp\left[-\frac{m\delta^2|\boldsymbol{v}|^2}{2}\right], \tag{2.17}$$

representing a family of flat-top profiles (see Fig. 2.8). While it is a Fourier-transformable function by construction, its non-negativity can be proved as follows. Equation (2.17) can be represented as

$$p(\boldsymbol{v}; \omega) = -\frac{\delta^2}{C_0} \sum_{m=1}^{M} \binom{M}{m} (-x)^m = \frac{\delta^2}{C_0}[1 - (1 - x)^M], \tag{2.18}$$

where $x = \exp[-\delta^2|\boldsymbol{v}|^2/2]$ Function $p(\boldsymbol{v})$ is manifestly nonnegative since $0 \leq x \leq 1$. We point out that this form of $p(\boldsymbol{v})$ is particularly simple, since it is clear that $(1-x)$ is a saturation function whose slope is controlled by index M.

Let us also set the Gaussian profile for function τ:

$$\tau(\boldsymbol{\rho}; \omega) = \exp[-|\boldsymbol{\rho}|^2/(4\sigma^2)]. \tag{2.19}$$

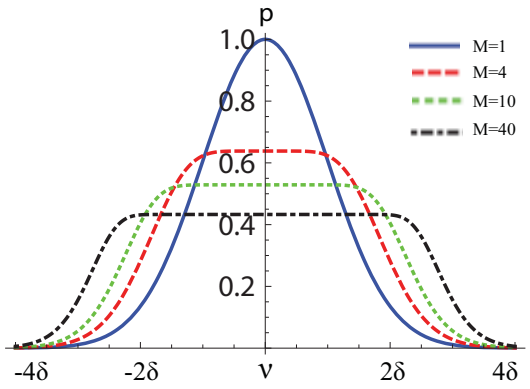

Figure 2.8: Illustration of the function p for several values of M.

Then, together with the weighting function $p(\boldsymbol{\upsilon})$ given by Eq. (2.17), we obtain on substituting them into Eq. (2.16) the cross-spectral density function of the form

$$W^{(0)}(\boldsymbol{\rho}_1, \boldsymbol{\rho}_2; \omega) = \frac{1}{C_0} \exp\left[-\frac{|\boldsymbol{\rho}_1|^2 + |\boldsymbol{\rho}_2|^2}{4\sigma^2}\right] \sum_{m=1}^{M} \frac{(-1)^{m-1}}{mM} \binom{M}{m} \exp\left[-\frac{|\boldsymbol{\rho}_2 - \boldsymbol{\rho}_1|^2}{2m\delta^2}\right], \tag{2.20}$$

which may be called multi-Gaussian Schell-model source.

We will now determine the cross-spectral density function of the field radiated by the source (2.20) to the far zone at two points specified by position vectors $\mathbf{r}_1 = r_1\mathbf{s}_1$ and $\mathbf{r}_2 = r_2\mathbf{s}_2$, with $\mathbf{s}_1^2 = \mathbf{s}_2^2 = 1$. The field in the far-zone of the source is given by the expression ([2], p. 240)

$$W^{(\infty)}(r_1\mathbf{s}_1, r_2\mathbf{s}_2; \omega) = (2\pi k)^2 \cos\theta_1 \cos\theta_2 \widetilde{W}^{(0)}(-k\mathbf{s}_{1\perp}, k\mathbf{s}_{2\perp}; \omega) \frac{\exp[ik(\mathbf{r}_2 - \mathbf{r}_1)]}{\mathbf{r}_1\mathbf{r}_2}, \tag{2.21}$$

where k is the wavenumber of the field, $\mathbf{s}_\perp$ is the projection of $\mathbf{s}$ onto the source plane, $\cos\theta = \mathbf{s}_z$, and

$$\widetilde{W}^{(0)}(\mathbf{f}_1, \mathbf{f}_2; \omega) = \frac{1}{(2\pi)^4} \int\int W^{(0)}(\boldsymbol{\rho}_1, \boldsymbol{\rho}_2; \omega) \times \exp[-i(\mathbf{f}_1 \cdot \boldsymbol{\rho}_1 + \mathbf{f}_2 \cdot \boldsymbol{\rho}_2)] d^2\boldsymbol{\rho}_1 d^2\boldsymbol{\rho}_2, \tag{2.22}$$

is the four-dimensional Fourier transform. On substituting from Eq. (2.20) first into Eq. (2.22) and then into Eq. (2.21), we obtain for the cross-spectral density $W^{(\infty)}(r_1\mathbf{s}_1, r_2\mathbf{s}_2)$ in the far field the formula

$$W^{(\infty)}(\mathbf{r}_1,\mathbf{r}_2;\omega) = \frac{1}{C_0}k^2\cos\theta_1\cos\theta_2\frac{\exp[ik(\mathbf{r}_2-\mathbf{r}_1)]}{\mathbf{r}_1\mathbf{r}_2}\sum_{m=1}^{M}\frac{(-1)^{m-1}}{mM}\binom{M}{m}\frac{1}{(a_m^2-b_m^2)}$$
$$\times\exp[-k^2(\alpha_m\mathbf{s}_{1\perp}^2+\alpha_m\mathbf{s}_{2\perp}^2-2\beta_m\mathbf{s}_{1\perp}\cdot\mathbf{s}_{2\perp})], \tag{2.23}$$

where

$$a_m = \frac{1}{2}\left(\frac{1}{2\sigma^2}+\frac{1}{m\delta^2}\right), \quad b_m = \frac{1}{2m\delta^2}, \tag{2.24}$$

$$\alpha_m = \frac{a_m}{4(a_m^2-b_m^2)}, \quad \beta_m = \frac{b_m}{4(a_m^2-b_m^2)}. \tag{2.25}$$

The far-field spectral density can be found by the formula $S^{(\infty)}(\mathbf{r};\omega) = W^{(\infty)}(\mathbf{r},\mathbf{r})$ and one obtains

$$S^{(\infty)}(\mathbf{r}) = \frac{k^2\cos^2\theta}{C_0|\mathbf{r}|^2}\sum_{m=1}^{M}\frac{(-1)^{m-1}}{mM}\binom{M}{m}\frac{\exp[-2k^2\mathbf{s}_\perp^2(\alpha_m-\beta_m)]}{(a_m^2-b_m^2)}. \tag{2.26}$$

In order for function $W^{(0)}(\boldsymbol{\rho}_1,\boldsymbol{\rho}_2)$ to generate a beam, the spectral density in Eq. (2.26) must be negligible except for directions within a narrow solid angle about the z-axis. This is so if ([2], Eq. [5.6-72])

$$\exp[-2k^2\mathbf{s}_\perp^2\theta^2(\alpha_m-\beta_m)] \approx 0, \tag{2.27}$$

for any $m = 1, ..., M$, unless $\mathbf{s}_\perp^2 \ll 1$, implying that

$$2k^2(\alpha_m-\beta_m) \ll 1, \tag{2.28}$$

or, in terms of the source parameters,

$$\frac{1}{4\sigma^2}+\frac{1}{m}\frac{1}{\delta^2}\ll\frac{2\pi^2}{\lambda^2},\quad m=1,...,M. \tag{2.29}$$

If the inequality holds for $m=1$ the rest of the set, for $m=2,...,M$ holds automatically. Thus the beam condition for the multi-Gaussian Schell-model sources is the same as that for the Gaussian Schell-model sources ([2], Eq. 5.6-73):

$$\frac{1}{4\sigma^2}+\frac{1}{\delta^2}\ll\frac{2\pi^2}{\lambda^2}. \tag{2.30}$$

Another possible class of sources with the correlation function of the form (2.12) can be introduced with the help of a quasi-homogeneous approximation. Namely, the cross-spectral density of such a source is of the form

$$\begin{aligned} W^{(0)}(\boldsymbol{\rho}_1,\boldsymbol{\rho}_2;\omega) &\approx \mathcal{S}\left(\frac{\boldsymbol{\rho}_1+\boldsymbol{\rho}_2}{2}\right)\mu(\boldsymbol{\rho}_1-\boldsymbol{\rho}_2;\omega)\\ &\approx \mathcal{S}\left(\frac{\boldsymbol{\rho}_1+\boldsymbol{\rho}_2}{2}\right)\widetilde{p}(\boldsymbol{\rho}_1-\boldsymbol{\rho}_2;\omega), \end{aligned} \tag{2.31}$$

under the assumption that function $\mathcal{S}$ is a slow function of its argument compared to μ. For this type of fields the far-field spectral density is given by ([2], p. 243)

$$S^{(\infty)}(\mathbf{r};\omega)=\frac{1}{|\mathbf{r}|^2}(2\pi k)^2\cos^2\theta\widetilde{F}(0)\widetilde{\mu}(k\mathbf{s}_\perp). \tag{2.32}$$

We also note that since the multi-Gaussian Schell-model and multi-Gaussian quasi-homogeneous sources have the same correlation function of type (1) their far fields are qualitatively similar for $M>1$, especially if $\delta\ll\sigma$.

Figure 2.9 shows several typical far fields radiated by the source in (2.20) with the following parameters: $\lambda=632$ nm, $\sigma=1$ mm, $\delta=0.1$ mm. It is clearly seen that a

beam with a Gaussian degree of coherence in the source plane monotonically decreases with the increase of angle θ, while beams with multi-Gaussian source correlations have flat profiles with different heights and steepness of the edges.

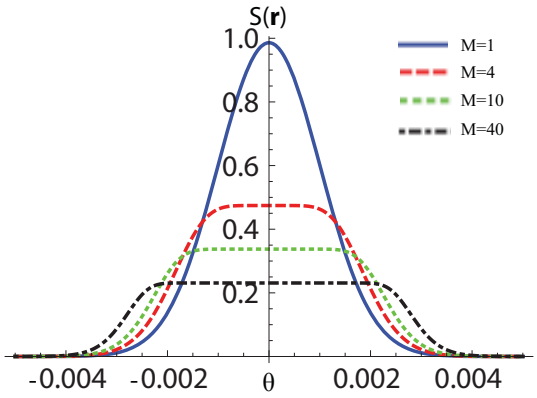

Figure 2.9: Far-field spectral density of the field generated by the multi-Gaussian Schell-model source vs. θ(degrees) for several values of M.

2.3.2 The analysis of beam evolution

In this section we explore the behavior of beam-like fields produced by multi-Gaussian Schell-model sources on propagation to different zones from the source in free space.

More specifically, we will examine the behavior of both the spectral density and the degree of coherence for such beams at any intermediate distance from the source. The paraxial free-space propagation law for the cross-spectral density function of a field to points $\mathbf{r}_1$ and $\mathbf{r}_2$ of the half-space $z > 0$ has the form of equation (1.33).

We first point out that for a classic scalar GSM beam, which corresponds to the case $M = 1$, the cross-spectral density matrix of the beam at distance z has been

shown to be [2]

$$\begin{aligned} W(\mathbf{r}_1,\mathbf{r}_2;\omega) =& \frac{1}{\Delta^2(z)}\exp\left[-\frac{(\mathbf{r}_1+\mathbf{r}_2)^2}{8\sigma^2\Delta^2(z)}\right] \\ & \times \exp\left[-\frac{(\mathbf{r}_1-\mathbf{r}_2)^2}{2\alpha^2\Delta^2(z)}\right]\exp\left[-ik\frac{(\mathbf{r}_2^2-\mathbf{r}_1^2)}{2R(z)}\right], \end{aligned} \tag{2.33}$$

where

$$\begin{aligned} &\alpha^2 = \left(\frac{1}{4\sigma^2}+\frac{1}{\delta^2}\right)^{-1}, \quad \Delta^2(z) = 1+\frac{z^2}{k^2\sigma^2\alpha^2}, \\ &R(z) = z\left(1+\frac{k^2\sigma^2\alpha^2}{z^2}\right). \end{aligned} \tag{2.34}$$

These expressions also follow from Eqs. (2.5)-(2.7) on ignoring the indexes i, j. By noting that the "m"-th term in the sum (2.20) can be evaluated in the same manner if one treats $\sqrt{m}\delta$ as a new variance, say δ_m. Then on summing all M such terms one obtains the formula

$$\begin{aligned} W(\mathbf{r}_1,\mathbf{r}_2;\omega) =& \frac{1}{C_0}\sum_{m=1}^{M}\binom{M}{m}\frac{(-1)^{m-1}}{m}\frac{1}{\Delta_m^2(z)}\exp\left[-\frac{(\mathbf{r}_1+\mathbf{r}_2)^2}{8\sigma^2\Delta_m^2(z)}\right] \\ & \times \exp\left[-\frac{(\mathbf{r}_1-\mathbf{r}_2)^2}{2\alpha_m^2\Delta_m^2(z)}\right]\exp\left[-ik\frac{(\mathbf{r}_2^2-\mathbf{r}_1^2)}{2R_m(z)}\right], \end{aligned} \tag{2.35}$$

where

$$\begin{aligned} &\alpha_m^2 = \left(\frac{1}{4\sigma^2}+\frac{1}{\delta_m^2}\right)^{-1}, \quad \Delta_m^2(z) = 1+\frac{z^2}{k^2\sigma^2\alpha_m^2}, \\ &R_m(z) = z\left(1+\frac{k^2\sigma^2\alpha_m^2}{z^2}\right). \end{aligned} \tag{2.36}$$

We will first consider the spectral density at any point $(\boldsymbol{\rho}, z)$ within the cross-

section of the beam:

$$S(\mathbf{r};\omega) = W(\mathbf{r},\mathbf{r};\omega) \\ = \frac{1}{C_0}\sum_{m=1}^{M}\binom{M}{m}\frac{(-1)^{m-1}}{m\Delta_m^2(z)}\exp\left[-\frac{\mathbf{r}^2}{2\sigma^2\Delta_m^2(z)}\right]. \tag{2.37}$$

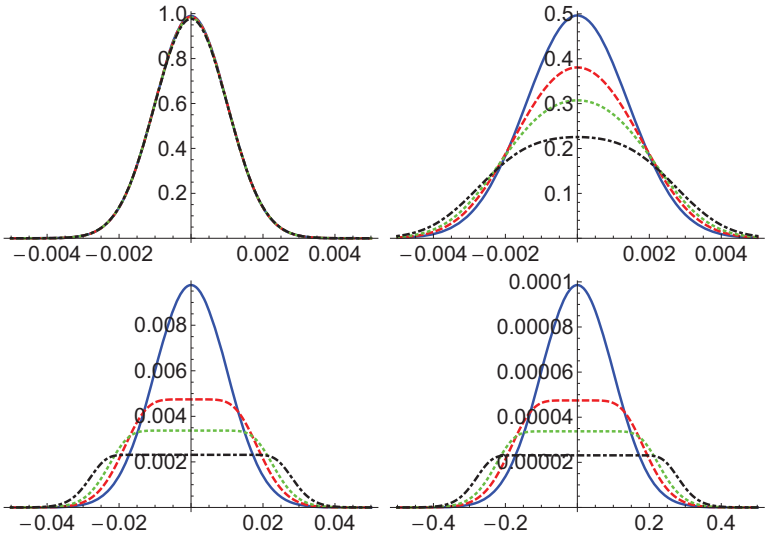

Figure 2.10: The transverse cross-section of the spectral density of the MGSM beam propagating in free space vs. $|\mathbf{r}|$ [m], at several distances from the source plane: A) 0.1 m; B) 1 m; C) 10 m, and D) 100 m. Several curves correspond to different values of M: $M = 1$ (solid blue curve), $M = 4$ (dashed red curve), $M = 10$ (dotted green curve) and $M = 40$ (dash-dotted black curve).

In Figure 2.10 we show the contours of the transverse cross-sections of a typical MGSM beam at several selected distances from the source and several values of index M. At sufficiently small distances from the source all curves preserve Gaussian shape (Fig. 2.10(A)), but as the propagation distance grows the transverse intensity profiles start to depend on the the index M: the larger the value of M the smaller its height at the beam's axis and flatter the profile become (Figs. 2.10(B)). At sufficiently large

distances, when the beam enters the far zone (see Fig. 2.10(C)), all contours with $M > 1$ assume the shapes having plateaus around the beam axis. Such plateaus are preserved but grow in width as the distance from the source is increased even more (compare Figs. 2.10(C) and 2.10(D)).

Without loss of generality, for the situation when $\mathbf{r}_d = 2\mathbf{r}_1 = -2\mathbf{r}_2$ we find at once, on using Eqs. (1.14) and (2.35)-(2.36) that

$$|\mu(\mathbf{r}_d, -\mathbf{r}_d; \omega)| = \frac{|W(\mathbf{r}_d, -\mathbf{r}_d; \omega)|}{S(0;\omega)} = \frac{\sum_{m=1}^{M} \binom{M}{m} \frac{(-1)^{m-1}}{m} \frac{1}{\Delta_m^2(z)} \exp\left[-\frac{\mathbf{r}_d^2}{2\alpha_m^2 \Delta_m^2(z)}\right]}{\sum_{m=1}^{M} \binom{M}{m} \frac{(-1)^{m-1}}{m} \frac{1}{\Delta_m^2(z)}}. \tag{2.38}$$

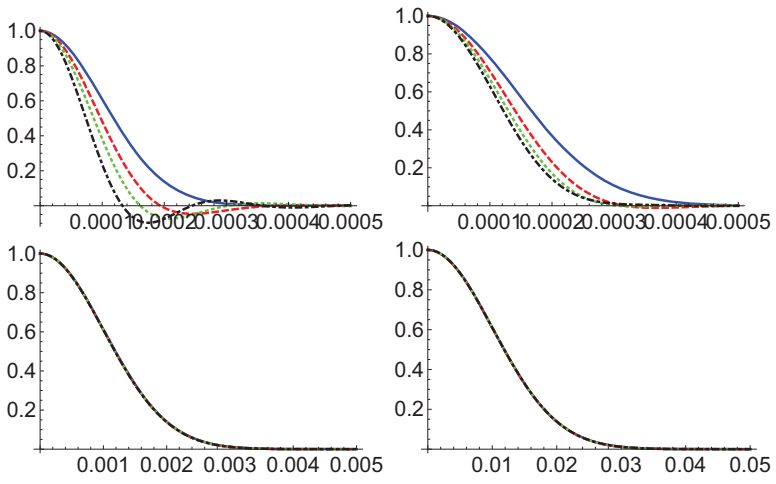

Figure 2.11: The modulus of the spectral degree of coherence of the MGSM beam propagating in free space vs. $|\mathbf{r}_d|$ [m], at the same distances from the source plane and the same values of M as in Fig. 2.10.

Figure 2.11 illustrates the behavior of $|\mu|$ on propagation in free space as a function of transverse difference variable $\mathbf{r}_d$ for several values of z and M. At relatively small

distances from the source the profiles of $|\mu|$ resemble that in the source plane (compare Fig. 2.11(A) with Fig. 1 of Ref. [33]). With growing distance, however, the shape of the curves becomes Gaussian-like while the dependence on M gradually disappears (Figs. 2.11(A)-2.11(C)). When the beam propagates in the far zone of the source, all the curves evolve in the same way: they remain Gaussian with monotonically increasing variance, being subjected to free-space diffraction (compare Figs. 2.11(C) and 2.11(D)).

2.4 Crystalline human eye lens' response to stochastic light

Almost always optical fields perceived by a human eye are partially coherent and partially polarized and in a number of cases have a beam-like nature. It is therefore crucial to be able to predict how the major properties of stochastic electromagnetic beams are modified on passing through the eye. Right after the entrance the light encounters the eye lens, known as the "aquula" ("water", Lat.) or "crystalline lens". Since the refractive power of the crystalline lens is approximately 18 dioptres, being roughly one-third of the eye's total power, it is the strongest optical element on the way of light to the retina and the eye nerve located at the back wall of the eye cavity.

For a recent mini-review of several existing models of the eye lens the reader is referred to [34]. The optical structure (see Fig. 2.12 for illustration) of this lens appears to be fairly well known for a long time (cf. [35]). Perhaps, the very first analytic model for the refractive index profile belongs to [36]:

$$\begin{aligned} n(r,d) = &-0.0062685(d-d_0)^2 + 0.0003834(d-d_0)^3 \\ &+ 1.406 - [0.00052375 + 0.00005735(d-d_0) \\ &+ 0.00027875(d-d_0)^2]r^2 - 0.000066717r^4 \end{aligned} \tag{2.39}$$

where r, d and d_0 are given in mm. The lens' total thickness $d = 3.6$ mm and the

distance from the entrance plane end to the plane with the highest refractive index $d_0 = 1.7$ mm. Other models for the refractive index profile of the lens were also suggested in [37] and [38].

One of the newer models for the crystalline eye lens was introduced in [39] (see also [40]-[41]). This model is based on the assumption that the variation of the refractive index in the radial direction is parabolic and, consequently, implies the ABCD-matrix determination. Namely, the lens is treated as a gradient-index [GRIN] medium limited either by plane-parallel or curved end faces with quadratic transverse refractive index, which is given, in the paraxial approximation and for a meridional section of the lens, by the distribution

$$n(r, d) = n_0(d) \left[1 - g^2(d) r^2/2\right], \tag{2.40}$$

where $n_0(d)$ is the index along the optical axis d and $g(d)$ is the gradient parameter describing the evolution of the transverse parabolic distribution.

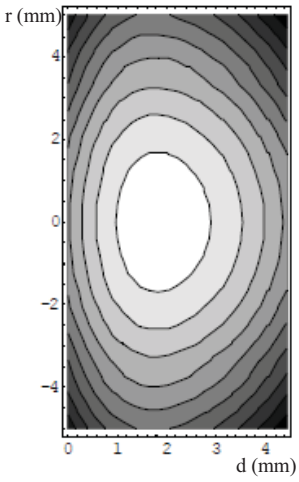

Figure 2.12: A typical distribution of the refractive index in the crystalline lens.

Among several analytical models of the crystalline eye lens, the GRIN lens, being

a first-order optical system, gained the widest popularity. It was treated in [39] as a quadratic phase transformer which has led to two versions called "plane-parallel end faces" and "curved end faces". Using both models propagation of a monochromatic lowest-order Gaussian beam was considered. The elements of the ABCD matrix of the GRIN profile slab lens were later determined by using the parabolic ray-path approximation in [34].

2.4.1 Beam interaction with the crystalline lens

In order to describe interaction of light with the crystalline lens we will employ the extended Huygens-Fresnel integral ([19], [20], [42], and [43]), and we will use the "curved end faces" model. Of special interest is whether the correlation properties of incident field have any influence on the intensity and polarization distribution of the light on the eye's retina.

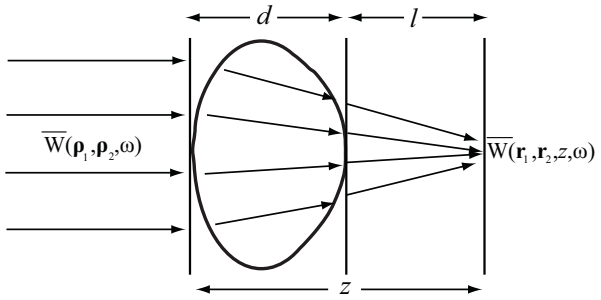

Figure 2.13: Illustration of notations used.

As a model for the initial beam we take the electromagnetic Gaussian Schell-model beam for which the elements of the cross-spectral density matrix have the form of Eq. (1.28). Propagation of each component of the correlation matrix through a paraxial optical ABCD system is given by Eq. (1.42). On substituting from Eq. (1.28) into Eq. (1.42) and performing integrations over the source plane one finds that the elements

of the cross-spectral density matrix of the beam in the plane $z > 0$, takes the form [20]

$$W_{ij}(\mathbf{r}_1, \mathbf{r}_2, z, \omega) = \frac{\sqrt{I_i I_j} B_{ij}}{Q_{ij}} exp\left[-\frac{|\mathbf{r}_1|^2 + |\mathbf{r}_2|^2}{4\sigma^2 Q_{ij}}\right] \times exp\left[-\frac{|\mathbf{r}_1 - \mathbf{r}_2|^2}{2\delta_{ij}^2 Q_{ij}}\right] exp\left[-\frac{ik(|\mathbf{r}_1|^2 - |\mathbf{r}_2|^2)}{2R_{ij}}\right], \tag{2.41}$$

where $Q_{ij} = A(z)^2 + (1 + 4\sigma^2/\delta_{ij}^2)B(z)^2/(4\sigma^4 k^2)$, $R_{ij} = B(z)Q_{ij}/(D(z)Q_{ij} - A(z))$. Equation (2.41) provides analytical description for propagation of the cross-spectral density matrix of the EGSMB through a paraxial optical system. By using Eq. (2.41) the intensity distribution (1.19) and polarization properties (1.20) of the beam everywhere within the system can be determined.

In order to carry out numerical evaluation of intensity and polarization characteristics of the EGSMB we will employ the model for the crystalline eye lens limited by curved end faces, introduced in [39] and further discussed in [40]-[41]. Because of the variable refractive index behavior the model is believed of being capable of accurately representing the optical structure of the eye lens. Following [39], the ray transfer matrix elements $A(d)$, $B(d)$, $C(d)$, $D(d)$ of the lens are given by the expressions

$$\begin{aligned} A(d) &= \Big[1 - \frac{g_e^2 d^2}{2} + \frac{d\dot{g}_e}{2g_e}\Big(1 - \frac{g_e^2 d^2}{6}\Big)\Big] - \frac{P_f d(1 - \frac{g_e^2 d^2}{6})}{n_e}, \\ B(d) &= \frac{n_1}{n_e} d\Big(1 - \frac{g_e^2 d^2}{6}\Big), \quad C(d) = -\frac{P_E(d)}{n_1'}, \\ D(d) &= \frac{n_1}{n_1'}\Big(-\Big[g_e^2 + \Big(\frac{\dot{g}_e}{2g_e}\Big)^2\Big] d\Big(1 - \frac{g_e^2 d^2}{6}\Big) \\ &+ \frac{P_b\Big[g_e^2 + \Big(\frac{\dot{g}_e}{2g_e}\Big)^2\Big] d\Big(1 - \frac{g_e^2 d^2}{6}\Big)}{n_e}\Big), \end{aligned} \tag{2.42}$$

where the back refractive power or equivalent power $P_E(d)$ of the lens is provided by

the formula

$$
\begin{aligned}
P_E(d) &= P_b H_f(d) + P_f \dot{H}_a(d) + P_G(d) - \frac{P_b P_f H_a(d)}{n_e} \\
&= P_b\Big[1 - \frac{g_e^2 d^2}{2} + \frac{\dot{g}_e}{2g_e} d\Big(1 - \frac{g_e^2 d^2}{6}\Big)\Big] \\
&+ P_f\Big(-\Big[g_e^2 + \Big(\frac{\dot{g}_e}{2g_e}\Big)^2\Big] d\Big(1 - \frac{g_e^2 d^2}{6}\Big)\Big) \\
&- n_e\Big[1 - \frac{g_e^2 d^2}{2} - \frac{\dot{g}_e}{2g_e} d\Big(1 - \frac{g_e^2 d^2}{6}\Big)\Big] - \frac{P_b P_f d\Big(1 - \frac{g_e^2 d^2}{6}\Big)}{n_e}.
\end{aligned}
\tag{2.43}
$$

The total $ABCD$ matrix of the lens with thickness d followed by free space propagation at distance l has the form

$$
\begin{pmatrix} A & B \\ C & D \end{pmatrix} = \begin{pmatrix} A(d) + lC(d) & B(d) + lD(d) \\ C(d) & D(d) \end{pmatrix}. \tag{2.44}
$$

2.4.2 Numerical examples

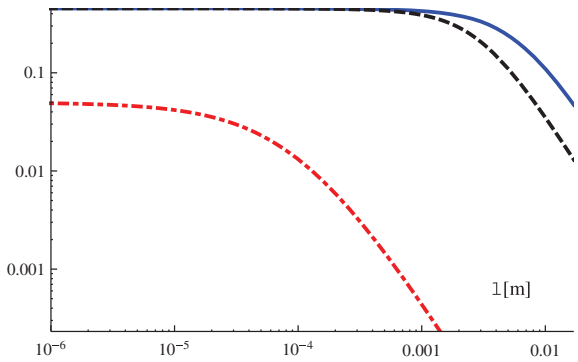

Figure 2.14: The normalized spectral density $S(\mathbf{r}, z, \omega)$ of the beam vs. propagation distance l [m] after the lens for: coherent beam, $\delta_{xx} = \delta_{yy} = \delta_{xy} = \delta_{yx} \to \infty$ (solid curve); partially coherent beam $\delta_{xx} = \delta_{yy} = 1.125 \times 10^{-4} m$ (dash-dotted curve), $\delta_{xy} = \delta_{yx} = 1.25 \times 10^{-4} m$, (C) nearly incoherent beam $\delta_{xx} = \delta_{yy} = 1.125 \times 10^{-5} m$, $\delta_{xy} = \delta_{yx} = 1.25 \times 10^{-5} m$ (dashed curve).

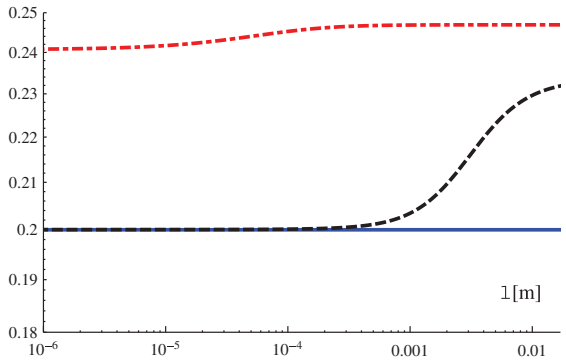

Figure 2.15: The spectral degree of polarization $P(\mathbf{r}, z, \omega)$ of the beams generated by the same sources as in Fig. 2.14 vs. propagation distance l [m] after the lens.

Equations (2.42) and (2.43) represent thickness-dependent (i.e. d-dependent) ABCD matrix elements of the curved end faces model of the GRIN lens. The parameters, with numerical values given in parenthesis, are, following [39]: g_e (0.03775 mm^{-1}) is the gradient parameter, $\dot{g}_e$ (0.0014 mm^{-2}) is its slope at $z = d$, n_e (1.386) is the edge index, n_1 (1.336) is the refractive index of the media in the object space, n_1' (1.336) is the refractive index of the media in the image space, P_f is the power of the front surface of the lens ($(n_c - n_1)/R_f$), P_b is the power of the back surface of the lens ($(n_1' - n_c)/R_b$), n_c (1.406) is the central refractive index, R_f ($12.7 - 0.058 \times age$ mm) is the variation of the front radius with age and R_b ($-5.9 + 0.015 \times age$ mm) is the variation of the back radius with age (age 30 is chosen in this analysis), $l = 17$ mm. The values of parameters of the EGSMB in the source plane are chosen as [12]: $\lambda = 550$ nm, $I_x = I_y = 1$, $B_{xx} = B_{yy} = 1$, $B_{xy} = B_{yx} = 0.2$, $d = 4$ mm, $\sigma = 0.1$ mm.

In Fig.2.14 we show the on-axis spectral density of the EGSMB as a function of propagation distance l after the crystalline lens, for several values of source correlation parameters. Figure 2.15 represents the degree of polarization vs. propagation distance l after the lens. Both the spectral density and the degree of polarization at the retina are intimately related to the correlation properties of the beam incident on the lens. We note that after passing through the lens the degree of polarization of the beam

still changes because of its stochastic nature [5].

2.5 Conclusion

To summarize, several important aspects of random beam analysis on its generation, free-space propagation, and passage through image forming systems have been discussed.

In section 2.2 we have derived the expressions for the elements of the 2×2 cross-spectral density matrix of an EGSM beam propagating in free space for two arbitrary points in the beam (not necessarily belonging to the same transverse cross-section) and then studied the changes in the SDCP. By a number of numerical examples we have demonstrated the dependence of the SDCP of the propagating beam on all of the parameters of the source. We considered separately the cases of uncorrelated and correlated components of the electric field in the source plane and also purely transverse and purely longitudinal SDCPs. In particular we found that the behavior of the SDCP of an EGSM beam depends strongly on the (constant) spectral degree of polarization in the source plane. Unlike the spectral degree of coherence and the spectral degree of polarization the SDCP may take on any non-negative value. Unlike the spectral degree of coherence, the transverse SDCP does not tend to 1 for sufficiently large distances from the source plane. Among the other not too obvious results is that the longitudinal SDCP saturates at certain (generally nonzero) values after the beam propagates over a sufficiently long distance in free space.

In section 2.3 we have introduced a family of functions whose Fourier transforms are multi-Gaussian functions for the source degree of coherence and employed them in the Schell-model and the quasi-homogeneous model. We have confirmed that such sources are physically genuine, determined the far fields they generate and showed that far fields have desirable features representing flat profiles which are useful in beam

shaping, optical trapping and tweezers. The novel family of correlation functions, while being visually similar to J_n-Bessel correlations, result in qualitatively different far-field patterns, possessing a flat intensity profile in the central part with a steep, adjustable drop at its edge.

In section 2.4 we have analyzed how electromagnetic stochastic beams propagate through the human crystalline eye lens. Our study revealed that the intensity and the polarization of light are drastically modified after passing through the eye lens. Hence the images formed by the eye are very sensitive to correlation properties of the incoming light. Moreover, since the effective focal length varies with the correlation properties of the incident light, the quality of the perceived image may also depend on it. We believe that our work is the very first to address interaction of light with arbitrary spectral, coherence and polarization properties by a human eye lens, and will potentially stimulate interest in using electromagnetic stochastic beams in applications involving eye medicine and cognitive science.

Chapter 3

Propagation of Electromagnetic Random Fields in the Atmosphere

3.1 Introductory remarks

The topic of interaction of electromagnetic random fields with linear random media, such as the atmospheric turbulence, has been previously explored to some extent. Among the most interesting phenomena in the beams in the presence of random media are the suppression of spectral shifts [44] and drastic changes in polarization properties ([45]). In this chapter we extend the existing knowledge by investigating the behavior of higher-order statistics of the beam and exploring the beam behavior in a double-pass propagation scenario.

The study of fluctuations in Stokes parameters of stochastic electromagnetic beams on propagation in turbulent atmosphere is presented first. Expressions are derived for the scintillation indexes (contrasts) of the Stokes parameters and their versions normalized by the instantaneous intensity in the case when the beam is generated by the electromagnetic Gaussian Schell-model source with uniform polarization. We illustrate our analytical results by a set of numerical examples.

An active bistatic LIDAR system operating through atmospheric turbulence is then considered. The illumination field is assumed to be an electromagnetic Gaussian-Schell model beam. The target surface is modeled as a combination of an isotropic phase screen governed by Gaussian statistics, to account for its roughness, and a Gaussian lens to account for its size and radius of curvature. With the help of

a recently developed tensor method for propagation of stochastic electromagnetic beams through the ABCD systems and random media we examine the evolution of states of coherence and polarization of the beam. In the case of an unresolved flat (planar) target we show that by comparing coherence and polarization properties of the illumination beam and of the return beam it is possible to predict the typical roughness of the target surface.

3.2 Fluctuations in the instantaneous Stokes parameters of stochastic electromagnetic beams propagating in the turbulent atmosphere

The possibility of the efficient use of scalar stochastic beams for optical systems which involve propagation through atmospheric turbulence was pointed out not that long ago [46]: the scintillation index of a stochastic beam is generally lower than that of the comparable monochromatic laser beam. Later it was also found [47] that, under certain conditions, the relative spreading of a stochastic beam might be weaker than that of a monochromatic laser beam. Based on these predictions an analysis of the FSO communication systems was made (see the references [48]-[50]) and it was found that, in fact, for certain atmospheric channels and for well-chosen sources of random beams the link performance may be significantly improved.

With the development of the unified theory of coherence and polarization [5] it became evident that the polarization properties of electromagnetic sources may also influence all the statistical properties of beams on propagation in vacuum and in random media. In particular, it was analyzed in [51] and [52] how the intensity fluctuations and fluctuations in the instantaneous Stocks parameters of stochastic electromagnetic beams evolve on propagation in free space, depending on coherence and polarization properties of their sources. In [53] it was demonstrated that, gener-

ally, the scintillation index of an unpolarized beam can be reduced by a factor of two, at best, compared to that of a polarized beam with the same intensity distribution and degree of coherence. Recently the possibility of reduction in scintillation with the help of a non-uniformly polarized monochromatic source (i.e. without use of source randomness) was also pointed out [54].

In this section we investigate whether in addition to the intensity, all the Stokes parameters can be used as information carriers. We develop expressions for the scintillation indexes of the instantaneous Stokes parameters of stochastic electromagnetic beams. For a wide class of stochastic electromagnetic beams we then numerically examine the behavior of such scintillation indexes and compare them with the conventionally used scintillation index based on fluctuations in the beam intensity. We assume that the beam propagates in clear-optical turbulence, i.e. depolarization of the beam due to scattering/absorption by aerosols is neglected.

3.2.1 General expressions for the statistics of the Stokes parameters

We begin by a brief review of the theoretical background relating to sources radiating stochastic electromagnetic beams. Let us assume that a planar source is located in the plane $z = 0$ and radiates a beam-like field propagating close to the positive z-axis through the atmosphere. Suppose the fluctuations in the beam at the source plane are wide-sense stationary and then its second-order statistical properties at points $\mathbf{r}_1'$ and $\mathbf{r}_1'$ and frequency ω may be characterized by the generalized Stokes parameters (Eq. (1.24)).

With the help of the extended Huygens-Fresnel integral principle adjusted for propagation in anisotropic and homogeneous atmosphere it can be readily shown, on

using Eqs. (1.24) and (1.37), that

$$\langle S_\alpha(\mathbf{r},\omega)\rangle = \frac{k^2}{(2\pi z)^2}\int\int \langle S_\alpha(\mathbf{r}_1',\mathbf{r}_2',\omega)\rangle\langle G^*(\mathbf{r},\mathbf{r}_1')G(\mathbf{r},\mathbf{r}_2')\rangle d^2r_1' d^2r_2', \quad (\alpha = 0,1,2,3), \tag{3.1}$$

where integration is performed twice over the planar source and $G(\mathbf{r},\mathbf{r}')$ is the Green's function of a point source. It follows from Eq. (1.38) and (1.39) that the propagation kernel for homogeneous and isotropic turbulence is:

$$\langle G^*(\mathbf{r},\mathbf{r}_1')G(\mathbf{r},\mathbf{r}_2')\rangle = \exp\left[-ik\frac{(\boldsymbol{\rho}-\mathbf{r}_1')^2-(\boldsymbol{\rho}-\mathbf{r}_2')^2}{2z}\right] \times \exp\left[-\frac{\pi^2k^2z}{3}(\mathbf{r}_1'-\mathbf{r}_2')^2\int_0^\infty \kappa^3\Phi_n(\kappa)d\kappa\right], \tag{3.2}$$

where $\Phi_n(\kappa)$ is the one-dimensional power spectrum of atmospheric fluctuations and $\boldsymbol{\rho}$ is the projection of vector $\mathbf{r}$ onto the source plane, i.e. $\mathbf{r} = (\boldsymbol{\rho}, z)$.

We will be interested in determining the scintillation indexes (contrasts of fluctuations) in the Stokes parameters S_α defined by the expressions

$$c[S_\alpha(\mathbf{r},\omega)] = \frac{\langle S_\alpha^2(\mathbf{r},\omega)\rangle - \langle S_\alpha(\mathbf{r},\omega)\rangle^2}{\langle S_\alpha(\mathbf{r},\omega)\rangle^2}, \quad (\alpha = 0,1,2,3). \tag{3.3}$$

Under the assumption that fluctuations in the beam propagating in the atmospheric turbulence are Gaussian it can be shown that [55]

$$c[S_0(\mathbf{r},\omega)] = \frac{1}{2}[1+P^2(\mathbf{r},\omega)], \tag{3.4}$$

and

$$c[S_\alpha(\mathbf{r},\omega)] = 1 + \frac{\langle S_0(\mathbf{r},\omega)\rangle^2}{2\langle S_\alpha(\mathbf{r},\omega)\rangle^2}[1-P^2(\mathbf{r},\omega)], \quad (\alpha = 1,2,3), \tag{3.5}$$

where

$$P(\mathbf{r},\omega)=\frac{\sqrt{\langle S_1(\mathbf{r},\omega)\rangle^2+\langle S_2(\mathbf{r},\omega)\rangle^2+\langle S_3(\mathbf{r},\omega)\rangle^2}}{\langle S_0(\mathbf{r},\omega)\rangle}, \tag{3.6}$$

is an alternative formula for the degree of polarization of the beam. We note here that the Gaussian approximation is legitimate only for strong fluctuation conditions, i.e. for sufficiently large propagation distances, or strong local fluctuations at points along the path.

Since usually on propagation in random media the Stokes parameters tend to zero with growing distance from the source, at the same rate as the spectral density does, it is also of interest sometimes to determine the contrasts in the normalized Stokes parameters, i.e. in the quantities

$$s_\alpha(\mathbf{r},\omega)=\frac{S_\alpha(\mathbf{r},\omega)}{S_0(\mathbf{r},\omega)},\quad(\alpha=0,1,2,3). \tag{3.7}$$

It was shown in [56] that under the assumption of Gaussian statistics the scintillation indexes of the normalized Stokes parameters defined as

$$c[s_\alpha(\mathbf{r},\omega)]=\frac{\langle s_\alpha^2(\mathbf{r},\omega)\rangle-\langle s_\alpha(\mathbf{r},\omega)\rangle^2}{\langle s_\alpha(\mathbf{r},\omega)\rangle^2},\quad(\alpha=1,2,3), \tag{3.8}$$

are given by the expressions

$$c[s_\alpha(\mathbf{r},\omega)]=\frac{(1-P)^2}{q_\alpha}\frac{2\Delta[P^2-Pq_\alpha^2]-q_\alpha^2[1-P^2]\Delta^2-4P^4+8q_\alpha^2P^2}{4P^2-4[P-P^3]\Delta+[1-P^2]^2\Delta^2}, \tag{3.9}$$

where

$$\Delta=\sinh^{-1}\left[\frac{P^2+q_\alpha}{\sqrt{[1-P^2][P^2-q_\alpha]}}\right]+\sinh^{-1}\left[\frac{P^2-q_\alpha}{\sqrt{[1-P^2][P^2-q_\alpha]}}\right], \tag{3.10}$$

and

$$q_\alpha = \frac{\langle S_\alpha \rangle}{\langle S_0 \rangle}. \tag{3.11}$$

3.2.2 Fluctuations in the Stokes parameters of Gaussian Schell-model beams

We will now apply the formulas of the previous section for the analysis of the fluctuations in the Stokes parameters of the most versatile class of random electromagnetic beams, the electromagnetic Gaussian Schell-model beams (see Eq. (1.28)). On substituting from Eq. (1.28) into Eq. (1.24) we find that the generalized Stokes parameters of such a source are

$$\begin{aligned}
\langle S_0(\mathbf{r}_1', \mathbf{r}_2', \omega)\rangle &= \exp\left[-\frac{r_1'^2 + r_2'^2}{4\sigma^2}\right]\left(I_x \exp\left[\frac{-(\mathbf{r}_1' - \mathbf{r}_2')^2}{2\delta_{xx}^2}\right] + I_y \exp\left[\frac{-(\mathbf{r}_1' - \mathbf{r}_2')^2}{2\delta_{yy}^2}\right]\right)\\
\langle S_1(\mathbf{r}_1', \mathbf{r}_2', \omega)\rangle &= \exp\left[-\frac{r_1'^2 + r_2'^2}{4\sigma^2}\right]\left(I_x \exp\left[\frac{-(\mathbf{r}_1' - \mathbf{r}_2')^2}{2\delta_{xx}^2}\right] - I_y \exp\left[\frac{-(\mathbf{r}_1' - \mathbf{r}_2')^2}{2\delta_{yy}^2}\right]\right)\\
\langle S_2(\mathbf{r}_1', \mathbf{r}_2', \omega)\rangle &= 2\sqrt{I_x I_y} Re[B_{xy}] \exp\left[-\frac{r_1'^2 + r_2'^2}{4\sigma^2}\right] \exp\left[\frac{-(\mathbf{r}_1' - \mathbf{r}_2')^2}{2\delta_{xy}^2}\right]\\
\langle S_3(\mathbf{r}_1', \mathbf{r}_2', \omega)\rangle &= 2\sqrt{I_x I_y} Im[B_{xy}] \exp\left[-\frac{r_1'^2 + r_2'^2}{4\sigma^2}\right] \exp\left[\frac{-(\mathbf{r}_1' - \mathbf{r}_2')^2}{2\delta_{xy}^2}\right],
\end{aligned} \tag{3.12}$$

Further, on substituting from Eq. (3.12) into Eq. (3.1) and after integrating we find that

$$\begin{aligned}
\langle S_0(\mathbf{r}, \omega)\rangle &= \frac{I_x}{\Delta_{xx}^2} \exp\left[-\frac{\boldsymbol{\rho}^2}{8\sigma^2\Delta_{xx}^2}\right] + \frac{I_y}{\Delta_{yy}^2} \exp\left[-\frac{\boldsymbol{\rho}^2}{8\sigma^2\Delta_{yy}^2}\right],\\
\langle S_1(\mathbf{r}, \omega)\rangle &= \frac{I_x}{\Delta_{xx}^2} \exp\left[-\frac{\boldsymbol{\rho}^2}{8\sigma^2\Delta_{xx}^2}\right] - \frac{I_y}{\Delta_{yy}^2} \exp\left[-\frac{\boldsymbol{\rho}^2}{8\sigma^2\Delta_{yy}^2}\right],\\
\langle S_2(\mathbf{r}, \omega)\rangle &= \frac{2\sqrt{I_x I_y} Re[B_{xy}]}{\Delta_{xy}^2} \exp\left[-\frac{\boldsymbol{\rho}^2}{8\sigma^2\Delta_{xy}^2}\right],\\
\langle S_3(\mathbf{r}, \omega)\rangle &= \frac{2\sqrt{I_x I_y} Im[B_{xy}]}{\Delta_{xy}^2} \exp\left[-\frac{\boldsymbol{\rho}^2}{8\sigma^2\Delta_{xy}^2}\right],
\end{aligned} \tag{3.13}$$

where

$$\Delta_{ij}^2 = 1 + \alpha_{ij} z^2 + \frac{2Mz^2}{k^2\sigma^2}, \tag{3.14}$$

with

$$\alpha_{ij} = \frac{1}{(k\sigma)^2}\left[\frac{1}{4\sigma^2} + \frac{1}{\delta_{ij}^2}\right] \tag{3.15}$$

and

$$M = \frac{1}{3}\pi^2 k^2 z \int_0^\infty \kappa^3 \Phi_n(\kappa) d\kappa. \tag{3.16}$$

In the case of the Tatarskii's power spectrum [17] the parameter M takes the form [57]

$$M = 0.55 C_n^2 l_0^{-1/3} k^2 z. \tag{3.17}$$

In these expressions C_n^2 is the refractive index structure parameter, l_0 is the inner scale of turbulence, and z is the propagation distance. The corresponding expression for the spectral density derived for scalar field can be found in [58]. On substituting from Eq. (3.13) into Eqs. (3.4) and (3.5) we finally can find the contrasts of the fluctuating Stokes parameters. Further, on substituting from Eq. (3.13) into Eq. (3.9) we can determine the contrasts in the normalized Stokes parameters. Since the derivation is straightforward and the final expressions are cumbersome we do not include them here but, instead, analyze the results numerically.

Unless it is stated otherwise we choose for the atmospheric channel the following set of parameters: $C_n^2 = 10^{-14} m^{-2/3}$, $l_0 = 1mm$, $z = 1km$. The parameters of the model source are carefully chosen in accord with realizability conditions and suitability for atmospheric propagation (cf. [59]). In particular, $\lambda = 0.628\mu m$, $\sigma = 2.5cm$, $I_x = 2.25$, $I_y = 1$, $B_{xy} = 0.2e^{-i\pi/6}$, $\delta_{xx} = 5mm$, $\delta_{yy} = 7.5mm$, $\delta_{xy} = \delta_{yx} = 10mm$.

Figure 3.1 demonstrates the evolution of the average Stokes parameters with grow-

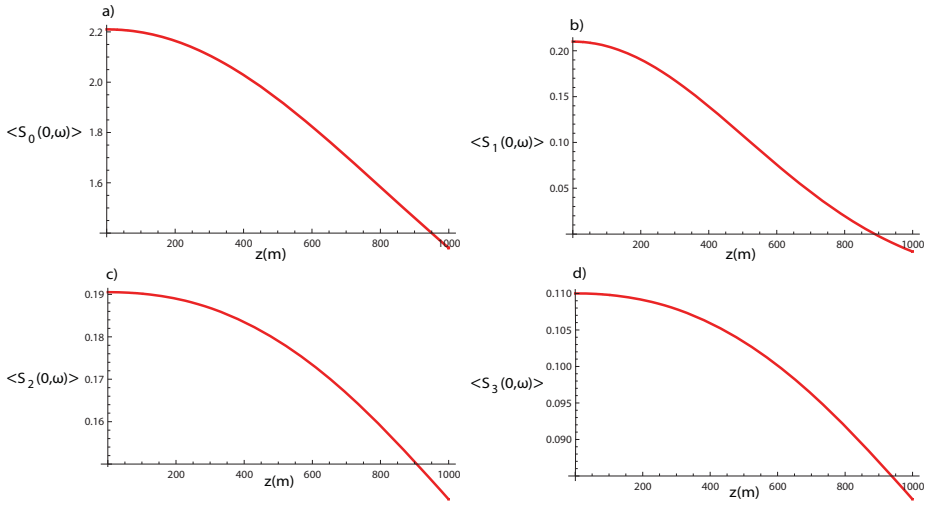

Figure 3.1: On-axis average Stokes parameters of an EMGSM beam propagating in turbulent atmosphere as a function of distance $z[m]$. (a) $\langle S_0(0,\omega)\rangle$, (b) $\langle S_1(0,\omega)\rangle$, (c) $\langle S_2(0,\omega)\rangle$, (d) $\langle S_3(0,\omega)\rangle$.

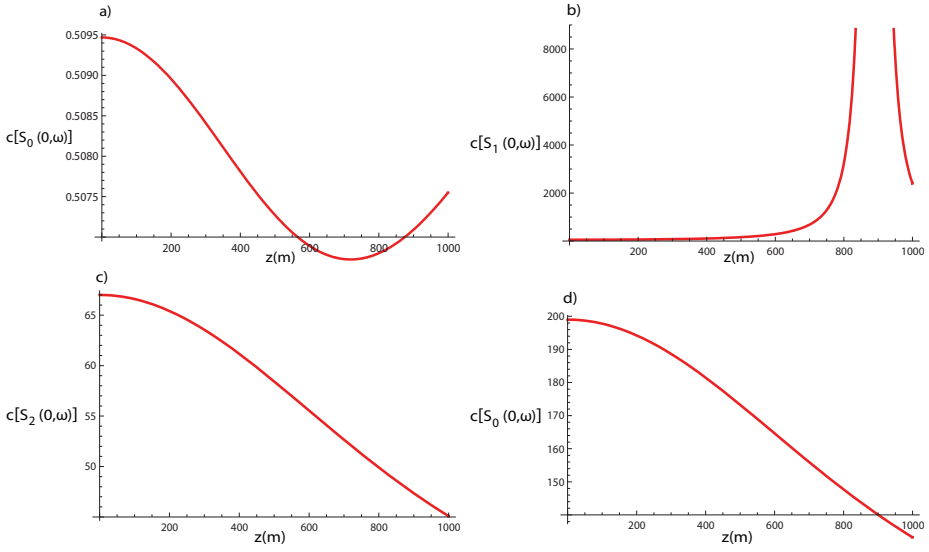

Figure 3.2: On-axis scintillation indexes of the instantaneous Stokes parameters of an EMGSM beam propagating in turbulent atmosphere as a function of distance $z[m]$. (a) $c[S_0(0,\omega)]$, (b) $c[S_1(0,\omega)]$, (c) $c[S_2(0,\omega)]$, (d) $c[S_3(0,\omega)]$.

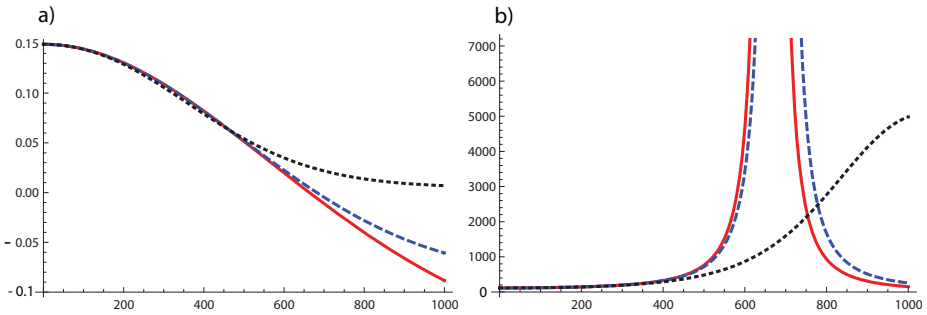

Figure 3.3: (a) Average Stokes parameter $\langle S_1(0,\omega)\rangle$ and (b) scintillation index $c[S_1(0,\omega)]$ as function of propagation distance $z[m]$ for $C_n^2 = 0$ (solid curves), for $C_n^2 = 10^{-14}m^{-2/3}$ (dashed curves) and for $C_n^2 = 10^{-13}m^{-2/3}$ (dotted curves). Parameters differ from the ones given in the text are: $I_x = 1.21$, $I_y = 1$.

ing distance z from the source. Figure 3.2 shows the same dependence but for the scintillation indexes of the four Stokes parameters. It is seen from Figs. 3.1 and 3.2 that even though the average Stokes evolve monotonically the scintillation indexes in the instantaneous Stokes parameters may have maxima and minima, and, moreover, tend to infinity at certain location. Especially complicated behavior is exhibited by $c[S_1(0,\omega)]$, since it might have zero in its denominator.

In Figure 3.3 we show the dependence of the average Stokes parameter S_1 (Figure 3.1(a)) and its scintillation index (Figure 3.1(b)) on the local strength of atmospheric turbulence (C_n^2). We see that with growing strength of turbulence the average Stokes parameter tends to zero faster and its scintillation index takes on lower values.

3.3 Sensing of semi-rough targets embedded in atmospheric turbulence by means of stochastic electromagnetic beams

The possibility of using coherence and polarization properties of the source in remote sensing and in recognition of targets embedded in random media is still a largely open problem and in majority of publications is confined to scalar treatment [60], [17]. Only recently a convenient technique which uses ABCD matrices together with

the extended Huygens-Fresnel integral developed in [61] was adopted to the GSM beam propagation in active LIDAR systems operating in the atmosphere (source- atmosphere- target- atmosphere- detector) [62] (see also [63] where a particular case of a perfectly smooth target was discussed in details). In Figure 3.4 we show a typical active LIDAR system, i.e. the one in which the properties of illumination can be adjusted. We also assume the LIDAR system to be bistatic, i.e. having sufficient separation distance between transmitter and receiver, in order to ignore possible backscatter amplification effects [17].

According to the tensor technique the source, the propagating beam, as well as all the optical elements in the system, are characterized by 4x4 tensors. If, as is assumed here, atmospheric turbulence and the target are isotropic, i.e. they affect both components of the electric field in the same way, they can be modeled with the help of scalar correlation functions, otherwise they can also be characterized by 4x4 tensors. We will use the electromagnetic Gaussian Schell-model beams [5] for our analysis since it is the only model beam introduced so far for which the tensor method was developed specifically for atmospheric propagation problems. Moreover several techniques were developed for synthesis of this class of beams in the laboratory (cf. [64]).

In almost all the previous studies, including [62], only the direct propagation problem through the LIDAR system has been discussed. In this section we will analyze the propagation of the spectral degree of coherence and the state of polarization of the beam, which were not analyzed before, and use the comparison between their distributions in the source plane and in the receiver plane for identification of some of the target characteristics, a typical roughness, for instance. In other words, we will tackle the inverse problem of target identification with the help of two easily practically accessible properties of the electromagnetic stochastic beams.

3.3.1 Propagation of an electromagnetic Gaussian Schell-model beam through the LIDAR system

We begin by a brief review of the theoretical development pertaining to propagation of the electromagnetic Gaussian Schell-model beam [EGSM] in the atmospheric LIDAR system. For detailed derivation of the formulas in this section the reader may consult with Ref. [62].

In the source (transmitter) plane each of the four elements of the cross-spectral density matrix [5] of an electromagnetic Gaussian Schell beam in its tensor notation is given by the expression

$$W_{\alpha\beta}(\widetilde{\mathbf{r}},0) = A_\alpha A_\beta B_{\alpha\beta} exp[-\frac{ik}{2}\widetilde{\mathbf{r}}^T \mathbf{M}^{-1}_{0\alpha\beta}\widetilde{\mathbf{r}}], \qquad (\alpha = x,y;\beta = x,y) \tag{3.18}$$

where $\widetilde{\mathbf{r}}$ is the 4×4 vector such that $\widetilde{\mathbf{r}} = (\mathbf{r}_1, \mathbf{r}_2)$, $\mathbf{r}_1$ and $\mathbf{r}_2$ being two-dimensional vectors in the source plane, $\mathbf{M}^{-1}_{0\alpha\beta}$ are the 4×4 matrices of the form

$$\mathbf{M}^{-1}_{0\alpha\beta} = \begin{pmatrix} \frac{1}{ik}(\frac{1}{2\sigma_\alpha^2} + \frac{1}{\delta^2_{\alpha\beta}})\mathbf{I} & \frac{i}{k\delta^2_{\alpha\beta}}\mathbf{I} \\ \frac{i}{k\delta^2_{\alpha\beta}}\mathbf{I} & \frac{1}{ik}(\frac{1}{2\sigma_\beta^2} + \frac{1}{\delta^2_{\alpha\beta}})\mathbf{I} \end{pmatrix}. \tag{3.19}$$

Parameters A_α, $B_{\alpha\beta}$, σ_α and $\delta_{\alpha\beta}$ entering Eq. (3.18) are independent of position but, in general, depend on the frequency. We assume that the realizability conditions [65] or [66] and the beam conditions [67] for the electromagnetic Gaussian-Schell model source hold. $\mathbf{I}$ is the 2x2 unit matrix. For uniformly polarized sources, sometimes also called isotropic, one must set $\sigma_x = \sigma_y = \sigma$ [67].

The elements of the cross-spectral density matrix of the beam propagating in the atmospheric turbulence from the source plane to the target plane, located at distance

l_1 and having focal length f_1, are given by the following expressions [62]

$$W_{\alpha\beta}(\widetilde{\mathbf{t}}, l_1) = \frac{A_\alpha A_\beta B_{\alpha\beta}}{[det(\widetilde{\mathbf{A}} + \widetilde{\mathbf{B}}\mathbf{M}_{0\alpha\beta}^{-1} + \widetilde{\mathbf{B}}\widetilde{\mathbf{P}_0})]^{1/2}} exp[-\frac{ik}{2}\widetilde{\mathbf{t}}^T \mathbf{M}_{1\alpha\beta}^{-1}\widetilde{\mathbf{t}}], \quad (\alpha = x, y; \beta = x, y), \tag{3.20}$$

where $\widetilde{\mathbf{t}} = (\mathbf{t}_1, \mathbf{t}_2)$, $\mathbf{t}_1$ and $\mathbf{t}_2$ are the two-dimensional vectors in the target plane. Also in Eq. (3.20) the 4×4 matrices in the exponential terms have the forms

$$\begin{aligned}\mathbf{M}_{1\alpha\beta}^{-1} =& (\widetilde{\mathbf{C}} + \widetilde{\mathbf{D}}\mathbf{M}_{0\alpha\beta}^{-1} + \widetilde{\mathbf{D}}\widetilde{\mathbf{P}_0})(\widetilde{\mathbf{A}} + \widetilde{\mathbf{B}}\mathbf{M}_{0\alpha\beta}^{-1} + \widetilde{\mathbf{B}}\widetilde{\mathbf{P}_0})^{-1} + \widetilde{\mathbf{P}}_0 + \\ & (\widetilde{\mathbf{B}}^{-1T} - \frac{1}{4}\widetilde{\mathbf{P}}_0^T)(\mathbf{M}_{0\alpha\beta}^{-1} + \widetilde{\mathbf{B}}^{-1}\widetilde{\mathbf{A}} + \widetilde{\mathbf{P}})^{-1}\widetilde{\mathbf{P}}_0,\end{aligned} \tag{3.21}$$

where auxiliary 4×4 matrices $\widetilde{\mathbf{A}}$, $\widetilde{\mathbf{B}}$, $\widetilde{\mathbf{C}}$ and $\widetilde{\mathbf{D}}$ can be shown to be given by the expressions

$$\begin{aligned}&\widetilde{\mathbf{A}} = \begin{pmatrix} \mathbf{A} & 0\mathbf{I} \\ 0\mathbf{I} & \mathbf{A}^* \end{pmatrix}, \widetilde{\mathbf{B}} = \begin{pmatrix} \mathbf{B} & 0\mathbf{I} \\ 0\mathbf{I} & -\mathbf{B}^* \end{pmatrix}, \widetilde{\mathbf{C}} = \begin{pmatrix} \mathbf{C} & 0\mathbf{I} \\ 0\mathbf{I} & -\mathbf{C}^* \end{pmatrix}, \\ &\widetilde{\mathbf{D}} = \begin{pmatrix} \mathbf{D} & 0\mathbf{I} \\ 0\mathbf{I} & \mathbf{D}^* \end{pmatrix},\end{aligned} \tag{3.22}$$

matrices $\mathbf{A}$, $\mathbf{B}$, $\mathbf{C}$ and $\mathbf{D}$ being the elements of the classic $ABCD$-matrix of the system:

$$\begin{pmatrix} \mathbf{A} & \mathbf{B} \\ \mathbf{C} & \mathbf{D} \end{pmatrix} = \begin{pmatrix} \mathbf{I} & l_1\mathbf{I} \\ (-1/f_1)\mathbf{I} & (1 - l_1/f_1)\mathbf{I} \end{pmatrix}. \tag{3.23}$$

At this stage the focusing properties of the target are already included in the analysis via the focal length f_1 of a Gaussian lens which is a part of the target model (see Fig.3.4).

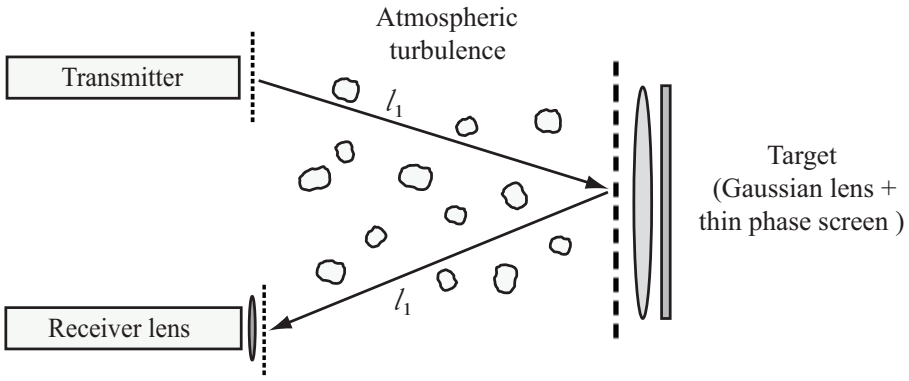

Figure 3.4: Schematic illustration of an active bistatic LIDAR system operating in the atmosphere.

Further, in Eqs. (3.20) and (3.21) the 4×4 matrix $\widetilde{\mathbf{P}}_0$ has the form

$$\widetilde{\mathbf{P}}_0 = \frac{2}{ik\rho_o^2} \begin{pmatrix} \mathbf{I} & -\mathbf{I} \\ -\mathbf{I} & \mathbf{I} \end{pmatrix}, \tag{3.24}$$

where ρ_o is the coherence radius of the spherical wave propagating in weak atmospheric turbulence with Kolmogorov power spectrum:

$$\rho_0 = (0.545k^2C_n^2l_1)^{-3/5}, \tag{3.25}$$

with k being the wave number of the propagating wave and C_n^2 being the refractive index structure parameter [17].

The elements of the transverse cross-spectral spectral density matrix of the beam at the receiver collecting lens located at distance l_1 from the target are given by the

expressions

$$W_{\alpha\beta}(\widetilde{\mathbf{v}}, 2l_1) = \frac{4\pi\beta^2 A_\alpha A_\beta B_{\alpha\beta}}{k^2[det(\widetilde{\mathbf{I}} + \widetilde{\mathbf{B}}\mathbf{M}_{1\alpha\beta}^{-1} + \widetilde{\mathbf{B}}\widetilde{\mathbf{T}} + \widetilde{\mathbf{B}}\widetilde{\mathbf{P}}_1)]^{1/2}[det(\widetilde{\mathbf{A}} + \widetilde{\mathbf{B}}\mathbf{M}_{0\alpha\beta}^{-1} + \widetilde{\mathbf{B}}\widetilde{\mathbf{P}_0})]^{1/2}}, \times exp[-\frac{ik}{2}\widetilde{\mathbf{v}}^T\mathbf{M}_{2\alpha\beta}^{-1}\widetilde{\mathbf{v}}] \tag{3.26}$$

where $\widetilde{\mathbf{v}} = (\mathbf{v}_1, \mathbf{v}_2)$, $\mathbf{v}_1$ and $\mathbf{v}_2$ are the two-dimensional vectors in the target plane and the 4×4 matrices $\mathbf{M}_{2\alpha\beta}^{-1}$ have the forms

$$\mathbf{M}_{2\alpha\beta}^{-1} = \widetilde{\mathbf{P}}_1 + \widetilde{\mathbf{B}}^{-1} - (\widetilde{\mathbf{B}}^{-1} - \frac{1}{2}\widetilde{\mathbf{P}}_1)^T(\mathbf{M}_{1\alpha\beta}^{-1} + \widetilde{\mathbf{T}} + \widetilde{\mathbf{B}}^{-1} + \widetilde{\mathbf{P}}_1)^{-1}(\widetilde{\mathbf{B}}^{-1} - \frac{1}{2}\widetilde{\mathbf{P}}_1). \tag{3.27}$$

In Eqs. (3.26) and (3.27) the 4×4 matrix $\widetilde{\mathbf{T}}$ represents the combination of the target size and the correlation function of its roughness, and β is the normalization parameter. According to the Goodman's model [68], $\widetilde{\mathbf{T}}$ is expressed in tensor notation [62], and has the form

$$\widetilde{\mathbf{T}} = \begin{pmatrix} -\frac{2i}{k}\left[\frac{1}{W_R^2} + \frac{1}{l_c^2}\right]\mathbf{I} & \frac{2i}{kl_c^2}\mathbf{I} \\ \frac{2i}{kl_c^2}\mathbf{I} & -\frac{2i}{k}\left[\frac{1}{W_R^2} + \frac{1}{l_c^2}\right]\mathbf{I} \end{pmatrix}, \tag{3.28}$$

with W_R being the r.m.s. width of the target and l_c is its r.m.s. transverse correlation width. The model can be used for a wide variety of targets in terms of their roughness and sizes. In particular, the surface roughness may vary from *smooth* ($\beta^2 = k^2/4\pi$, $l_c \to \infty$), to *Lambertian* ($\beta^2 = T_0^2/\pi l_c^2$, $l_c \to 0$), T_0 is the r.m.s. target reflection coefficient; and its size can range from *point* ($W_R \to 0$) to *unbounded* ($W_R \to \infty$).

3.3.2 Sensing by the spectral degree of coherence

In this section we will first investigate propagation of the spectral degree of coherence of the EGSM beam in the atmospheric LIDAR system and then will use this knowledge for solving one related inverse problem. The spectral degree of coherence at two spatial positions, say $\boldsymbol{\rho}_1$ and $\boldsymbol{\rho}_2$, which can be vectors in the source, target, collector planes as well any other two positions within the LIDAR system, was defined by the expression (1.14). In this study we will only be interested in the absolute value of this quantity which represents a fully coherent beam if its value is 1 and incoherent beam if its value is 0.

In Fig. 3.5. we demonstrate typical evolution of the degree of coherence of the beam in three planes, transverse to direction of propagation of the beam showing its modulus: source [Figs. 3.5(A), 3.5(D) and 3.5(G)]; target [Figs. 3.5(B), 3.5(E) and 3.5(H)] and collector [Figs. 3.5(C), 3.5(F) and 3.5(I)] planes. In the upper row of the plot [Fig. 3.5(A), 3.5(B) and 3.5(C)] we show the changes in the modulus of the degree of coherence of a beam generated by a nearly incoherent source. We see that in this case the degree of coherence only broadens on passage through the system. In this case among the three competing mechanisms that affect coherence, source correlations, roughness of the target and atmospheric turbulence, the first dominates. In the second row [Fig. 3.5(D), 3.5(E) and 3.5(F)] we see the evolution of the absolute value of the degree of coherence in the case when the beam is initially partially coherent. We notice that degree of coherence does not change significantly on passage through the LIDAR, since the effect of turbulence and the target is practically compensated by the source correlations. Moreover, as we will later show, it is possible to find, for a given LIDAR setup, the source that generates the beam whose degree of coherence at the collecting lens plane is the same as in the source plane. In the third row [Fig. 3.5(G), 3.5(H) and 3.5(I)] we show the case where the source is

assumed to be almost coherent and the degree of coherence of the propagating beam can only decrease on passage through the LIDAR due to the cumulative effect of atmospheric turbulence and source correlations. After considering these three generic cases, especially the case of a partially coherent source (second row) we can conclude that: *if the degree of coherence remains approximately the same on passage through the LIDAR system then r.m.s. target roughness is approximately the same as initial r.m.s. source correlation widths.*

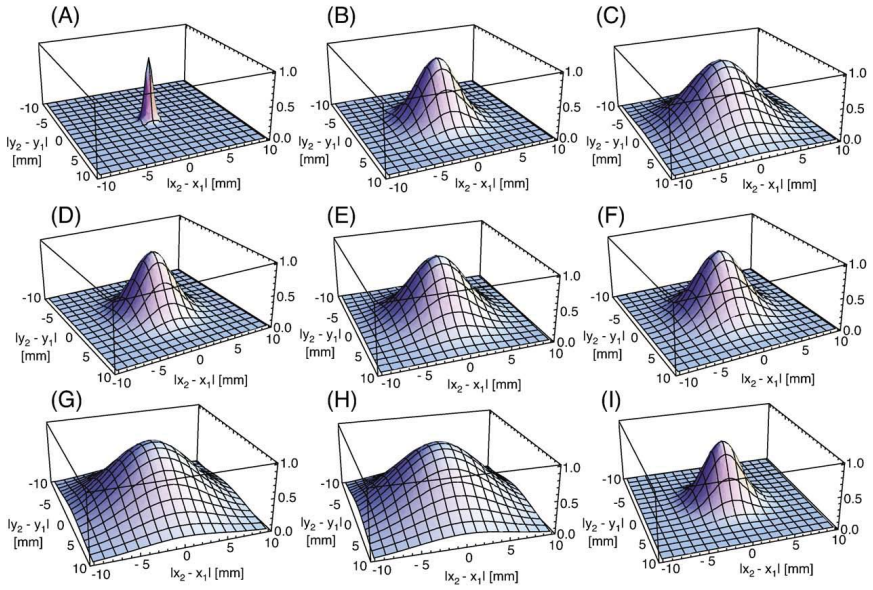

Figure 3.5: Evolution of the modulus of the spectral degree of coherence of the beam passing through the LIDAR system. The source plane (A), (D), (G), the target plane (B), (E), (H); the collecting lens plane (C), (F), (I). The parameters of the source and system are chosen to be: $\lambda = 1.55\mu m$, $C_n^2 = 10^{-14} m^{-2/3}$, $L = 500m$, $l_c = 1cm$; $\sigma_x = \sigma_y = 2.5cm$, $A_x = A_y = 1$. (A), (B), (C): $l_c = 1cm$, $\delta_{yy} = \delta_{xx} = 1mm$, (D), (E), (F) $l_c = 5mm$, $\delta_{yy} = \delta_{xx} = 5mm$; (G), (H), (I) $l_c = 1mm$, $\delta_{yy} = \delta_{xx} = 1cm$.

We will now employ the information of Fig. 3.5 for solving one inverse problem of target recognition. We will restrict ourselves to the case when the target is unbounded and planar, i.e. $W_R \to \infty$ and $f_1 \to \infty$ and will solely focus our attention on estimation of the r.m.s. width of target surface l_c.

It will be sufficient to consider the following example. Let us first fix the value of target roughness parameter, say at $l_c = 2mm$ and assume that it is known to the observer at the transceiver. Then we will compare in Fig. 3.6 the pairs of curves of the degree of coherence in the source (solid curves) and in the collecting lens (dashed curves) planes for six sets of source correlation coefficients. The case when the two curves are the closest to each other must provide an estimate of l_c: it should be approximately the same as the correlation coefficients. In Fig. 3.6(D) the two curves almost overlap - consequently the correlation coefficient $l_c \approx 5mm$. Since the actual value of l_c is $2mm$ we conclude that this fast technique can provide an estimate of the typical target roughness valid at least on the same order of magnitude. Multiple simulations that were run for various source, system and target parameters confirm this conclusion.

3.3.3 Sensing by the state of polarization

We will now turn to a more accurate technique for estimation of target roughness the one which involves measurement of polarization properties of the beam. Typically, the polarization state is acquired with the help of a set of four Stokes parameters (see Eq. (1.21)).

In Fig. 3.7 we demonstrate typical changes that the Stokes parameters of an electromagnetic Gaussian Schell-model beam undergo on passage through the LIDAR system. From this figure we notice that, similarly to the spectral density of the beam [62], the Stokes parameters broaden and the absolute values of maxima at the center of the beam can only decrease.

In Fig. 3.8 we show a typical evolution of the polarization ellipse (see Eqs. (1.22)-(1.23)) in the LIDAR system for both types of sources uniformly and non-uniformly polarized. We notice that in the case of the uniformly polarized source (Fig. 3.8, left

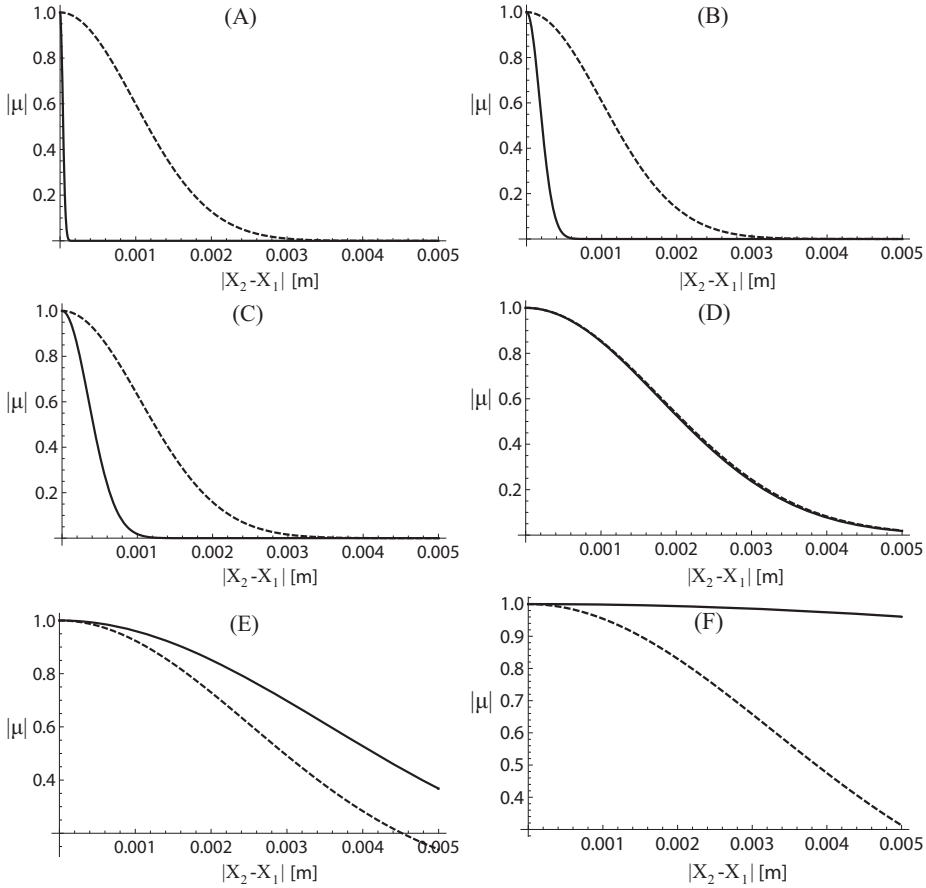

Figure 3.6: Comparison of the modulus of the degree of coherence in the source plane (solid curves) with that in the collector plane (dashed curves). The parameters of the source, system and target are: $\lambda = 1.55\mu m$, $C_n^2 = 10^{-14} m^{-2/3}$, $L = 1km$, $\sigma_x = \sigma_y = 2.5cm$; $A_x = A_y = 1$, $\delta_{xx} = \delta_{yy} = \delta$, $B_{xy} = 0$. (A) $\delta = 0.1mm$; (B) $\delta = 0.5mm$; (C) $\delta = 1mm$; (D) $\delta = 5mm$; (E) $\delta = 1cm$; (F) $\delta = 5cm$.

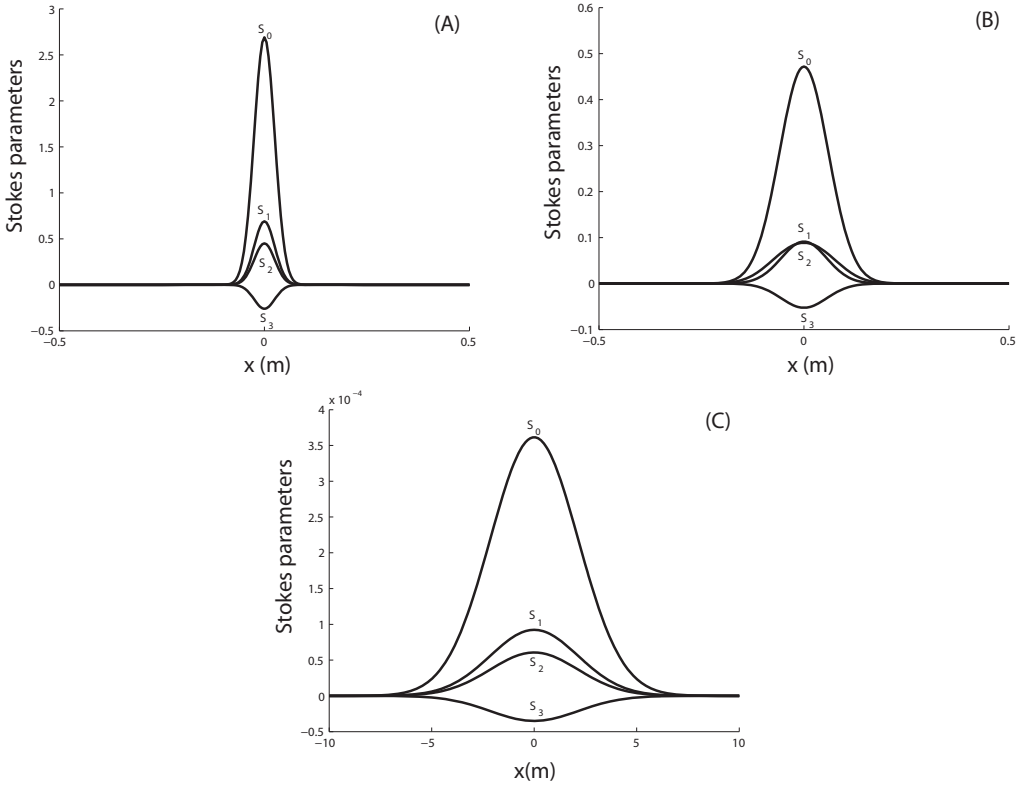

Figure 3.7: Propagation of Stokes parameters through a LIDAR system: (A) in the source plane; (B) in the target plane; (C) Collecting lens plane. Source, system and target parameters are chosen to be: $l_1 = 1.5km$, $f_1 = 10^6 m$, $W_R = 1m$, $l_c = 0.1mm$, $\lambda = 0.6328\mu m$, $A_x = 1.3$, $A_y = 1$, $B_{xy} = 0.2e^{-i\pi/6}$, $\sigma_x = \sigma_y = 2.5cm$, $\delta_{xx} = 5mm$, $\delta_{yy} = 7.5mm$, $\delta_{xy} = 1cm$.

column) the ellipse slightly rotates on passage from the source plane [Fig. 3.8(A)] to target plane [Fig. 3.8(C)] and then rotates back to its original value on passage from target to collector [Fig. 3.8(E)]. This effect is similar to line-of sight propagation of the polarization state of the beam at long distances. In this case the target acts on the beam the same way as long distance propagation in the atmosphere [69]. We also notice even though we have started from uniformly polarized beam in the target plane the polarization ellipses have different orientations; further in the collector plane the ellipses again acquire the same orientation. The same can be easily verified about the other normalized polarization properties such as degree of polarization (see also [62]) and the ellipticity of the beam (ratio of the semiaxes).

In the case of the non-uniformly polarized source (Fig. 3.8, right column) the ellipse typically rotates at a very large angle on a passage from the source [Fig. 3.8(B)] to the target [Fig. 3.8(D)] and does not change on propagation from target to collector [Fig. 3.8(F)], never returning to its original orientation. Such phenomenon is in agreement with results obtained for line-of sight propagation of non-uniformly polarized beams in atmospheric turbulence [70].

We now turn to the solution of the related inverse problem that we have already treated in the previous section. As we will now illustrate, it is possible in a number of situations to accurately predict the target surface r.m.s. width l_c, from the knowledge of the initial source correlations and the orientation angle of the on-axis polarization ellipse in the collecting lens plane. In Fig. 3.9(A), after fixing the source and system parameters, we plot the on-axis orientation angle of the polarization ellipse of the beam in the collecting plane, varying with l_c. All the correlation widths of the beam in the source plane were selected in the range from $1mm$ to $1cm$. We can see from the plot that the orientation angle θ in the collecting lens plane varies only when l_c goes through the same range of values. It is true for different values of C_n^2, even though for stronger turbulence (dotted curve) the range of variation becomes smaller.

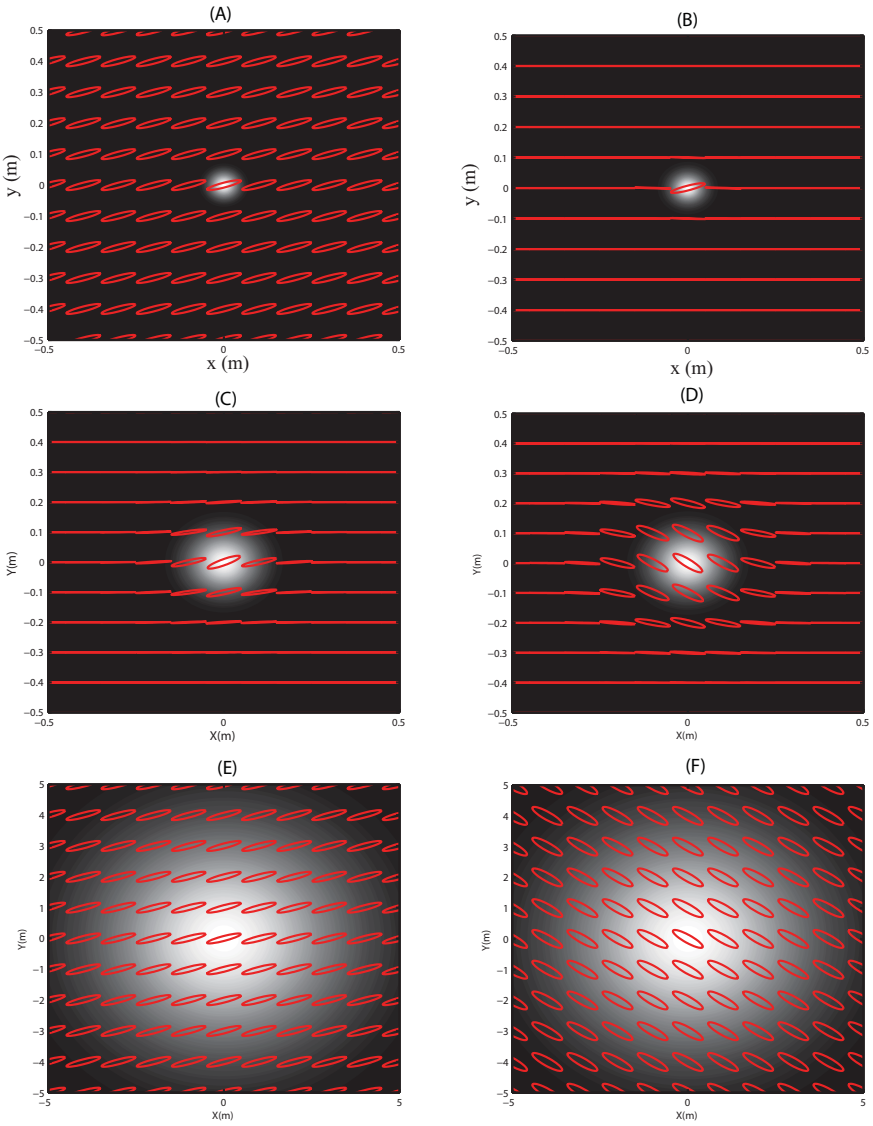

Figure 3.8: Propagation of polarization ellipses through a LIDAR system in case of a uniformly polarized source (with $\sigma_x = \sigma_y = 2.5cm$) (A), (C) and (E) and non-uniformly polarized source ($\sigma_x = 2.5cm$, $\sigma_y = 3.5cm$) (B), (D) and (F). Figures (A), (B) source plane; (C), (D) target plane; (E), (F) collecting lens plane. The other parameters of the source and of the system are the same as in Fig. 3.7.

In Figs. 3.9(B) and 3.9(C) we show the same setup as in Fig. 3.9(A) but for different incident beam parameters. In particular, in Fig. 3.9(B) the source correlations are all chosen to be in the range from $0.1mm$ to $1mm$ and we see that the variation of θ with l_c occurs exactly in the same range. Similarly for Fig. 3.9(C) the range of initial source correlations was chosen to be $6cm$ to $10cm$ and we find that, even though very slightly, θ varies in this range. Based on this analysis we can make the following conclusion: *if the source correlation coefficients are approximately equal to the r.m.s transverse target surface roughness l_c polarization properties of the beam in the collecting lens plane vary sharply with l_c.* This remark can be now used to solve the related inverse problem, i.e. the problem of finding l_c from the knowledge of initial beam correlations and changes in polarization state, for instance orientation angle "*theta*".

Let us consider the following example. Suppose the unbounded flat target has r.m.s. correlation width $l_c = 2mm$, which is not known at the transceiver. We aim to recover the value of l_c by analyzing the variation of the orientation angle θ with the source correlation parameters. In order to establish an efficient and legitimate "tuning" of the source correlations we will fix the initial correlations at starting values $\delta_{xx}^{(0)} = 6 \times 10^{-5}m$, $\delta_{yy}^{(0)} = 7.5 \times 10^{-5}m$ and $\delta_{yy}^{(0)} = 8.5 \times 10^{-5}m$. In order to establish the range of variation of these parameters we will multiply them by parameter $u \in [1; 1000]$. In Fig. 3.10 we show the variation of the orientation angle θ versus u. We see that when $u \approx 30$, which corresponds to the set of correlation coefficients $\delta_{xx} = 30 \times 6 \times 10^{-5} = 1.8mm$, $\delta_{yy} = 30 \times 7.5 \times 10^{-5} = 2.2mm$ and $\delta_{xy} = 30 \times 8.5 \times 10^{-5} = 2.5mm$, the change in θ is the largest. This implies that l_c should have approximately the same values. By recalling that l_c was initially chosen to be $2mm$ we find that the estimation is, in fact, very precise, and moreover is always exactly the average value of δ_{xx} and δ_{yy}, as this and multitude of other runs show.

Although our calculations in Figs. 3.9 and 3.10 pertain to uniformly polarized

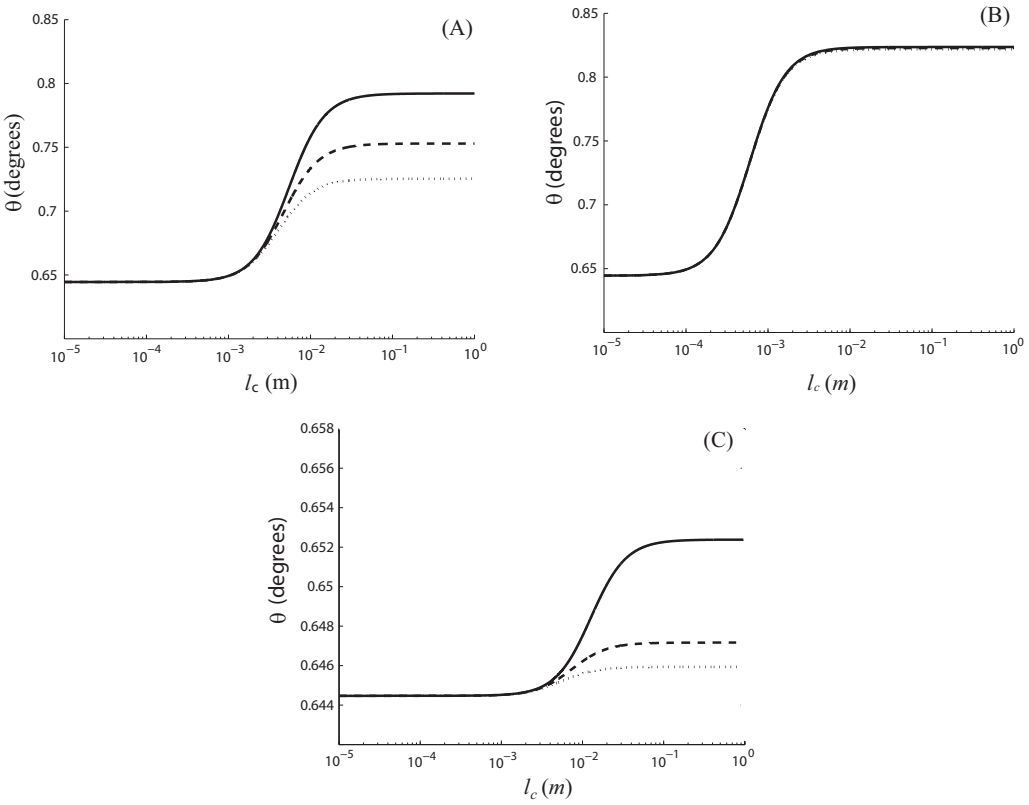

Figure 3.9: Orientation angle of the polarization ellipse at the collecting lens plane versus r.m.s. target surface roughness l_c for free space scenario (solid curve), for $C_n^2 = 5 \times 10^{-14}$ (dashed curve) and for $C_n^2 = 10^{-13}$ (dotted curve). Source and system parameters are: $\sigma_x = \sigma_y = 2.5cm$; $A_x = 0.1$; $A_y = 0.9$; $B_{xy} = 0.1$; $\lambda = 1.55 \times 10^{-6}m$, $l_1 = 1km$. (A) $\delta_{xx} = 6mm$; $\delta_{yy} = 7.5mm$; $\delta_{xy} = 8.5mm$; (B) $\delta_{xx} = 0.6mm$; $\delta_{yy} = 0.75mm$; $\delta_{xy} = 0.85mm$ (C) $\delta_{xx} = 6cm$; $\delta_{yy} = 7.5cm$; $\delta_{xy} = 8.5cm$.

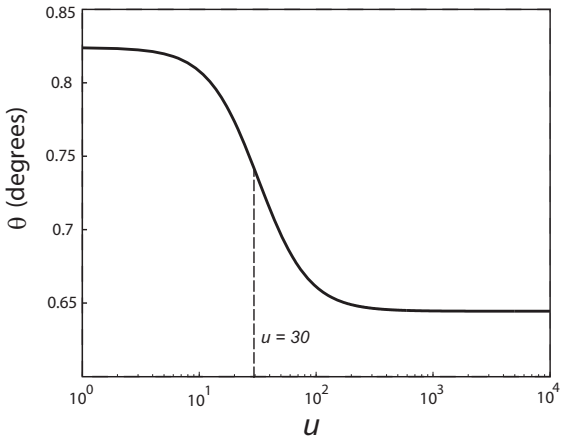

Figure 3.10: Variation of the orientation angle θ at the collecting lens with scaling parameter u. All other parameters of the source and of the system are the same as in Fig. 3.9.

sources similar results can be obtained in case when the source is non-uniformly polarized.

3.4 Conclusion

We have derived the expressions for the contrasts (scintillation indexes) of the Stokes parameters of GSM beams on propagation in turbulent atmosphere, and performed careful numerical analysis of the results. In particular, we revealed that some of the Stokes parameters have an undefined scintillation index at certain distances, others possess different trends compared with the intensity-based scintillation index. Our predictions can be used for creation of optical communication schemes which use Stokes parameters as information carriers.

We suggest two methods for estimation of r.m.s. surface roughness, l_c, of a target embedded in the turbulent atmosphere. Both methods are based on correlation-induced changes in electromagnetic stochastic beams on propagation. The first technique uses the degree of coherence of the electromagnetic beam which can be directly

measured [5], [71]. The second technique suggests measurement of the Stokes parameters and then calculation of one of the normalized polarization properties, say, the orientation angle of the polarization ellipse. While the method involving the measurement of the degree of coherence of the beam provides a rough estimate of l_c (on the order of magnitude), the technique based on the polarization state measurement recovers l_c with a remarkable accuracy. In any case the information that stochastic electromagnetic beams may carry in many circumstances is sufficient for identification of the nature of the target.

Chapter 4

Scattering of Random Light Beams

4.1 Description

Using the angular spectrum representation of fields and the first Born approximation we develop a theory of scattering of scalar waves with arbitrary spectral composition and correlation properties from collections of particles which have either deterministic or random distributions of the index of refraction and locations. An example illustrating the far-field intensity and the far-field spectral degree of coherence produced on scattering of a model field from deterministic collections of several particles with Gaussian potentials is considered.

Further, using scattering matrices and the angular spectrum representation of waves, we develop the analytical theory of scattering of random scalar waves from random collections of particles, valid under the first Born approximation. We demonstrate that in the calculation of far-field statistics, such as the spectral density and the spectral degree of coherence, the knowledge of the pair-structure factor of the collection is crucial. We illustrate our analytical approach by considering a numerical example involving scattering of two partially correlated plane waves from a random distribution of spheres.

A three-dimensional multi-Gaussian function, being a finite sum of Gaussian functions, is adopted for modeling a spherically symmetric scatterer with a semisoft boundary, i.e. one that has a continuous and adjustable drop in the index of refraction. A Gaussian sphere and a hard sphere are the two limiting cases when the number of terms in multi-Gaussian distribution is one and infinity, respectively. The

effect of the boundary's softness on the intensity distribution of the scattered wave is revealed. The generalization of the model to random scatterers with semisoft boundaries is also outlined.

4.2 Scattering of scalar light fields from collections of particles

In a recent publication [72] a new theory was developed that makes it possible to study scattering of scalar fields of arbitrary spectral composition and coherence properties from deterministic and random continuous scatterers. The combination of scattering matrix theory and the angular spectrum decomposition of fields employed in Ref. [72] made the treatment of complex phenomenon of scattering complete and simple. Following Ref. [72] we will first review the theory of scattering of scalar fields with arbitrary spectral and coherence properties from static deterministic or random media. Let us first consider a monochromatic scalar field at a point with position vector $\mathbf{r}$ and frequency ω, $U^{(i)}(\mathbf{r};\omega)e^{-i\omega t}$, propagating into the half-space $z > 0$. Its space-dependent part can be represented in the form of the angular spectrum of plane waves

$$U^{(i)}(\mathbf{r};\omega) = \iint a^{(i)}(\mathbf{u};\omega)e^{ik(\mathbf{u}_\perp\cdot\mathbf{r}+u_z z)}d^2\mathbf{u}_\perp, \tag{4.1}$$

where integration extends over the u_x, u_y plane. Here $k = \omega/c$ is the wave-number, c being the speed of light in vacuum; $\mathbf{u} = (u_x, u_y, u_z)$ is a unit vector, $\mathbf{u}_\perp = (u_x, u_y, 0)$ and

$$u_z = \sqrt{1 - |\mathbf{u}_\perp|^2}, \quad when \quad |\mathbf{u}_\perp| \leq 1 \quad (homogeneous \quad waves) \tag{4.2a}$$

$$= i\sqrt{|\mathbf{u}_\perp|^2 - 1}, \quad when \quad |\mathbf{u}_\perp| > 1 \quad (evanescent \quad waves). \tag{4.2b}$$

It was shown in Refs. [72] and [73] that the total field produced on scattering,

being the sum of the incident and the scattered fields, can be calculated by the formula

$$U^{(t)}(\mathbf{r};\omega) = \iint a^{(t)}(\mathbf{u};\omega) e^{ik(\mathbf{u}_\perp \cdot \mathbf{r} \pm u_z z)} d^2\mathbf{u}_\perp, \tag{4.3}$$

where the scattering amplitude of the total scattered field is given by the expression

$$a^{(t)}(\mathbf{u},\omega) = \mathbb{S}(\mathbf{u},\mathbf{u}',\omega) a^{(i)}(\mathbf{u}',\omega), \tag{4.4}$$

$\mathbb{S}$ being the spectral scattering matrix. The positive or negative sign in Eq. (4.3) must be chosen for forward-scattering and back-scattering portions of the scattered field, respectively.

If the field incident on the scatterer is stochastic, wide-sense statistically stationary, then its second-order, two-point spatial correlation properties (in the frequency domain) can be characterized by the cross-spectral density function (Eq. (1.57)), or by its angular correlation function

$$\mathcal{A}^{(i)}(\mathbf{u}_1,\mathbf{u}_2;\omega) = \langle a^{(i)*}(\mathbf{u}_1;\omega) a^{(i)}(\mathbf{u}_2;\omega)\rangle, \tag{4.5}$$

which can be shown to be the four-dimensional Fourier transform of $W^{(i)}$ [72]. The cross-spectral density matrix of the total scattered field then becomes

$$\begin{aligned} W^{(t)}(\mathbf{r}_1,\mathbf{r}_2;\omega) &= \langle U^{(t)*}(\mathbf{r}_1;\omega) U^{(t)}(\mathbf{r}_2;\omega)\rangle \\ &= \iiiint \mathbb{M}(\mathbf{u}_1,\mathbf{u}_2;\mathbf{u}_1',\mathbf{u}_2';\omega) \mathcal{A}^{(i)}(\mathbf{u}_1',\mathbf{u}_2';\omega) \\ &\quad \times e^{ik(\mathbf{u}_2\cdot\mathbf{r}_2 - \mathbf{u}_1\cdot\mathbf{r}_1)} d^2\mathbf{u}_{1\perp} d^2\mathbf{u}_{2\perp} d^2\mathbf{u}_{1\perp}' d^2\mathbf{u}_{2\perp}', \end{aligned} \tag{4.6}$$

where

$$\mathbb{M}(\mathbf{u}_1,\mathbf{u}_1',\mathbf{u}_2,\mathbf{u}_2';\omega) = \mathbb{S}^*(\mathbf{u}_1,\mathbf{u}_1';\omega)\mathbb{S}(\mathbf{u}_2,\mathbf{u}_2';\omega). \tag{4.7}$$

is the pair scattering matrix [72].

Under the first Born approximation the scattering matrix may be expressed in terms of the scattering potential in a simple manner. Let $n(\mathbf{r},\omega)$ be the refractive index distribution throughout the scatterer. The scattering potential $F(\mathbf{r},\omega)$ was given in terms of the refractive index (Eq. (1.49)), in this situation the *pair-scattering matrix* of the total field takes the form

$$\mathbb{M}(\mathbf{u}_1,\mathbf{u}_2;\mathbf{u}_1',\mathbf{u}_2';\omega)=\tilde{F}^*[k(\mathbf{u}_1-\mathbf{u}_1'),\omega]\tilde{F}[k(\mathbf{u}_2-\mathbf{u}_2'),\omega]. \tag{4.8}$$

where tilde denotes the two dimensional Fourier transform. In the case when the scatterer is random the expression above generalizes to

$$\mathbb{M}(\mathbf{u}_1,\mathbf{u}_1',\mathbf{u}_2,\mathbf{u}_2';\omega)=\langle\mathbb{S}^*(\mathbf{u}_1,\mathbf{u}_1';\omega)\mathbb{S}(\mathbf{u}_2,\mathbf{u}_2';\omega)\rangle_{rm}, \tag{4.9}$$

where $\langle\cdot\rangle_{rm}$ denotes the average taken over the ensemble of realizations of the scattering medium.

In particular, in the far field of the scatterer the total field $U^{(t)}$ and the cross-spectral density function $W^{(t)}$ along directions specified by unit vectors $\mathbf{u}_1$ and $\mathbf{u}_2$ reduce to the forms [72]:

$$U^{(t)}(r\mathbf{u},\omega)\approx\pm\frac{2\pi i u_z}{k}\frac{e^{ikr}}{r}\int\mathbb{S}(\mathbf{u},\mathbf{u}',\omega)a^{(i)}(\mathbf{u}',\omega)d^2\mathbf{u}_\perp', \tag{4.10}$$

$$\begin{aligned}W^{(t)}(r\mathbf{u}_1,r\mathbf{u}_2;\omega)\approx\pm\frac{4\pi^2}{k^2r^2}u_{z1}u_{z2}\int\int\mathbb{M}(\mathbf{u}_1,\mathbf{u}_2;\mathbf{u}_1',\mathbf{u}_2';\omega)\\ \times\mathcal{A}^{(i)}(\mathbf{u}_1',\mathbf{u}_2';\omega)d^2\mathbf{u}_1'd^2\mathbf{u}_2'.\end{aligned} \tag{4.11}$$

With the help of the cross-spectral density function $W^{(t)}(\mathbf{r}_1,\mathbf{r}_2;\omega)$ (Eq.(4.6)) we may at once determine the spectrum $S^{(t)}(\mathbf{r};\omega)$ (Eq.(1.15)) and the spectral degree of coherence $\mu^{(t)}(\mathbf{r}_1,\mathbf{r}_2;\omega)$ (Eq.(1.14)) of the total field.

Suppose that light is being scattered from a static collection of particles of L

different types which occupy domain D (see Fig. 4.1). To characterize the response of such a collection to the incident light the discrete-particle model is then used, in which the scattering potential $F(\mathbf{r},\omega)$ of the collection can be represented by a finite sum of potentials of individual scatterers, i.e.

$$F(\mathbf{r},\omega) = \sum_{l=1}^{L}\sum_{m=1}^{M_l} f_l(\mathbf{r}-\mathbf{r}_m,\omega), \tag{4.12}$$

where $\mathbf{r}_m$ is the location of a scattering center, f_l is the scattering potential of the scatterer of type l, M_l is the number of particles of type l.

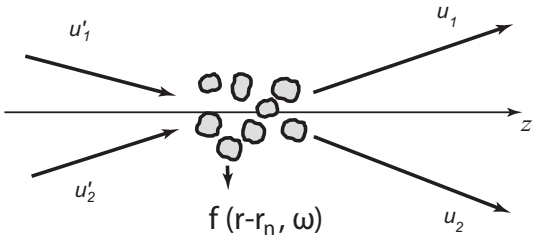

Figure 4.1: Notation relating to the scattering of two correlated plane waves from a collection of particles.

In the case when the collection is static but random one can characterize its response with the help of the correlation function of the scattering potential which reduces for the particulate medium to the form [Ref. [5], Sec. 6.3.1]

$$\begin{aligned} C_F(\mathbf{r}_1,\mathbf{r}_2,\omega) &= \langle F^*(\mathbf{r}_1,\omega)F(\mathbf{r}_2,\omega)\rangle_{rm} \\ &= \sum_{l=1}^{L}\sum_{j=1}^{L}\sum_{m=1}^{M_l}\sum_{n=1}^{N_j}\langle f_l^*(\mathbf{r}-\mathbf{r}_m,\omega)f_j(\mathbf{r}-\mathbf{r}_n,\omega)\rangle_{rm}. \end{aligned} \tag{4.13}$$

If all particles in the collection are identical the summations over indexes l and j in

the expressions (4.12) and (4.13) may be omitted and they become

$$F(\mathbf{r},\omega)=\sum_{n=1}^{N} f(\mathbf{r}-\mathbf{r}_n,\omega), \tag{4.14}$$

$$C_F(\mathbf{r}_1,\mathbf{r}_2,\omega)=\sum_{m=1}^{M}\sum_{n=1}^{N}\langle f^*(\mathbf{r}_1-\mathbf{r}_m,\omega)f(\mathbf{r}_2-\mathbf{r}_n,\omega)\rangle_{rm}. \tag{4.15}$$

In scattering from collections of particles by scalar wave-fields several cases should be differentiated. The incident field can be either deterministic or stochastic and, besides, particles can form a deterministic (Sec. 4.2.1) or random collection (Sec. 4.2.3).

4.2.1 Scattering from deterministic collections

We begin by considering the simplest situation when the incident field, say $U^{(i)}(\mathbf{r},\omega)$, is deterministic and it is scattered from a deterministic collection of particles, i.e. the distribution of the refractive index within particles and their locations are deterministic. In this case the scattering potential of the system of n (identical) particles is given by Eq. (4.14).

In this case, within the validity of the first Born approximation the scattering matrix takes the form (Ref. [72], Eq. (35))

$$\mathbb{S}(\mathbf{u},\mathbf{u}',\omega)=\mathcal{F}[F(\mathbf{r},\omega)]=\sum_{n=1}^{N}\mathcal{F}[f(\mathbf{r}-\mathbf{r}_n,\omega)]. \tag{4.16}$$

where $\mathcal{F}$ denotes two-dimensional Fourier transform.

On performing Fourier transforms of potentials of individual particles with the

help of variables $\mathbf{R}_n = \mathbf{r} - \mathbf{r}_n$ (n=1...N) we find that

$$\mathbb{S}(\mathbf{u}, \mathbf{u}', \omega) = \sum_{n=1}^{N} e^{-i\mathbf{r}_n \cdot \mathbf{K}} \tilde{f}[\mathbf{K}, \omega], \tag{4.17}$$

where $\mathbf{K} = k(\mathbf{u} - \mathbf{u}')$ is the so-called momentum-transfer vector.

The total scattered field produced on scattering can be found with the help of Eqs. (4.3), (4.4) and (4.17) to be

$$\begin{aligned} U^{(t)}(\mathbf{r}, \omega) = \sum_{n=1}^{N} \iint e^{-i\mathbf{r}_n \cdot \mathbf{K}} \tilde{f}[\mathbf{K}, \omega] \\ \times a^{(i)}(\mathbf{u}', \omega) e^{-ik(\mathbf{u}_\perp \cdot \mathbf{r} \pm u_z z)} d^2\mathbf{u}_\perp d^2\mathbf{u}'_\perp. \end{aligned} \tag{4.18}$$

In the far-zone of the scatterer the total field reduces to the expression involving single integral, i.e.

$$U^{(t)}(r\mathbf{u}, \omega) = \pm \frac{2\pi i u_z}{k} \frac{e^{ikr}}{r} \sum_{n=1}^{N} e^{-ik\mathbf{r}_n \cdot \mathbf{u}} \int e^{ik\mathbf{r}_n \cdot \mathbf{u}'} \tilde{f}[\mathbf{K}, \omega] a^{(i)}(\mathbf{u}', \omega) d^2\mathbf{u}'_\perp. \tag{4.19}$$

We will now consider the case when the field incident on the system of particles is stochastic and is characterized by the cross-spectral density function $W^{(i)}(\mathbf{r}_1, \mathbf{r}_2, \omega)$. The cross-spectral density function of the total scattered field is then given by expression (4.6). Noting that [see Eq. (4.17)]

$$\mathbb{S}^*(\mathbf{u}_1, \mathbf{u}'_1, \omega) \mathbb{S}(\mathbf{u}_2, \mathbf{u}'_2, \omega) = \sum_{m=1}^{M} \sum_{n=1}^{N} e^{-i[\mathbf{K}_2 \cdot \mathbf{r}_n - \mathbf{K}_1 \cdot \mathbf{r}_m]} \tilde{f}^*(-\mathbf{K}_1, \omega) \tilde{f}(\mathbf{K}_2, \omega), \tag{4.20}$$

where $\mathbf{K}_\alpha = k(\mathbf{u}_\alpha - \mathbf{u}'_\alpha) \quad (\alpha = 1, 2)$, we find, on substituting from Eq. (4.20) into

Eq. (4.6) that

$$W^{(t)}(\mathbf{r}_1,\mathbf{r}_2,\omega)=\sum_{m=1}^{M}\sum_{n=1}^{N}\iiiint e^{-i[\mathbf{K}_2\cdot\mathbf{r}_n-\mathbf{K}_1\cdot\mathbf{r}_m]}\tilde{f}^*(-\mathbf{K}_1,\omega)\tilde{f}(\mathbf{K}_2,\omega) \times\mathcal{A}^{(i)}(\mathbf{u}_1',\mathbf{u}_2',\omega)e^{ik(\mathbf{u}_2\cdot\mathbf{r}_2-\mathbf{u}_1\cdot\mathbf{r}_1)}d^2\mathbf{u}_{1\perp}d^2\mathbf{u}_{2\perp}d^2\mathbf{u}_{1\perp}'d^2\mathbf{u}_{2\perp}'. \tag{4.21}$$

In the far zone of the scattering volume the last equation reduces to the formula

$$W^{(t)}(r\mathbf{u}_1,r\mathbf{u}_2,\omega)=\pm\frac{4\pi^2}{k^2r^2}u_{1z}u_{2z}\sum_{m=1}^{M}\sum_{n=1}^{N}\iint e^{-i[\mathbf{K}_2\cdot\mathbf{r}_n-\mathbf{K}_1\cdot\mathbf{r}_m]} \times\tilde{f}^*(-\mathbf{K}_1,\omega)\tilde{f}(\mathbf{K}_2,\omega)\mathcal{A}^{(i)}(\mathbf{u}_1',\mathbf{u}_2',\omega)d^2\mathbf{u}_{1\perp}'d^2\mathbf{u}_{2\perp}'. \tag{4.22}$$

4.2.2 Application of the theory to two partially correlated polychromatic plane waves incident on a deterministic medium

As an application to the theory discussed in Sec. 4.2.1 we consider the incident field $U^{(i)}$ which consists of two mutually correlated polychromatic plane waves propagating along directions $\mathbf{u}_1'$ and $\mathbf{u}_2'$, and scattered from a collection of spheres. The spectral amplitude $a^{(i)}(\mathbf{u}',\omega)$ of the incident field has the form

$$a^{(i)}(\mathbf{u}',\omega)=a^{(i)}(\mathbf{u}_1',\omega)\delta^{(2)}(\mathbf{u}'-\mathbf{u}_1')+a^{(i)}(\mathbf{u}_2',\omega)\delta^{(2)}(\mathbf{u}'-\mathbf{u}_2'), \tag{4.23}$$

$\delta^{(2)}(\mathbf{u})$ being the spherical Dirac delta-function.

On substituting from Eq. (4.23) into Eq. (4.5), we find that the angular correlation

function of the incident field takes the form

$$\begin{aligned}\mathcal{A}^{(i)}(\mathbf{u}_1', \mathbf{u}_2'; \omega) = &\mathfrak{a}(\mathbf{u}_1', \mathbf{u}_1'; \omega)\delta^{(2)}(\mathbf{u}' - \mathbf{u}_1')\delta^{(2)}(\mathbf{u}' - \mathbf{u}_1') \\ &+ \mathfrak{a}(\mathbf{u}_2', \mathbf{u}_2'; \omega)\delta^{(2)}(\mathbf{u}' - \mathbf{u}_2')\delta^{(2)}(\mathbf{u}' - \mathbf{u}_2') \\ &+ \mathfrak{a}(\mathbf{u}_1', \mathbf{u}_2'; \omega)\delta^{(2)}(\mathbf{u}' - \mathbf{u}_1')\delta^{(2)}(\mathbf{u}' - \mathbf{u}_2') \\ &+ \mathfrak{a}(\mathbf{u}_2', \mathbf{u}_1'; \omega)\delta^{(2)}(\mathbf{u}' - \mathbf{u}_2')\delta^{(2)}(\mathbf{u}' - \mathbf{u}_1'),\end{aligned} \tag{4.24}$$

where the angular correlation function $\mathfrak{a}(\mathbf{u}_1', \mathbf{u}_2'; \omega)$ is assumed to be Gaussian, i.e

$$\mathfrak{a}(\mathbf{u}_p', \mathbf{u}_q'; \omega) = \mathfrak{a}_{pq} e^{-\frac{k^2\Delta^2}{2}(\mathbf{u}_q' - \mathbf{u}_p')^2} \qquad (p, q = 1, 2), \tag{4.25}$$

where $\mathfrak{a}_{pq}$ and Δ may depend, in general, on frequency ω.

Suppose that the scatterers are spherical centered at points $\mathbf{r}_c = (x_n, y_n, z_n)$, having a three-dimensional (soft) Gaussian potential

$$f(\mathbf{r}_n; \omega) = Bexp\left[-\frac{(x - x_n)^2 + (y - y_n)^2 + (z - z_n)^2}{2\sigma^2}\right]. \tag{4.26}$$

The variance σ^2 is taken to be independent of position but, in general, will depend on the frequency. On calculating three-dimensional Fourier transform of the expression (4.26) we find that

$$\widetilde{F}(\mathbf{K}; \omega) = B(2\pi)^{(3/2)}\sigma^3 e^{-K^2\sigma^2/2} \sum_{n=1}^{N} e^{ix_nK_x} e^{iy_nK_y} e^{iz_nK_z}. \tag{4.27}$$

On substituting from Eq. (4.47) into Eq. (4.8) and setting $\mathbf{K} = k(\mathbf{u} - \mathbf{u}')$ we find that, within the accuracy of the first Born approximation, the pair scattering matrix

has the form

$$\begin{aligned}
&\mathbb{M}^{(1)}(\mathbf{u}_1,\mathbf{u}_2;\mathbf{u}_1',\mathbf{u}_2';\omega) = B^2(2\pi)^3\sigma^6 \\
&\times \big(e^{-\frac{k^2\sigma^2}{2}(\mathbf{u}_1-\mathbf{u}_1')^2}\sum_{n=1}^{N} e^{-ikx_n(u_{1x}-u_{1x}')}e^{-iky_n(u_{1y}-u_{1y}')}e^{-ikz_n(u_{1z}-u_{1z}')}\big) \\
&\times \big(e^{-\frac{k^2\sigma^2}{2}(\mathbf{u}_2-\mathbf{u}_2')^2}\sum_{n=1}^{N} e^{ikx_n(u_{2x}-u_{2x}')}e^{iky_n(u_{2y}-u_{2y}')}e^{ikz_n(u_{2z}-u_{2z}')}\big).
\end{aligned} \tag{4.28}$$

When we substitute from Eqs. (4.25) and (4.28) (with the help of Eq. (4.24)) first into Eq. (4.11) and then into Eq. (1.15) we obtain the formula for the spectral density of the far field

$$\begin{aligned}
&S^{(t)}(r\mathbf{u};\omega) = \frac{B^2(2\pi)^5\sigma^6 u_z^2}{k^2r^2}\times \\
&\Bigg\{ e^{-k^2\sigma^2(\mathbf{u}-\mathbf{u}_1')^2}\big(\sum_{n=1}^{N} e^{-ikx_n(u_x-u_{1x}')}e^{-iky_n(u_y-u_{1y}')}e^{-ikz_n(u_z-u_{1z}')} \\
&\times \sum_{n=1}^{N} e^{ikx_n(u_x-u_{1x}')}e^{iky_n(u_y-u_{1y}')}e^{ikz_n(u_z-u_{1z}')}\big)\mathfrak{a}_{11} \\
&+ e^{-k^2\sigma^2(\mathbf{u}-\mathbf{u}_2')^2}\big(\sum_{n=1}^{N} e^{-ikx_n(u_x-u_{2x}')}e^{-iky_n(u_y-u_{2y}')}e^{-ikz_n(u_z-u_{2z}')} \\
&\times \sum_{n=1}^{N} e^{ikx_n(u_x-u_{2x}')}e^{iky_n(u_y-u_{2y}')}e^{ikz_n(u_z-u_{2z}')}\big)\mathfrak{a}_{22} + \\
&2e^{-\frac{k^2\sigma^2}{2}(\mathbf{u}-\mathbf{u}_1')^2}e^{-\frac{k^2\sigma^2}{2}(\mathbf{u}-\mathbf{u}_2')^2}e^{-\frac{k^2\Delta^2}{2}(\mathbf{u}_2'-\mathbf{u}_1')^2} \\
&\times Re\Big\{\mathfrak{a}_{12}\big(\sum_{n=1}^{N} e^{-ikx_n(u_x-u_{1x}')}e^{-iky_n(u_y-u_{1y}')}e^{-ikz_n(u_z-u_{1z}')} \\
&\times \sum_{n=1}^{N} e^{ikx_n(u_x-u_{2x}')}e^{iky_n(u_y-u_{2y}')}e^{ikz_n(u_z-u_{2z}')}\big)\Big\}\Bigg\}.
\end{aligned} \tag{4.29}$$

In Fig. 4.2 we show distributions of 1, 2, 5 and 10 spheres that we used for all our numerical examples (Figs. 3-6). The parameters used for all of the numerical calculations are: $\lambda = 0.633\times 10^{-6}m$, $B = 1$, $a_1 = 0.6e^{i\pi/7}$, $a_2 = 0.9e^{i\pi/6}$.

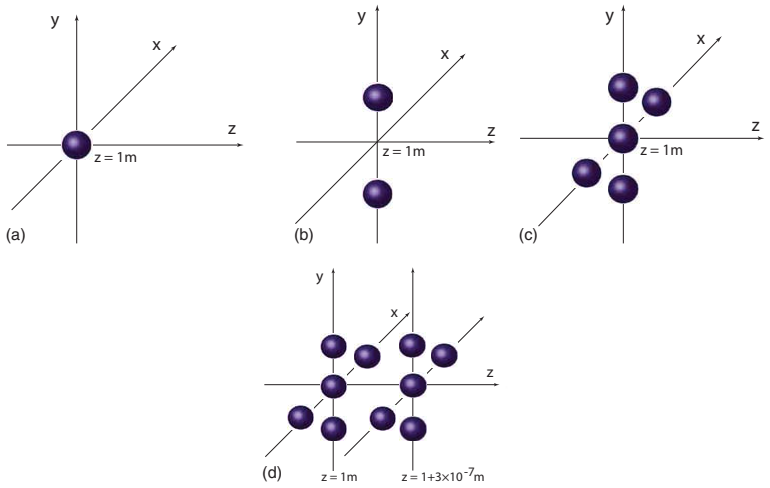

Figure 4.2: The coordinates of the particles, (a) $(0, 0, 1m)$, (b) $(0, 3 \times 10^{-7}m, 1m)$, $(0, -3 \times 10^{-7}m, 1m)$, (c) $(0, 0, 1m)$, $(0, 3 \times 10^{-7}m, 1m)$, $(0, -3 \times 10^{-7}m, 1m)$, $(3 \times 10^{-7}m, 0, 1m)$, $(-3 \times 10^{-7}m, 0, 1m)$, (d) $(0, 0, 1m)$, $(0, 3 \times 10^{-7}m, 1m)$, $(0, -3 \times 10^{-7}m, 1m)$, $(3 \times 10^{-7}m, 0, 1m)$, $(-3 \times 10^{-7}m, 0, 1m)$, $(0, 0, 1 + 3 \times 10^{-7}m)$, $(0, 3 \times 10^{-7}m, 1 + 3 \times 10^{-7}m)$, $(0, -3 \times 10^{-7}m, 1 + 3 \times 10^{-7}m)$, $(3 \times 10^{-7}m, 0, 1 + 3 \times 10^{-7}m)$, $(-3 \times 10^{-7}m, 0, 1 + 3 \times 10^{-7}m)$.

In Figs. 4.3-4.5 we illustrate the behavior of the spectral density of the far field calculated from Eq.(4.29) and normalized by the factor $B^2(2\pi)^5\sigma^6 u_z^2/k^2r^2$. By these sets of contour-plots we show the dependence of spectral density distribution on various parameters of the incident field and of the particle system. Angles θ and ϕ are the polar and the azimuthal angles of the unit vector $\mathbf{u}$ in spherical coordinates, i.e. $u_x = cos\theta cos\phi$, $u_y = cos\theta sin\phi$, $u_z = sin\theta$. Angles $\theta'_{1,2}$, $\phi'_{1,2}$ are the polar and azimuthal angles of vectors $\mathbf{u}'_{1,2}$ in spherical coordinates. For figures 3-5 we have chosen the directions of the incident field to be: $\theta'_1 = -\pi/4$; $\phi'_1 = -\pi/3$; $\theta'_2 = \pi/6$; $\phi'_2 = \pi/5$.

In Fig. 4.3 we show the behavior in spectral density of far fields as a number of particles in the system grows from 1 to 10 [see Fig. 4.2], provided the size of the individual particles as well as correlation and directions of the incident plane waves are kept fixed. One can see that with the increase of the number of particles from 1 to 5 [see figures 4.3(a)-4.3(c)] the distribution becomes more localized around two centers corresponding to directions of the incident plane waves. However, for larger number of particles, e.g. 10, [Fig. 4.3(d)], the localization becomes less pronounced again.

In Fig. 4.4 the spectral density of the far field is shown for four different values of the scaled size of the particles, $k\sigma$. As the size decreases the interference effects disappear (Fig. 4.4(a)) and the distribution becomes more localized (compare peak values in Figs. 4.4(a) and 4.4(b)). However with further decrease of $k\sigma$ the localization becomes less noticeable [Figs. 4.4(c) and 4.4(d)].

In Fig. 4.5 we compare the changes in far-field spectral density with the scaled degree of correlation $k\Delta$ of the incident plane waves. Figures 4.5(c) and 4.5(d) refer to 2-particles system. One can readily see that for two-particle system the influence of $k\Delta$ is less evident (compare 4.5(c) and 4.5(d)).

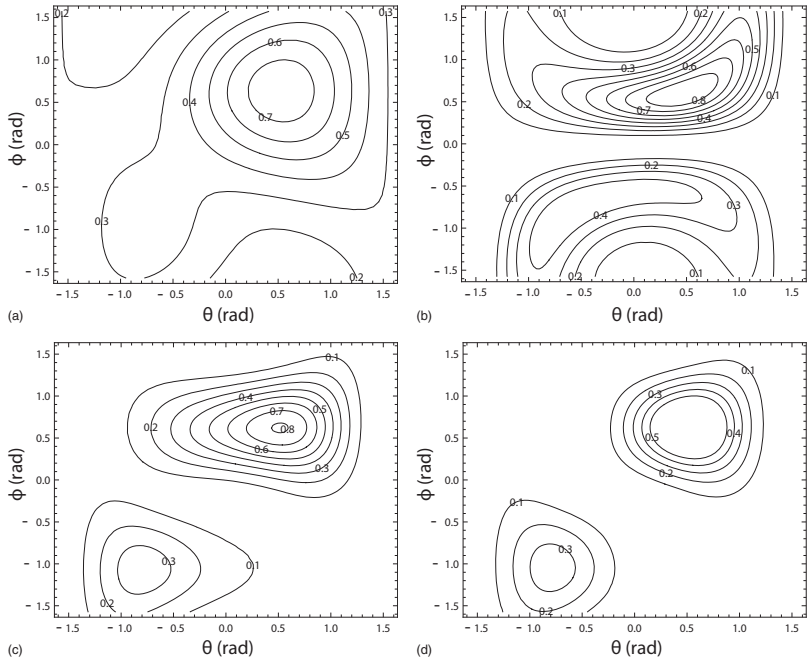

Figure 4.3: Contours of the spectral density of the far field produced by scattering of two correlated plane waves on particles with Gaussian potential. The parameters σ and Δ are kept fixed: $k\sigma = 1$, $k\Delta = 1$, (a) 1 particle; (b) 2 particles; (c) 5 particles; (d) 10 particles.

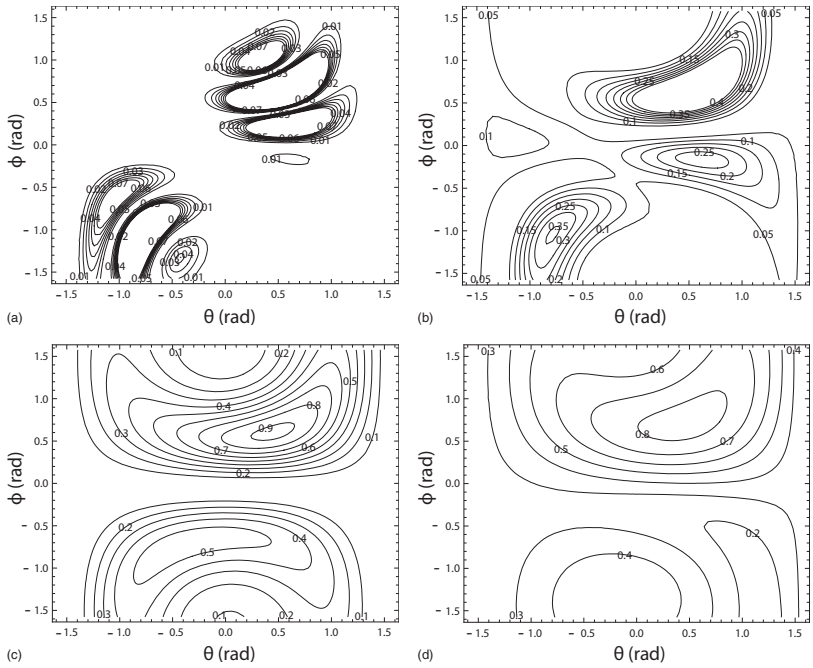

Figure 4.4: Contours of the spectral density of the far field produced by scattering of two correlated plane waves on two particles with Gaussian potential. The parameter Δ is kept fixed: $k\Delta = 1$, (a) $k\sigma = 3$; (b) $k\sigma = 1.5$ (c) $k\sigma = 0.9$; (d) $k\sigma = 0.5$.

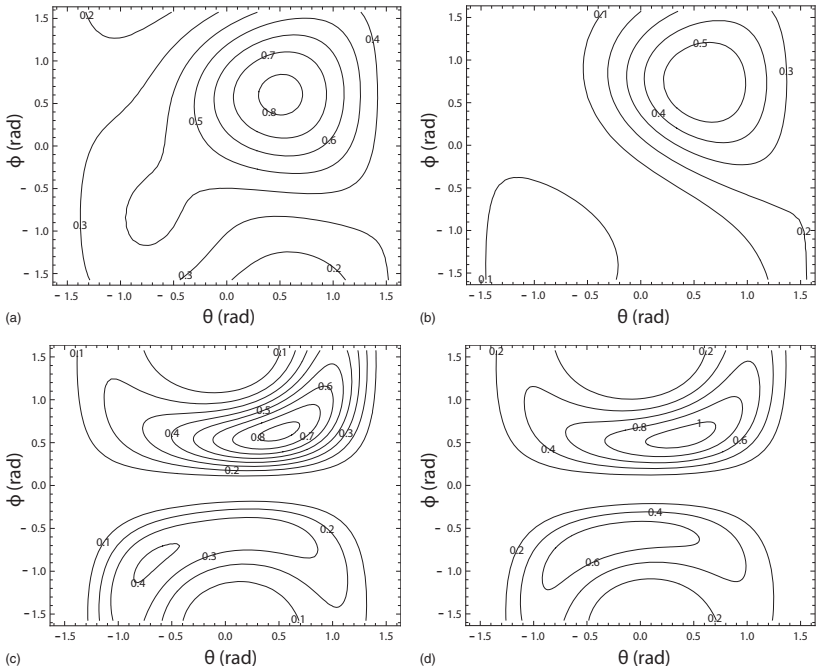

Figure 4.5: Contours of the spectral density of the far field, produced by scattering of two correlated plane waves on two particles with Gaussian potential. The parameter σ is kept fixed: $k\sigma = 1$, (a) One particle, $k\Delta = 10$; (b) One particle, $k\Delta = 0.1$; (c) Two particles, $k\Delta = 10$; (d) Two particles, $k\Delta = 0.1$.

On substituting from Eqs. (4.25) and (4.28) (with the help of (4.24)) first into Eq. (4.11) and then into Eq. (1.14) we now obtain the expression for the spectral degree of coherence of the far field produced on scattering of two correlated plane waves on the collection of spheres with Gaussian potentials

$$
\begin{aligned}
\mu^{(t)}(r\mathbf{u}_1, r\mathbf{u}_2;\omega) &= \frac{1}{\sqrt{S^{(t)}(r\mathbf{u}_1;\omega)}\sqrt{S^{(t)}(r\mathbf{u}_2;\omega)}}\times \\
&\Bigg\{ e^{-\frac{k^2\sigma^2}{2}(\mathbf{u}_1-\mathbf{u}_1')^2}\Big(\sum_{n=1}^{N} e^{-ikx_n(u_{1x}-u_{1x}')}e^{-iky_n(u_{1y}-u_{1y}')}e^{-ikz_n(u_{1z}-u_{1z}')}\Big) \\
&\times e^{-\frac{k^2\sigma^2}{2}(\mathbf{u}_2-\mathbf{u}_1')^2}\Big(\sum_{n=1}^{N} e^{ikx_n(u_{2x}-u_{1x}')}e^{iky_n(u_{2y}-u_{1y}')}e^{ikz_n(u_{2z}-u_{1z}')}\Big)\mathfrak{a}_{11} \\
&+ e^{-\frac{k^2\sigma^2}{2}(\mathbf{u}_1-\mathbf{u}_2')^2}\Big(\sum_{n=1}^{N} e^{-ikx_n(u_{1x}-u_{2x}')}e^{-iky_n(u_{1y}-u_{2y}')}e^{-ikz_n(u_{1z}-u_{2z}')}\Big) \\
&\times e^{-\frac{k^2\sigma^2}{2}(\mathbf{u}_2-\mathbf{u}_2')^2}\Big(\sum_{n=1}^{N} e^{ikx_n(u_{2x}-u_{2x}')}e^{iky_n(u_{2y}-u_{2y}')}e^{ikz_n(u_{2z}-u_{2z}')}\Big)\mathfrak{a}_{22} \\
&+ \Bigg[e^{-\frac{k^2\sigma^2}{2}(\mathbf{u}_1-\mathbf{u}_1')^2}\Big(\sum_{n=1}^{N} e^{-ikx_n(u_{1x}-u_{1x}')}e^{-iky_n(u_{1y}-u_{1y}')}e^{-ikz_n(u_{1z}-u_{1z}')}\Big) \\
&\times e^{-\frac{k^2\sigma^2}{2}(\mathbf{u}_2-\mathbf{u}_2')^2}\Big(\sum_{n=1}^{N} e^{ikx_n(u_{2x}-u_{2x}')}e^{iky_n(u_{2y}-u_{2y}')}e^{ikz_n(u_{2z}-u_{2z}')}\Big)\mathfrak{a}_{12} \\
&+ e^{-\frac{k^2\sigma^2}{2}(\mathbf{u}_1-\mathbf{u}_2')^2}\Big(\sum_{n=1}^{N} e^{-ikx_n(u_{1x}-u_{2x}')}e^{-iky_n(u_{1y}-u_{2y}')}e^{-ikz_n(u_{1z}-u_{2z}')}\Big) \\
&\times e^{-\frac{k^2\sigma^2}{2}(\mathbf{u}_2-\mathbf{u}_1')^2}\Big(\sum_{n=1}^{N} e^{ikx_n(u_{2x}-u_{1x}')}e^{iky_n(u_{2y}-u_{1y}')}e^{ikz_n(u_{2z}-u_{1z}')}\Big)\mathfrak{a}_{21}\Bigg] \\
&\times e^{-\frac{k^2\Delta^2}{2}(\mathbf{u}_1'-\mathbf{u}_2')^2}\Bigg\}.
\end{aligned}
\tag{4.30}
$$

Figure 4.6 shows the behavior of the modulus of the spectral degree of coherence, $|\mu^{(t)}(r\mathbf{u}_1, r\mathbf{u}_2;\omega)|$, of the far-field calculated from Eq. (4.30). We assume that the plane waves are incident on the collection of spheres along directions specified by polar angles $\phi_1' = \pi/2$, $\phi_2' = -\pi/2$ and azimuthal angles $\theta_1' = \theta_2' = 0.3$ rad. The modulus of the degree of coherence of the scattered field was calculated as a function

of the angle $\theta_d = \theta_2 - \theta_1$, while the other angles were kept fixed: $\theta_1 = 0$, $\phi_1 = \pi/2$, $\phi_2 = \pi/2$.

In Fig. 4.6(a) the behavior of $|\mu^{(t)}(r\mathbf{u}_1, r\mathbf{u}_2; \omega)|$ for four collections of particles (see Fig. 4.2) is plotted. The appearance of interference effects is obviously seen starting from the case $n = 2$. Figure 4.6(b) shows the influence of different values of σ on scattering from five particles when $k\Delta = 1$. In Fig. 4.6(c) we illustrate the effect of the scaled correlation parameter $k\Delta$ of the incident plane waves on the scattered spectral density scattered from five particles, while the scaled size of the spheres $k\sigma$ is kept fixed.

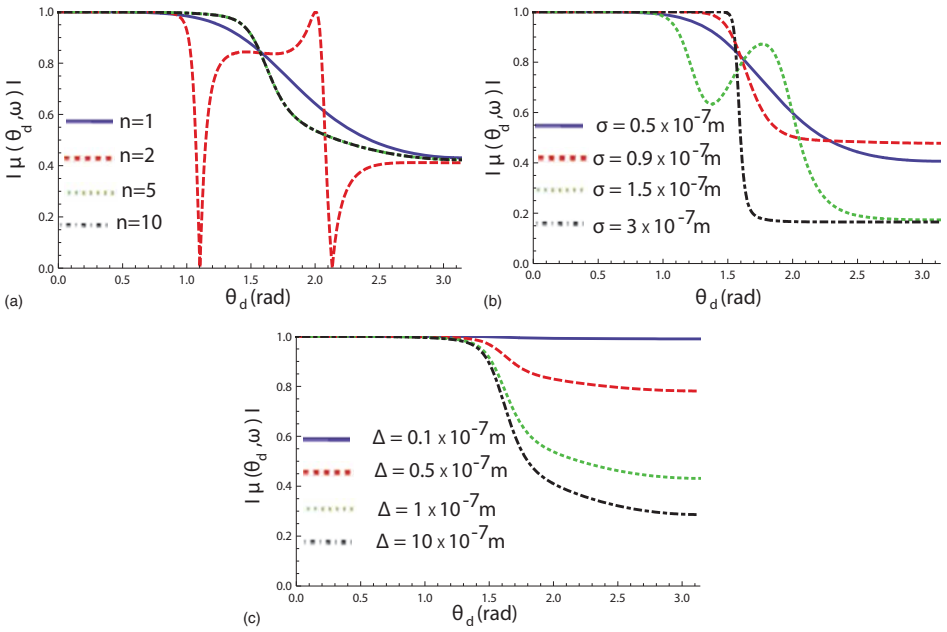

Figure 4.6: Modulus of the spectral degree of coherence of the far-field as a function of $\theta_d = \theta_2 - \theta_1$ where $\theta_1 = 0$, produced by scattering of two correlated plane waves, (a) on different number of particles ($k\sigma = 1$, $k\Delta = 1$); (b) on five particles, for different σ values ($k\Delta = 1$); (c) on five particles, for different Δ values ($k\sigma = 1$).

4.2.3 Scattering from random collections of particles: Pair-structure factor

In this section we develop the theory of scattering of scalar fields with arbitrary spectral and coherence properties from random collections of particles (deterministic potentials, random locations) which we characterize by a pair-structure factor (c.f. [74]). Pair-structure factor is a generalization of the conventional structure factor accounting for the change in correlation properties of light at two given directions of incidence and two given directions of scattering. We stress that the knowledge of the pair-structure factor makes it possible to predict of not only spectral but also coherence properties of scattered light, even in case when the incident wave has more complex structure than a plane wave. In order to deal with scattering of scalar fields with arbitrary spectral and correlation properties we use their plane wave (angular) representation. By considering a numerical example we illustrate how the spectral and correlation properties of scattered radiation depend on spectral and correlations properties of illumination, as well as on the size and locations of individual particles and their correlation properties.

Let us consider a collection of N identical particles with scattering potentials $f(\mathbf{r};\omega)$ being deterministic functions of position $\mathbf{r} = (x, y, z)$ and frequency ω, but with centers randomly distributed in scattering volume V. The scattering potential of each particle is a simple function of the index of refraction $n(\mathbf{r})$, namely Eq. (1.49). The scattering potential $F(\mathbf{r};\omega)$ of the whole collection is then given by the expression (4.14). Generally, for description of light scattering from random medium a spectral pair-scattering matrix of the form [75]

$$\mathbb{M}(\mathbf{u}_1, \mathbf{u}_1'; \mathbf{u}_2, \mathbf{u}_2'; \omega) = \langle \mathbb{S}^*(\mathbf{u}_1, \mathbf{u}_1'; \omega) \mathbb{S}(\mathbf{u}_2, \mathbf{u}_2'; \omega) \rangle_{rm} \tag{4.31}$$

may be employed, where the angular brackets with subscript "rm" denote statistical average taken over the realization of the medium. In this equation $\mathbb{S}(\mathbf{u}, \mathbf{u}'; \omega)$ is the ordinary scattering matrix which describes the change in the amplitude of a plane wave incident along direction $\mathbf{u}'$ and scattered along direction $\mathbf{u}$. It was shown [75] that within the accuracy of the first Born approximation the scattering matrix is related to the scattering potential of the scatterer by the expression

$$\mathbb{S}[\mathbf{K}; \omega] = \widetilde{F}(\mathbf{r}; \omega), \tag{4.32}$$

where $\mathbf{K} = k(\mathbf{u} - \mathbf{u}')$ is called the momentum transfer vector, and the bar denotes the (spatial) three-dimensional Fourier transform. On substituting from Eq. (1.49) into Eq. (4.32) we find that

$$\begin{aligned} \mathbb{S}(\mathbf{K}; \omega) &= \sum_{n=1}^{N} \widetilde{f}(\mathbf{r} - \mathbf{r}_n, \omega) \\ &= \sum_{n=1}^{N} e^{-i\mathbf{r}_n \cdot \mathbf{K}} \widetilde{f}(\mathbf{K}, \omega). \end{aligned} \tag{4.33}$$

Further, on substituting from Eq. (4.33) into Eq. (4.31) we find that

$$\mathbb{M}(\mathbf{K}_1, \mathbf{K}_2; \omega) = \widetilde{f}^*(\mathbf{K}_1, \omega) \widetilde{f}(\mathbf{K}_2, \omega) \mathbb{Q}(\mathbf{K}_1, \mathbf{K}_2; \omega) \tag{4.34}$$

where

$$\mathbb{Q}(\mathbf{K}_1, \mathbf{K}_2; \omega) = \langle \sum_{n=1}^{N} \sum_{m=1}^{N} e^{-i[\mathbf{r}_m \cdot \mathbf{K}_2 - \mathbf{r}_n \cdot \mathbf{K}_1]} \rangle_{rm} \tag{4.35}$$

is the *pair-structure factor* of the collection (cf. Ref. [74]). It provides the measure of correlation (similarity) between waves along transfer vectors $\mathbf{K}_1$ and $\mathbf{K}_2$. If the momentum transfer vectors coincide, i.e. if $\mathbf{K}_1 = \mathbf{K}_2$ then the pair-structure factor

reduces to the ordinary structure factor $\mathcal{S}(\mathbf{K})$, viz.

$$\mathcal{S}(\mathbf{K};\omega) = \langle \sum_{n=1}^{N} \sum_{m=1}^{N} e^{-i\mathbf{K}[\mathbf{r}_m - \mathbf{r}_n]} \rangle_{rm} \tag{4.36}$$

It is seen from Eq. (4.34) that, in addition to the scattering potential $f(\mathbf{r})$ of an individual particle, the knowledge of the pair-structure factor is sufficient for determining all the second-order statistical properties of fields produced on scattering from a collection of particles while the knowledge of the structure factor $\mathcal{S}(\mathbf{K};\omega)$, together with $f(\mathbf{r})$, is not. Only in a very restricted number of cases, such as the determination of the spectrum at a particular direction of scattering of a plane wave, one can rely solely on the knowledge of $\mathcal{S}(\mathbf{K};\omega)$ and $f(\mathbf{r})$ [76].

Note that by normalizing the pair-structure factor according to the formula

$$q(\mathbf{K}_1, \mathbf{K}_2; \omega) = \frac{\mathbb{Q}(\mathbf{K}_1, \mathbf{K}_2; \omega)}{\sqrt{\mathcal{S}(\mathbf{K}_1;\omega)}\sqrt{\mathcal{S}(\mathbf{K}_2;\omega)}} \tag{4.37}$$

we obtain a complex-valued quantity whose absolute value varies between 0 and 1 and which may be regarded as a *degree of angular correlation* of the collection of scatterers. Such measure is similar to the spectral degree of coherence of optical fields but rather describes the ability of a random medium to "decorrelate" light.

In order to illustrate the importance of the pair-structure factor for scattering of random light we now assume, without loss of generality, that it can be described by a Schell-model, vis.,

$$\mathbb{Q}(\mathbf{K}_1, \mathbf{K}_2; \omega) = \sqrt{S(\mathbf{K}_1)S(\mathbf{K}_2)}q(|\mathbf{K}_2 - \mathbf{K}_1|) \tag{4.38}$$

i.e. q depends on the distance between the two momentum transfer vectors. Assume

also that

$$q(|\mathbf{K}_2 - \mathbf{K}_1|) = exp\left[-\frac{|\mathbf{K}_2 - \mathbf{K}_1|^2}{(k\delta)^2}\right], \tag{4.39}$$

where σ^2 is the normalized variance of Gaussian distribution. A typical structure factor of a collection entering Eq. (4.38) can be found in Ref. [77].

We will now recall the general basic equations relating to the statistical properties of random waves scattered from random media. For more detailed derivation of these expressions see Refs. [78] and [75]. Let us assume that the incident field $U^{(i)}(\mathbf{r}, \omega)$ in the source plane is described with the help of the cross-spectral density function

$$W^{(i)}(\mathbf{r}_1, \mathbf{r}_2, \omega) = \langle U^{*(i)}(\mathbf{r}_1, \omega) U^{(i)}(\mathbf{r}_2, \omega) \rangle \tag{4.40}$$

or its angular correlation function

$$\begin{aligned} \mathcal{A}^{(i)}(\mathbf{u}_1, \mathbf{u}_2, \omega) = \frac{k^4}{(2\pi)^4} \iiiint\limits_{-\infty}^{\infty} W^{(i)}(\mathbf{r}_1, \mathbf{r}_2, \omega) \\ \times exp[-i(\mathbf{u}_1\mathbf{r}_1 + \mathbf{u}_2\mathbf{r}_2)] d^2\mathbf{r}_1 d^2\mathbf{r}_2, \end{aligned} \tag{4.41}$$

where $\mathbf{u}_1$, $\mathbf{u}_2$ are unit vectors and the integration is performed over the entire source plane ([2], Sect. 5.6.3).

It was shown in Ref. [78] that the cross-spectral density function of the total (incident + scattered) field in the far zone of the scatterer is given by the expression

$$\begin{aligned} W^{(t)}(r\mathbf{u}_1, r\mathbf{u}_2, \omega) = \ \pm \frac{4\pi^2}{k^2 r^2} u_{1z} u_{2z} \iint \widetilde{f}(\mathbf{K}_1) \widetilde{f}(\mathbf{K}_2) \\ \times \mathbb{Q}(-\mathbf{K}_1, \mathbf{K}_2) \mathcal{A}^{(i)}(\mathbf{u}'_1, \mathbf{u}'_2, \omega) d^2\mathbf{u}'_{1\perp} d^2\mathbf{u}'_{2\perp}, \end{aligned} \tag{4.42}$$

where $r = |\mathbf{r}|$ and both integrations extend only over the homogeneous part of the angular spectrum.

For the spectral density $S^{(t)}(r\mathbf{u};\omega)$, and the spectral degree of coherence $\mu^{(t)}(r\mathbf{u}_1, r\mathbf{u}_2;\omega)$ of the total far field produced on scattering we will use the formulas (1.15) and (1.14), from these expressions and Eq. (4.42) one can see explicitly that both the spectral density and the spectral degree of coherence of scattered light depend on the pair-structure factor of the collection.

4.2.4 Application to the pair of correlated plane waves scattered by random collection

We will now illustrate our analytical development by considering scattering of two mutually correlated polychromatic plane waves propagating along directions $\mathbf{u}_1'$ and $\mathbf{u}_2'$ by a model random collection.

It was found in Ref. [75] that the angular correlation function of correlated plane waves has the form of (4.24) with (4.25). Suppose that the scatterers centered at positions $\mathbf{r}_n = (x_n, y_n, z_n)$ have three-dimensional (soft) Gaussian potentials given by Eq. (4.26). The correlation properties of the collection are assumed to be described by Eqs. (4.38) and (4.39).

In Figure 4.7 the contour plots of the spectral density of the far field produced on scattering are shown for two values of the variance of pair-structure factor δ. On the horizontal scale, θ is the polar angle of the far-field and on the vertical scale, ϕ is the azimuthal angle of the far-field which are related to components of the unit vector $\mathbf{u}$ by the expression: $u_x = cos\theta cos\phi$, $u_y = cos\theta sin\phi$, $u_z = sin\theta$. Figure 4.8 illustrates the modulus of the spectral degree of coherence as a function of difference $(\theta_d = \theta_1 - \theta_2)$ between two directions in the far field. It is clear from figures 4.7 and 4.8 that correlation properties of the scatterers can significantly modify the intensity distribution and coherence properties of the scattered light.

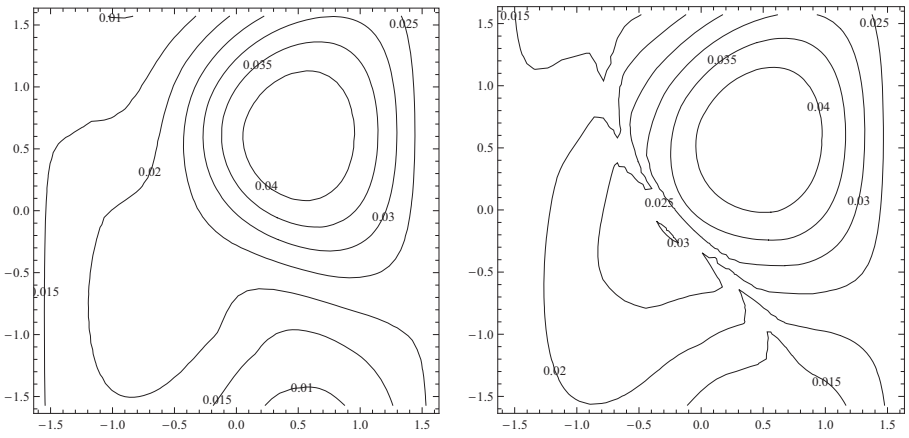

Figure 4.7: Contours of the spectral density of the far field: a) $\delta = 10^{-7}m$, b) $\delta = 10^{-6}m$, The other parameters are: $\lambda = 632.8nm$, $\Delta = 10^{-7}m$ $\sigma = 10^{-7}m$, $\theta_1' = -\pi/4$, $\phi_1' = -\pi/3$, $\theta_2' = \pi/6$, $\phi_2' = \pi/5$, $\theta_2 = \theta_1$, $\phi_2 = \phi_1$.

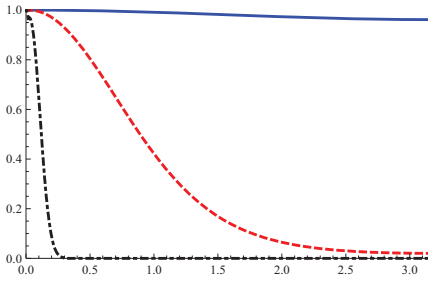

Figure 4.8: Modulus of the degree of coherence as a function of $\theta_d = \theta_1$, when $\theta_2 = 0$: dashed curve $\delta = 10^{-7}m$, dotted curve $\delta = 5 \times 10^{-7}m$, dot-dashed curve $\delta = 10^{-6}m$. The other parameters are: $\lambda = 632.8nm$, $\sigma = 10^{-7}m$; $\Delta = 10^{-7}m$; $\theta_1' = -\pi/4$; $\phi_1' = -\pi/3$; $\theta_2' = \pi/6$; $\phi_2' = \pi/5$; $\phi_1 = \pi/2$; $\phi_2 = \pi/2$.

4.3 Scattering of light from particles with semisoft boundaries

In potential scattering theory of light the distribution of the refractive index within a spherically-shaped scatterer can be fairly arbitrary, in principle (cf. [21], Ch. 13). However, in practice only two models for the refractive index distribution are routinely used: a Gaussian (soft-edge) sphere [5] and a hard-edge sphere [79]. In what follows we introduce a family of spherically symmetric scatterers with variable rate of change in the index of refraction at their edges, which we will refer to as "edge softness". Needless to say, both the hard-edge model and the Gaussian model, while being mathematically handy, are only the idealizations: scatterers with semi-soft edges are more realistic.

The original idea of a profile which has a flat center and an adjustable slope at the edge belongs to Gori [80] who used, to construct a flat-topped optical beam, a superposition of several Gaussian functions with different heights and widths. This idea has also been used for modeling edges in disk read-out systems [81]. Even though flat profiles can be expressed via various mathematical functions, such as Gegenbauer polynomials, Fermi-Dirac distribution, or much studied super-Gaussian function [82], the model introduced in [80] has the advantage of leading to tractable analytical results.

The other important type of a scatterer that we introduce is a hollow sphere with adjustable softness of its shell, on both inner and outer sides. Such model can be employed for instance in problems involving scattering from bubbles. We will show how a linear combination of 3D multi-Gaussian functions can efficiently serve this purpose, just like superposition of 2D multi-Gaussian beams has led to an important class of dark-hollow beams [83].

In briefly reviewing the potential scattering theory we fully rely on Ref. [5], Ch. 6. When a polychromatic spatially coherent plane wave field

$$U^{(i)}(\mathbf{r},\omega) = S^{(i)}(\omega)e^{ik\mathbf{s}_0\cdot\mathbf{r}}, \tag{4.43}$$

with spectral density $S^{(i)}(\omega)$, wave number $k = c/\omega$, c being the velocity of light in vacuum, ω angular frequency, at position $\mathbf{r}$, is incident, from direction $\mathbf{s}_0$, on a scatterer occupying volume D, then the spectral density of the scattered field $U^{(s)}(r\mathbf{s},\omega)$ in the far-zone of the scatterer along direction $\mathbf{r} = r\mathbf{s}$ ($|\mathbf{s}| = 1, |\mathbf{r}| = r$) can be expressed as

$$S^{(s)}(r\mathbf{s},\omega) = \frac{1}{r^2}S^{(i)}(\omega)\widetilde{C}_F[-k(\mathbf{s}-\mathbf{s}_0), k(\mathbf{s}-\mathbf{s}_0), \omega]. \tag{4.44}$$

Here $\widetilde{C}_F$ is the six-dimensional spatial Fourier transform:

$$\widetilde{C}_F(\mathbf{K}_1,\mathbf{K}_2,\omega) = \int_D\int_D C_F(\mathbf{r}_1',\mathbf{r}_2',\omega)e^{-i(\mathbf{K}_1\cdot\mathbf{r}_1'+\mathbf{K}_2\cdot\mathbf{r}_2')}d^3r_1'd^3r_2', \tag{4.45}$$

with $K = k(\mathbf{s}-\mathbf{s}_0)$ and C_F being the spatial correlation function of the scattering potential, Eq. (1.64) for random medium, Eq. (1.66) for deterministic medium.

On substituting from either Eq. (1.66) for deterministic scatterers or from Eq. (1.64) for random scatterers into Eqs. (4.44)-(4.45) one can determine the angular distribution of the far-field scattered spectral density.

4.3.1 Models of potentials with adjustable edges

A spherical scatterer centered at a point with position vector $\mathbf{r} = (0,0,d)$, without loss of generality, and a potential that has adjustable edge softness can be modeled

much like a multi-Gaussian beam [80] or aperture [81], i.e. via the sum:

$$F(\mathbf{r};\omega) = \frac{B}{C_0}\sum_{m=1}^{M}\frac{(-1)^{m-1}}{M}\binom{M}{m}e^{-m\frac{x^2+y^2+(z-d)^2}{2\sigma^2}}. \tag{4.46}$$

with $C_0 = \sum_{m=1}^{M}\frac{(-1)^{m-1}}{M}\binom{M}{m}$ being the normalization factor. Here variance σ^2 can be a constant or depend on ω. Figure 4.9 illustrates the soft-edge profiles versus radial distance from the center of the particle for several values of summation index M.

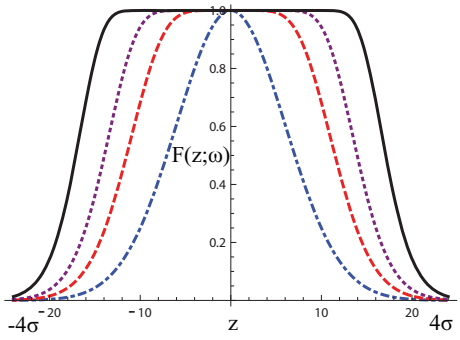

Figure 4.9: Scattering potential for solid particles calculated from Eq. (4.46) for several values of M: $M = 1$ dot-dashed curve , $M = 4$ dashed curve, $M = 10$ dotted curve and $M = 40$ solid thick curve.

The angular distribution of the spectral density of a plane wave scattered by a particle with potential (4.46) can be readily found from Eq. (4.44) to have the form

$$\begin{aligned} S^{(s)}(r\mathbf{s};\omega) =& \frac{B^2(2\pi)^5\sigma^6 s_z^2}{k^2r^2C_0^2}\Bigg(\sum_{m=1}^{M}\frac{(-1)^{m-1}}{M}\binom{M}{m}(1/m)^3 \\ &\times \exp\left[-k^2\sigma^2(\mathbf{s}-\mathbf{s}_0)^2/m\right]\Bigg)^2 \end{aligned} \tag{4.47}$$

For modeling hollow scatterers with semi-soft boundaries (bubbles, see also Fig. 4.10) it is sufficient to consider the following linear combination of two multi-Gaussian

functions

$$F(\mathbf{r};\omega) = \frac{B}{C_0}\sum_{m=1}^{M}\frac{(-1)^{m-1}}{M}\left(e^{-m\frac{x^2+y^2+(z-d)^2}{2\sigma_o^2}} - e^{-m\frac{x^2+y^2+(z-d)^2}{2\sigma_p^2}}\right), \tag{4.48}$$

in similarly with the model for the dark-hollow beams [83]. On substituting from Eq. (4.48) into Eq. (4.44) we find that the spectral density of a plane wave scattered from a bubble-like scatterer has the form

$$S^{(s)}(r\mathbf{s};\omega) = \frac{B^2(2\pi)^5\sigma^6 s_z^2}{k^2 r^2 C_0^2}\left(\sum_{m=1}^{M}\frac{(-1)^{m-1}}{Mm^3}\left(e^{-\frac{k^2\sigma_o^2(\mathbf{s}-\mathbf{s}_0)^2}{m}} - e^{-\frac{k^2\sigma_p^2(\mathbf{s}-\mathbf{s}_0)^2}{m}}\right)\right)^2. \tag{4.49}$$

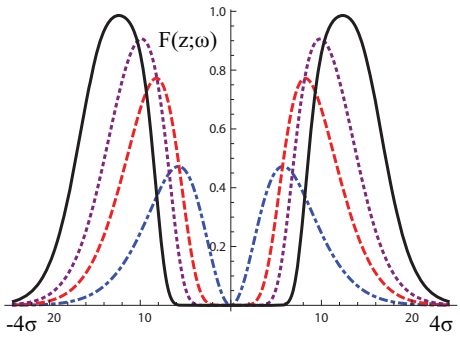

Figure 4.10: Same as in Fig. 4.9 but calculated from Eq. (4.48).

In order to introduce a random scatterer with semi-soft edges we can use for the correlation function C_F in Eq. (1.64) either of the Schell-model form [5],

$$C_F(\mathbf{r}_1,\mathbf{r}_2,\omega) = \sqrt{I_F(\mathbf{r}_1,\omega)}\sqrt{I_F(\mathbf{r}_2,\omega)}\mu_F(\mathbf{r}_2-\mathbf{r}_1,\omega), \tag{4.50}$$

with $I_F(\mathbf{r}_1,\omega) = C_F(\mathbf{r},\mathbf{r},\omega)$ or of the quasi-homogeneous form [5]

$$C_F(\mathbf{r}_1,\mathbf{r}_2,\omega) = I_F\left(\frac{\mathbf{r}_1+\mathbf{r}_2}{2},\omega\right)\mu_F(\mathbf{r}_2-\mathbf{r}_1,\omega), \tag{4.51}$$

where μ_F is the degree of spatial correlation which is assumed to be a function varying with $\mathbf{r}_2 - \mathbf{r}_1$ much faster than I_F varies with $\mathbf{r}$. It has been shown in Ref. [84] that for spherical sources and, hence, scatterers one should be careful with the choice of μ_F, some of the frequently used 2D correlation functions might not be legitimate for the 3D spherically symmetric model. On the other hand, a 3D Gaussian function

$$\mu_F^{(G)}(\mathbf{r}_2 - \mathbf{r}_1, \omega) = \exp\left(-\frac{|\mathbf{r}_1 - \mathbf{r}_2|^2}{2\delta^2}\right) \tag{4.52}$$

has been shown to be applicable, for instance. On substituting from Eqs. (4.51)-(4.52) together with either Eq. (4.46) or Eq. (4.48) into Eqs. (4.44)-(4.45) one can readily determine the spectral density of the field scattered from the random scatterer with semi-soft boundaries. We also note that the multi-Gaussian model can be readily extended to the incident random light waves [72], collections of particles [85], and elliptically-shaped scatterers.

4.3.2 Numerical examples

For the numerical analysis it is convenient to represent the coordinates of the direction vector $\mathbf{s}$ in the spherical system: $s_x = \cos\theta\cos\phi$, $s_y = \cos\theta\sin\phi$, $s_z = \sin\theta$ where θ and ϕ are the polar and the azimuthal angles, respectively.

We will now illustrate the usefulness of the models introduced by numerical calculations of the angular distribution of the spectral density of a plane wave scattered to the far field. In Fig. 4.11 we present the contourplot of the far-field spectral density (see Eq. (4.47)), depending on polar and azimuthal angles of the unit vector $\mathbf{s}$ for (a) soft-edge $M = 1$ and (b) semi-soft edge $M = 40$ solid scattering potential. The parameters used for numerical curves are: $\lambda = 632$nm, $\sigma = \frac{1}{2k}$, $\phi' = 0$, $\theta' = 0$. Figure 4.12 shows the far-field spectral density calculated from Eq. (4.49) for (a) soft-edge $M = 1$ and (b) semi-soft edge $M = 40$ hollow potential and demonstrates that the

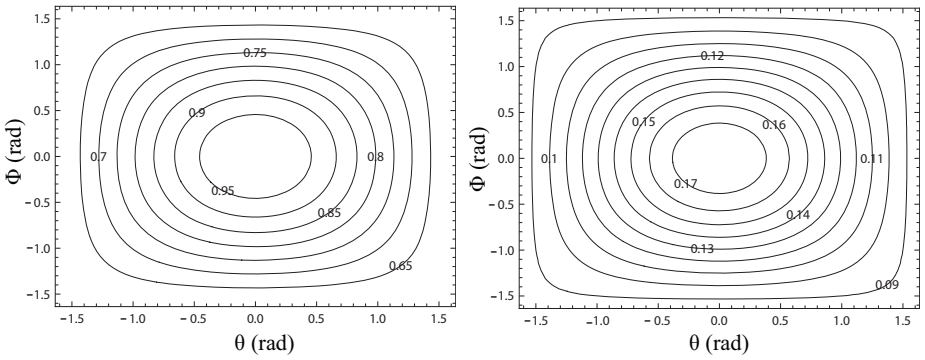

Figure 4.11: Contourplot of the spectral density of the the far field, calculated from Eq.(4.47), for: a) M=1, b) M=40.

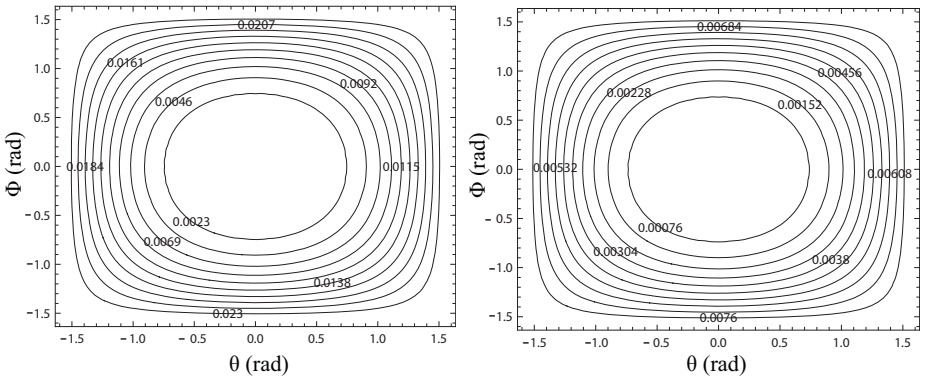

Figure 4.12: Same as Fig. 4.11 but calculated from Eq. (4.49).

effect of edge softness is very well pronounced.

4.4 Conclusion

Various aspects of scattering of fields from media confined to a localized volume were considered here, under a very general assumption that both the incident wave and the scatterer can be of either deterministic or random nature. The only assumption that we have made is the one of weak scattering, hence our results are pertinent to particles whose refractive indexes have values close to unity.

In section 4.2 we have developed the theory for far-field scattering of electromagnetic fields of deterministic and random nature from collections of discrete particles which have either deterministic or random locations. It enables scattering of fields with practically arbitrary spectral and coherence properties from particulate media in the most rigorous possible manner, while previously the majority of calculations were done for a single monochromatic or, at best, a polychromatic plane wave. From the example that we have considered, that involve scattering of two mutually correlated plane waves on several particles with Gaussian potentials, it is seen how the spectral density and the state of coherence of the far field depend on directions of the plane waves, their degree of correlation and, of course, on all the properties of the collection of scatterers. Although our analysis is limited only to collections for which the boundaries of the individual particles are soft and multiple scattering effects are neglected. In many practical cases our calculations are very relevant, e.g., in scattering of a random light beam from a tenuous collection of cells suspended in a solution. If the size of a cell is on the order of the wavelength then interference effects dominate multiple scattering effects and the first Born approximation is sufficient for obtaining an adequate solution.

In section 4.3 we have introduced a model for a scatterer with a flat potential in

its center and adjustable change in the refractive index at its edge, with the help of a 3D multi-Gaussian function. We have also shown how a linear combination of multi-Gaussian functions can be used to model shell-like scatterers, also with adjustable shell thickness. Our numerical examples illustrate that the softness of the boundary (thickness of the shell) of the scattering medium can significantly affect the angular distribution of the scattered field. This model could potentially be used to assess the role of hard boundaries on electromagnetic scattering, as it is known that field discontinuities at such boundaries can play a significant role [86]. Spherical scatterers can also readily extended to elliptical, cylindrical and parallelepiped-like shapes which can be useful in practice (c.f. [87]).

Chapter 5

Summary

In all the chapters included in this dissertation we explore generation and the behavior of random optical fields on propagation in vacuum, deterministic and random linear media, whether discrete or continuous, and we develop some of the applications which benefit from these findings. Among the major contributions of the author to the field are the following:

- Introduction of a novel class of sources with arbitrary intensity profiles which form constant-intensity profiles throughout the far zone.
- Analytical prediction of random light evolution in the human's crystalline lens.
- Development of novel techniques for target sensing in the presence of a random media by means of random light.
- Tractable modeling of particle's edges for easy applications of potential scattering theory.
- The seminal description of the dependence between the correlation properties of particles in the scattering collection and the properties of the scattered light.

All of the findings are based on the rigorous theoretical foundations involving Maxwell's equations and the classical statistical optics. They do not possess any heuristic or engineering types of modeling. The potential applications of the introduced ideas and techniques range from medicine to communications, from sensing of the environment to optical material processing.

References

[1] F. Zernike, "The concept of degree of coherence and its application to optical problems", Physica 5, 785-795 (1938).

[2] L. Mandel and E. Wolf, *Optical Coherence and Quantum Optics* (Cambridge, Cambridge University Press, 1995).

[3] R. Hanbury Brown and R. Q. Twiss, "Interferometry of the intensity fluctuations in light. I. Basic theory: the correlation between photons in coherent beams of radiation", Proc of the Royal Society of London A 242, 300-324 (1957).

[4] E. Collett, and E. Wolf, "New equivalence theorems for planar sources that generate the same distributions of radiant intensity", J. Opt. Soc. Am. 69, 942-950 (1979).

[5] E. Wolf, *Introduction to the Theory of Coherence and Polarization of Light* (Cambridge, Cambridge University Press, 2007).

[6] D. F. V. James, "Change of polarization of light beams on propagation in free space", J. Opt. Soc. Am. A 11, 1641-1643 (1994).

[7] C. M. V. Vliet, *Equilibrium and Non-equilibrium Statistical Mechanics* (World Scientific, 2008).

[8] T. Shirai, "Polarization properties of a class of electromagnetic Gaussian Schell-model beams which have the same far-zone intensity distribution as a fully coherent laser beam", Opt. Commun. 256, 197 (2005).

[9] O. Korotkova, and Emil Wolf, "Generalized Stokes parameters of random electromagnetic beams", Opt. Lett. 30, 198-200 (2005).

[10] F. Gori, M. Santarsiero, G. Piquero, R. Borghi, A. Mondello, and R. Simon, "Partially polarized Gaussian Schell-model beams", J. Opt. A: Pure Appl. Opt. 3, 1 (2001).

[11] O. Korotkova, M. Salem, and E. Wolf, "Beam conditions for radiation generated by an electromagnetic Gaussian Schell-model source", Opt. Lett. 29, 1173-1175 (2004).

[12] H. Roychowdhury, and O. Korotkova, "Realizability conditions for electromagnetic Gaussian Schell-model sources", Opt. Commun. 249, 379-385 (2005).

[13] O. Korotkova, and E. Wolf, "Spectral degree of coherence of a random three-dimensional electromagnetic field", Opt. Soc. Am. A 21, 2382-2385 (2004).

[14] M. A. Alonso, O. Korotkova, and E. Wolf, "Propagation of the electric correlation matrix and the van CittertZernike theorem for random electromagnetic fields", Journal of Modern Optics 53, 969-978 (2006).

[15] W. Gao, "Spectral changes of the light produced by scattering from tissue", Opt. Lett. 35, 862-864 (2010).

[16] Wanrong Gao and Olga Korotkova, "Changes in the state of polarization of a random electromagnetic beam propagating through tissue", Opt. Commun. 270, 474-478 (2007).

[17] L. C Andrews and R. L. Phillips, *Laser Beam Propagation in the Turbulent Atmosphere* (2nd edition, SPIE press, Bellington, 2005).

[18] O. Korotkova, J. Pu, and E. Wolf, "Spectral changes in electromagnetic stochastic beams propagating through turbulent atmosphere", Journal of Modern Optics 55, 1199-1208 (2008).

[19] S.A. Collins, Jr., "Lens-system diffraction integral written in terms of matrix optics", J. Opt. Soc. Am. A 60, 1168-1177 (1970).

[20] B. Lu, and L. Pan, "Propagation of vector Gaussian Schell-model beams through a paraxial optical ABCD system", Opt. Commun. 205, 7-16 (2002).

[21] M. Born and E. Wolf, *Principles of Optics* (Cambridge, Cambridge University Press, 7th Edition, 1999).

[22] A. Ishimaru, *Wave Propagation and Scattering in Random Media* (Wiley-IEEE Press, 1999, vol.1).

[23] J. Ellis, A. Dogariu, "Complex degree of cross-polarization", Opt. Lett. 29, 536-538 (2004).

[24] T. Shirai, and E. Wolf, "Correlations between intensity fluctuations in stochastic electromagnetic beams of any state of coherence and polarization", Opt. Commun. 272, 289-292 (2007).

[25] A. T. Friberg, and R. J. Sudol, "The spatial coherence properties of Gaussian Schell-model beams", Opt. Acta 30, 1075 (1983).

[26] A. C. Schell, *The Multiple Plate Antenna*, (Doctoral Dissertation, MIT, Sect. 7.5, 1961).

[27] F. Gori, G. Guattari and C. Padovani, "Modal expansion for J_0-correlated Schell-model sources", Opt. Comm. 64, 311-316 (1987).

[28] S.A. Ponomarenko, "A class of partially coherent beams carrying optical vortices", J. Opt. Soc. Am. A 18, 150-156 (2001).

[29] H. Lajunen, T. Saastamoinen, "Propagation characteristics of partially coherent beams with spatially varying correlations", Opt. Lett. 36, 4104-4106 (2011).

[30] F. Gori and M. Santarsiero, "Devising genuine spatial correlation functions", Opt. Lett. 32, 3531-3533 (2007).

[31] F. Gori, "Flattened gaussian beams", Opt. Comm. 107, 335-341 (1994).

[32] S. Sahin, G. Gbur, O. Korotkova, "Scattering of light from particles with semi-soft boundaries", Opt. Lett. 36, 3957-3959 (2011).

[33] S. Sahin, and O. Korotkova, "Light sources generating far fields with tunable flat profiles", Opt. Lett. 37, in press.

[34] J. A. Diaz, "ABCD matrix of the human lens gradient-index profile: applicability of the calculation methods", Appl. Opt. 47, 195-205 (2008).

[35] L. Matthiessen, "Untersuchungen über den Aplanatismus und die Periscopie der Krystalllinsen in den Augen der Fische," Pfluegers Arch. Gesamte Physiol. Menschen Tiere 21, 287-307 (1880).

[36] A. Gullstrand, Helmholtz's Handbuch der Physiologischen Optik, 3rd ed., Vol. 1, Appendix II, pp. 301-358 (English translation edited by J. P. Southall, Optical Society of America, 1924).

[37] G. Smith, D.A. Atchison, and B. K. Piercionek, "Modeling the power of the aging human eye," J. Opt. Soc. Am. A 9, 2111-2117 (1992).

[38] Y. Huang and D. T. Moore, "Human eye modeling using a single equation of gradient index crystalline lens for relaxed and accomodated states", Proc. SPIE 6342, 63420D (2006).

[39] M.T. Flores-Arias, M.V. Perez, C. Bao, A. Castelo, and C. Gomez-Reino, "Gradient-index human lens as a quadratic phase transformer", Journal of Modern Optics 53, 495-506 (2006).

[40] M.V. Perez, C. Bao, M.T. Flores-Arias, M.A. Rama, and C.G. Reino, "Description of gradient-index crystalline lens by a first-order optical system", J. Opt. A: Pure Appl. Opt. 7, 103-110 (2005).

[41] M. A. Rama, M. V. Perez, C. Bao, M.T. Flores-Arias, and C.G. Reino, "Gradient-index crystalline lens model: A new method for determining the paraxial properties by the axial and field rays", Opt. Commun. 249, 595-609 (2005).

[42] A.T. Friberg, J. Turunen, "Imaging of Gaussian Schell-model sources", J. Opt. Soc. Am. A 5, 713 (1988).

[43] S. Sahin and O. Korotkova, "Crystalline human eye lens response to stochastic light", Opt. Lett. 36, 2970-2972 (2011).

[44] J. Pu, and O. Korotkova, "Propagation of the degree of cross-polarization in the turbulent atmosphere", Opt. Commun. 282, 1691-1698 (2009).

[45] O. Korotkova, M. Salem and E. Wolf, "The far-zone behavior of the degree of polarization of partially coherent beams propagating through atmospheric turbulence", Opt. Comm. 233, 225-230 (2004).

[46] V. A. Banakh, V. M. Buldakov, V.L. Mironov, "Intensity fluctuations of a partially coherent light beam in a turbulent atmosphere", Opt. Spectrosk. 54, 626-629 (1983).

[47] G. Gbur, E. Wolf, "Spreading of partially coherent beams in random media", J. Opt. Soc Am. A 19, 1592-1598, (2002).

[48] J. C. Ricklin, F. M. Davidson, "Atmospheric optical communication with a Gaussian Schell beam", J. Opt. Soc. Am. A 20, 856-866 (2003).

[49] O. Korotkova, L. C. Andrews and R. L. Phillips, "A model for a partially coherent Gaussian beam in atmospheric turbulence with application in LaserCom", Opt. Eng. 43, 330-341 (2004).

[50] T. J. Schulz. "Optimal beam for propagation through random media", Opt. Lett. 30, 1093-1095 (2005).

[51] O. Korotkova, "Changes in the intensity fluctuations of a class of random electromagnetic beams on propagation", J. Opt. A: Pure and Appl. Opt. 8, 30-37 (2006).

[52] O. Korotkova, "Changes in statistics of the instantaneous Stokes parameters of a quasi-monochromatic electromagnetic beam on propagation", Opt. Comm. 261, 218-224 (2008).

[53] O. Korotkova, "Scintillation index of a random electromagnetic beam propagating in random media", Opt. Comm. 281, 2342-2348 (2008).

[54] Y. Gu, O. Korotkova and G. Gbur, "Scintillation of non-uniformly polarized beams in atmospheric turbulence", Opt. Lett. 34, 2261-2263 (2009).

[55] C. Brosseau, *Fundamentals of Polarized Light: A Statistical Optics Approach* (Wiley, New York, 1998).

[56] C. Brosseau, "Statistics of the normalized Stokes parameters for a Gaussian stochastic plane wave field", Appl. Opt. 34, 4788 (1995).

[57] M. Salem, O. Korotkova, A. Dogariu, E. Wolf, "Polarization changes in partially coherent electromagnetic beam propagating through the turbulent atmosphere", Waves in Random Media 14, 513-523 (2004).

[58] J. C. Ricklin and F. M. Davidson, "Atmospheric turbulence effects on a partially coherent Gaussian beam: implications for free-space laser communication", J. Opt. Soc Am. A 19, 1794-1802 (2002).

[59] O. Korotkova, M. Salem, A. Dogariu, E. Wolf, "Changes in the polarization ellipse of random electromagnetic beams propagating through turbulent atmosphere", Waves in Random and Complex Media 15, 353-364 (2005).

[60] V. A. Banakh, *Lidar in a Turbulent Atmosphere* (Artech House, 1987).

[61] Q. Lin, Y. Cai, "Tensor ABCD law for partially coherent twisted anisotropic Gaussian-Schell model beams," Opt. Lett. 27, 216-218 (2002).

[62] O. Korotkova, Y. Cai, E. Watson, "Stochastic electromagnetic beams for LIDAR systems operating in turbulent atmosphere", Appl. Physics B 94, 681-690 (2009).

[63] Y. Cai, O. Korotkova, H. T. Eyyubogllu, Y. Baykal, "Active laser radar systems with stochastic electromagnetic beams in turbulent atmosphere", Opt. Express 16, 15834-15846 (2008).

[64] T. Shirai, O. Korotkova and E. Wolf, "A method of generating electromagnetic Gaussian Schell-model beams" J. Opt. A: Pure Appl. Opt. 7 232-237 (2005).

[65] H. Roychowdhury and O. Korotkova, "Realizability conditions for electromagnetic Gaussian Schell-model sources" Opt. Comm. 249, 379-385 (2005).

[66] F. Gori, M. Santarsiero, R. Borghi, V. Ramirez-Sanchez, "Realizability condition for electromagentic Schell-model sources", J. Opt. Soc. Am A 25, 1016-1021 (2008).

[67] O. Korotkova, M. Salem and E. Wolf, "Beam conditions for radiation generated by an electromagnetic Gaussian Schell-model source", Opt. Lett. 29, 1173-1175 (2004).

[68] J. W. Goodman, "Statistical properties of laser speckle patterns", Chap. 2 in Laser Speckle and Related Phenomena, J. C. Dainty, Ed. (Springer-Verlag, Berlin, 1975).

[69] O. Korotkova, M. Salem and E. Wolf, "The far-zone behavior of the degree of polarization of partially coherent beams propagating through atmospheric turbulence", Opt. Comm. 233, 225-230 (2004).

[70] X. Du, D. Zhao, O. Korotkova, "Changes in the statistical properties of stochastic anisotropic electromagnetic beams on propagation in the turbulent atmosphere", Opt. Express 15, 16909-16915 (2007).

[71] P. Meemon, M. Salem, K. Lee, M. Chopra, J.P. Rolland, "Determination of the correlation matrix of a broadband stochastic electromagnetic light beam", J. Mod. Opt. 55, 2765-2776 (2008).

[72] O. Korotkova and E. Wolf, "Scattering Matrix Theory for stochastic scalar fields", Phys. Rev. E 75, 056609 (2007).

[73] S. Sahin and O. Korotkova, "Scattering of scalar light fields from collections of particles", Phys. Rev. A 78, 063815 (2008).

[74] G. Gbur and E. Wolf, "Determination of density correlation functions from scattering of polychromatic light", Opt. Comm. 168, 39-45 (1999).

[75] O. Korotkova and E. Wolf, "Scattering Matrix Theory for stochastic scalar fields", Phys. Rev. E 75, 056609 (2007).

[76] A. Dogariu, E. Wolf, "Spectral changes produced by static scattering on a system of particles", Opt. Lett. 23, 1340-1342 (1998).

[77] J. M. Ziman, *Models of Disorder* (Cambridge University Press, 1979).

[78] S. Sahin and O. Korotkova, "Scattering of random light from deterministic collections of particles", Phys. Rev. A. 78, 063815 (2008)

[79] T. van Dijk, D.G. Fischer, T.D. Visser and E. Wolf, "Effects of Spatial Coherence on the Angular Distribution of Radiant Intensity Generated by Scattering on a Sphere", Phys. Rev. Lett. 104, 173902 (2010).

[80] F. Gori, "Flattened gaussian beams", Opt. Commun. 107, 335341 (1994).

[81] Y. Li, H. Lee, E. Wolf, "Effect of edge rounding and sloping of sidewalls on the readout signal of the information pits on optical disks", Opt. Eng. 42, 27072720 (2003).

[82] S. De Silvestri, P. Laporta, V. Magni and O. Svelto, "Solid-state laser unstable resonators with tapered reflectivity mirrors: the super-Gaussian approach", IEEE J. Quantum Electron QE-24, 1172 (1988).

[83] J. Yin, W. Gao, and Y. Zhu, "Generation of dark hollow beams and their applications," in Progress in Optics, Vol. 44, E. Wolf, ed., North-Holland, Amsterdam, 119204 (2003).

[84] F. Gori and O. Korotkova, "Modal expansion for spherical homogeneous sources", Opt. Comm. 282, 3859-3861 (2009).

[85] S. Sahin and O. Korotkova, "Effect of the pair-structure factor of a particulate medium on scalar wave scattering in the first Born approximation", Opt. Lett. 34, 1762-1764 (2009).

[86] T. D. Visser, and E. Wolf, "Potential scattering with field discontinuities at the boundaries", Phys. Rev. E 59, 2355-2360 (1999).

[87] Howard R. Gordon, "Rayleigh-Gans scattering approximation: surprisingly useful for understanding backscattering from disk-like particles", Opt. Exp. 15, 5572 (2007).